THE UNIVERSITY OF MICHIGAN

INDUSTRY PROGRAM OF THE COLLEGE OF ENGINEERING

OXIDATION OF AMMONIA OVER A SUPPORTED RUTHENIUM CATALYST

Thomas J. Schriber

A dissertation submitted in partial fulfillment
of the requirements for the degree of
Doctor of Philosophy in the
University of Michigan
Department of Chemical and Metallurgical Engineering
1964

May, 1964

IP-670

ACKNOWLEDGEMENTS

This research was conducted in the Department of Chemical and Metallurgical Engineering at the University of Michigan under the direction of Professor Giuseppe Parravano. Special thanks go to Professor Parravano and to the members of the doctoral committee for suggestions and guidance during the course of the work.

Thanks are also due to Doctors Ewald Wicke and Kurt Hedden, both of the Institute of Physical Chemistry at the University of Muenster in Muenster, Germany, and to Doctor Georg-Maria Schwab, of the Institute of Physical Chemistry at the University of Munich, for friendly and provocative discussions concerning heterogeneous catalysis.

The author recognizes a debt of gratitude to the National Science Foundation for three pre-doctoral fellowships, to the Fulbright Commission for a Fulbright Grant to Germany and to the International Nickel Company both for personal support for one year and for generous funds to provide the experimental equipment for this investigation.

TABLE OF CONTENTS

		Page
ACKNOWLEDGEMENTS		ii
LIST OF TABLES		v
LIST OF FIGURES		vi
LIST OF APPENDICES		viii
NOMENCLATURE		ix
ABSTRACT		xii
I	INTRODUCTION	1
II	SURVEY OF THE LITERATURE	7
	A. Laboratory Scale Reactors for Gas-Solid Systems	7
	B. Previous Studies of the Heterogeneous Catalytic Oxidation of Ammonia	10
	C. Ruthenium as a Catalyst	16
III	EXPERIMENTAL EQUIPMENT	18
	A. Description of Flow Sequence	18
	B. Flow Meter Bank	20
	C. Molten Salt Bath	20
	D. Reactor	21
	E. Back Pressure Regulator	23
	F. Recycle Pump	24
	G. Surge Cylinders	25
	H. Sample Valve	26
	I. Vapor Fractometer	27
	J. Printing Integrator and Recorder	28
	K. The Catalyst	28
IV	EXPERIMENTAL TECHNIQUES	30
	A. Feed Composition	30
	B. Flowmeter Calibration	30
	C. Pump Calibration	31
	D. Vapor Fractometer Calibration	32
	E. Catalytic Activity of Reactor System	33
	F. Catalytic Activity of Alumina Carrier	34

TABLE OF CONTENTS (CONT'D)

		Page
G.	Experimental Procedure	35
H.	Reaction Products	36
I.	Range of Variables	37
J.	Stability of Catalyst	38
K.	Check on Differential Conditions	39
L.	Data Reproducibility	40
M.	Reversibility of Water Adsorption	42
N.	Removal of Water from Recycle Stream	43
O.	Presence of Hydrogen	45
V	EXPERIMENTAL RESULTS	46
A.	Influence of Ammonia Pressure on Total Rate of Ammonia Oxidation	46
B.	Influence of Nitrogen on Rate of Product Formation	46
C.	Influence of Nitrous Oxide on Rate of Product Formation	50
D.	Influence of Ammonia on Rate of Product Formation	54
E.	Influence of Oxygen on Rate of Product Formation	57
F.	Influence of Water on Rate of Product Formation	60
G.	Influence of Mass Transfer on Rate of Product Formation	63
H.	Stability of Catalyst and Check on Differential Conditions	65
I.	Influence of Ammonia on Relative Rate of Nitrous Oxide Formation	65
VI	DISCUSSION OF RESULTS	71
A.	Influence of Partial Pressures on Reaction Rates	71
B.	Influence of Mass Transfer on Reaction Rates	74
C.	Formulation of Reaction Mechanism	75
D.	Rate Equations Corresponding to Proposed Mechanism	78
E.	Evaluation of Constants in Rate Equations	82
F.	Theoretical and Experimental Heats of Adsorption	83
G.	Theoretical and Experimental Adsorption Equilibrium Constant b_o; Entropies of Adsorption	89
H.	Apparent and True Activation Energies	95
I.	Absolute Rate Theory	98
VII	SUMMARY AND CONCLUSIONS	102
APPENDICES		105
BIBLIOGRAPHY		144

LIST OF TABLES

Table		Page
III-1	Physical Properties of Catalyst.....	29
IV-1	Reproducibility of Measurements with Used Catalyst.	41
IV-2	Reproducibility of Measurements with Two Catalyst Charges.....	41
VI-1	Experimental and Theoretical Values of b_o.....	91
VI-2	Experimental and Theoretical Values of Adsorption Entropy.....	94
VI-3	Experimental Pre-Exponential Factors in Power Rate Law.....	101
A-1	Flowmeter Calibration Measurements.....	105
B-1	Experimental Values of Partial Pressures and Rates of Product Formation.....	110
C-1	Measurements Used to Evaluate Activation Energy in Power Rate Law.....	124
D-1	Numerical Values Used in Mass Transfer Equation.....	131
D-2	Numerical Values Used in Heat Transfer Equation.....	136
E-1	Values of Constants in Rate Equations and Percentage Deviations of Data Fit.....	139
F-1	Free Energy Functions of Ammonia, Oxygen and Water..	140

LIST OF FIGURES

Figure		Page
1.1	Oxidation of Ammonia to Nitrous Oxide and Nitrogen..	5
3.1	Experimental Apparatus.....	19
3.2	Reactor Section.....	21
3.3	Integration of Reactor in Recycle Loop.....	22
5.1	Influence of Ammonia on Total Rate of Ammonia Oxidation, Pressure 280 cm Hg, 5.3 Volume Percent Ammonia in Feed.....	47
5.2	Influence of Ammonia on Total Rate of Ammonia Oxidation, Pressure 280 cm Hg, 16.5 Volume Percent Ammonia in Feed.....	48
5.3	Influence of Ammonia on Total Rate of Ammonia Oxidation, Pressure 176 cm Hg, 16.5 Volume Percent Ammonia in Feed.....	49
5.4	Influence of Nitrogen and Nitrous Oxide on Rate of Product Formation at 296°C.....	51
5.5	Influence of Nitrogen and Nitrous Oxide on Rate of Product Formation at 310°C.....	52
5.6	Influence of Nitrogen and Nitrous Oxide on Rate of Product Formation at 345°C.....	53
5.7	Influence of Ammonia on Rate of Nitrogen Formation..	55
5.8	Influence of Ammonia on Rate of Nitrous Oxide Formation.....	56
5.9	Influence of Oxygen on Rate of Nitrogen Formation...	58
5.10	Influence of Oxygen on Rate of Nitrous Oxide Formation.....	59
5.11	Influence of Water on Rate of Nitrogen Formation....	61
5.12	Influence of Water on Rate of Nitrous Oxide Formation.....	62
5.13	Rate of Ammonia Oxidation vs. Ammonia Pressure.....	64

LIST OF FIGURES (CONT'D)

Figure		Page
5.14	Influence of Mass Transfer on Rate of Ammonia Oxidation.....	66
5.15	Stability of Catalyst and Check on Differential Conditions at 246°C.....	67
5.16	Stability of Catalyst and Check on Differential Conditions at 322°C.....	68
5.17	Influence of Ammonia on Relative Rate of Nitrous Oxide Formation.....	70
6.1	Illustration of Steps in Proposed Reaction Mechanism	79
6.2	Mechanism for Reaction Between Adsorbed Ammonia and One Dissociatively Adsorbed Oxygen.....	80
6.3	Mechanism for Reaction Between Adsorbed Ammonia and Two Dissociatively Adsorbed Oxygens.....	81
6.4	Temperature Dependence of Rate Equation Constants...	84
6.5	Mechanism 1 for Adsorption of Oxygen and Water on Ruthenium.....	85
6.6	Mechanism 2 for Adsorption of Oxygen and Water on Ruthenium.....	87
A.1	Flowmeter Calibration Curves for 9.7 Volume Percent Ammonia, Balance Oxygen, Feed.....	106
A.2	Flowmeter Calibration Curves for Helium, Nitrogen and Nitrous Oxide.....	108
C.1	Plot for Evaluation of Rate Constants.....	119
C.2	Plot for Evaluation of Rate Constants.....	120
C.3	Plot for Evaluation of Power Rate Law Activation Energy.....	125
D.1	Experimental Temperature Rise in Reactant Stream....	134

LIST OF APPENDICES

Appendix		Page
A	CALIBRATION OF FLOW METERS	105
B	EXPERIMENTAL DATA	109
C	SAMPLE CALCULATIONS	115
	1. Calculation of Reaction Rates and Partial Pressures from Raw Data	115
	2. Evaluation of Constants in Rate Equations	118
	3. Calculation of Experimental Heat of Adsorption	121
	4. Calculation of Theoretical Heat of Adsorption	121
	5. Calculation of the Experimental b_O	122
	6. Calculation of the Theoretical b_O	123
	7. Calculation of the Experimental Entropy of Adsorption	123
	8. Calculation of E for Power Rate Law	123
	9. Calculation of Power Rate Law Experimental Pre-Exponential Factor	124
	10. Calculation of Power Rate Law Theoretical Pre-Exponential Factor	126
	11. Calculation of Percentage Surface Covered by Atomic Oxygen	127
	12. Validity of Assumption that Number of Reaction Sites Equals Number of Ruthenium Atoms	127
	13. Calculation of Theoretical Entropy of Adsorption of Oxygen	128
D	HEAT AND MASS TRANSFER CONSIDERATIONS	130
	1. Calculation of Pressure Drop Between Bulk Gas and Catalyst Surface	130
	2. Calculation of Temperature Drop Between Bulk Gas and Catalyst Surface	132
	3. Relationship Between Mass Transfer Coefficient and Reactor Diameter	138
E	VALUES OF CONSTANTS IN RATE EQUATIONS	139
F	FREE ENERGY FUNCTIONS OF AMMONIA, OXYGEN AND WATER	140
G	DETERMINATION OF REACTION RATES IN A STIRRED FLOW SYSTEM	141

NOMENCLATURE

a	Ammonia exponent in power rate law, nitrogen data
a_m	External pellet area per unit mass
a_p	External pellet area per pellet
B_{NH_3}	Coefficient used in approximation of Langmuir adsorption isotherm for ammonia
B_{O_2}	Coefficient used in approximation of Langmuir adsorption isotherm for oxygen
b	Oxygen exponent in power rate law, nitrogen data
b_A	Adsorption equilibrium constant of species A
$(b_o)_A$	Pre-exponential factor in equation relating adsorption equilibrium constant of species A to temperature
C_p	Heat capacity
c	Water Exponent in power rate law, nitrogen data
D	Reactor diameter
D_A	Diffusivity of component A
d	Ammonia exponent in power rate law, nitrous oxide data
E	Activation energy associated with power rate law equation
E	Internal energy
e	Oxygen exponent in power rate law, nitrous oxide data
f	Water exponent in power rate law, nitrous oxide data
G	Free energy
G	Superficial mass velocity
H	Enthalpy
h	Planck's constant
j_D	j-factor for mass transfer

K_A	Overall rate coefficient in rate equation for formation of species A
k	Boltzmann's constant
k	Mass transfer coefficient
k_A	Rate constant corresponding to slow step in formation of species A
k_o	Power rate law pre-exponential factor
M_m	Average molecular weight of gas
m	Exponent in power rate law
n	Exponent in power rate law
p	Total gas pressure
p_A	Partial pressure of gas species A
p_f	Gas film pressure
p_o	Standard gas pressure
R	Gas constant
r	Rate of reaction
S	Entropy
T	Temperature
v	Superficial linear velocity
W	Weight
X_A	Electronegativity of species A
Δ	Difference
ΔE	Activation energy
ΔH	Heat of reaction
ϵ	Porosity
λ_A	Heat of adsorption of species A

μ	Polar moment of metal-adsorbed species bond
μ	Viscosity
θ_{NH_3}	Fraction of catalyst surface covered with ammonia
θ_O	Fraction of catalyst surface covered with atomic oxygen
ϕ_A	Free energy function of species A
ρ	Density
τ	Contact time

Subscripts

apparent	Denotes apparent activation energy
exptl	Experimental value of quantity subscripted
theo	Theoretical value of quantity subscripted
true	Denotes true activation energy

ABSTRACT

A stirred flow reactor has been used to study the kinetics of the oxidation of ammonia with oxygen over 0.5 weight percent ruthenium supported on 1/8 inch cylindrical alumina pellets. The experimental system featured rapid recycling of 98% or more of the reactor effluent and concurrent product withdrawal and fresh feed makeup. This experimental approach facilitated close temperature control, rapid mass transport to the catalyst surface and uniform reaction conditions over the whole length of the catalyst bed.

Experimentation was conducted at six temperatures in the range 246 - 345°C. Reaction pressures from 176 to 280 cm Hg (2.3 - 3.7 atmospheres) were used. Feed composition during most of the work was 5.3, 9.6 and 16.5 mole percent ammonia, the balance in each case being oxygen. The reactor effluent was analyzed by gas chromatography. Products of reaction were nitrogen, nitrous oxide and water.

Rates of formation of both nitrogen and nitrous oxide were found to depend on the partial pressures of ammonia, oxygen and water and to be independent of nitrogen and nitrous oxide. Increasing water pressure inhibited both rates to the same extent. Increasing ammonia pressure favored the relative rate of formation of nitrous oxide. Increasing temperature also favored nitrous oxide formation. The maximum nitrous oxide yield realized in this work was about 45%. It was shown experimentally that mass transport did not influence product distribution and was not the slow step controlling the reaction rate.

Rate equations were developed to express the rates of formation of nitrogen and nitrous oxide. Constants appearing in these equations were calculated as a function of temperature and were found to fit the experimental data within $\pm$ 3.2%. Temperature dependence of the constants was used to calculate apparent activation energies and heats and entropies of adsorption. The heats of adsorption were compared with values predicted theoretically on the basis of an adsorption mechanism and use of Pauling's equation for single bond energies. The entropies of adsorption were compared with the theoretical values which result when the adsorbed species has lost three degrees of translational freedom during the adsorption process. A power rate law data fit was used to compare the observed reaction rates with those predicted by absolute rate theory and order-of-magnitude agreement resulted. A reaction mechanism which is consistent with all the experimental observations in this study was developed.

The rate equations corresponding to the rate of formation of nitrogen and nitrous oxide, respectively, are:

$$r_{N_2} = \frac{K_{N_2} p_{O_2} p_{NH_3}}{(1 + b_{O_2}^{1/2} p_{O_2}^{1/2} + b_{H_2O} p_{H_2O})^2}$$

and

$$r_{N_2O} = \frac{K_{N_2O} p_{O_2} p_{NH_3}^{1.35}}{(1 + b_{O_2}^{1/2} p_{O_2}^{1/2} + b_{H_2O} p_{H_2O})^2}$$

I INTRODUCTION

The science of chemical kinetics concerns itself with the rates of chemical reactions and with those factors upon which reaction rates depend. It addresses itself also to the problem of explaining observed rates and their dependencies in terms of postulated models, known as reaction mechanisms. These mechanisms propose to indicate the stages through which molecules and the various intermediate species move in passing from reactants to products. Fundamentally, then, chemical kinetics involves the details of transition from one state to another and the time required for the transition.

One can easily appreciate that kinetics will be of interest both to chemical engineers and to chemists. The chemical engineer must have at his disposal knowledge both of reaction rates and of their environmental dependency before he can satisfactorily design the equipment in which reactions are conducted on a commercial scale. The details of a particular reaction mechanism can facilitate this goal by suggesting how to optimize reaction conditions relative to such important factors as product yield and degree of conversion.

Whereas the chemical engineer might use a proposed reaction mechanism as an aid in reactor design, the chemist is more directly concerned with the mechanism itself. The chemist is often interested in measuring reaction rates and rate dependencies chiefly because such measurements provide the most general method of determining the mechanism of a reaction. This is not to say that reaction mechanisms can be uniquely specified solely on the basis of rate measurements. Experimental results can in general be

interpreted on the basis of several conceivable mechanisms. More experimentation or even a basically different experimental approach may sometimes then be conceived and conducted to test the hypotheses, eliminating several of them or possibly all but one.

Whichever ultimate purpose rate measurements are intended to serve, great pains must be taken to insure that the measurements are precise, i.e., that the influence of such variables as temperature and concentration are carefully distinguished independently of one another. This is particularly true in heterogeneous catalysis, where heat and mass transfer play important roles and the danger of overlapping effects is especially acute. Consider the steps that are involved in a gas phase reaction over a solid catalyst: first there is transport of reactants to the exterior catalyst surface, followed possibly by diffusion into the catalyst pores; then adsorption of some or all reactants takes place; adsorption is followed by reaction of the adsorbed species, either only with other adsorbed species or possibly with gas-phase species; desorption of products must then occur; and, finally, the last step is diffusion from the catalyst interior and surface back to the bulk gas stream. A further complication is that while this series of steps takes place, the necessary heat requirements must be supplied to or removed from the catalyst.

In the simplified approach taken to this complex phenomenon, one of the steps other than heat transfer is assumed to be so relatively slow that all other steps may be considered to be in a state of equilibrium. Measuring the reaction rate is then equivalent to measuring the rate of the slow step. It is clear that if the measured rates are to be related to a

reaction mechanism, then the slow step must be a chemical step, i.e., adsorption, reaction on the surface, or desorption. The condition of turbulence that the required rapid mass transport implies may also result in interfacial partial pressures being approximately equal to those in the bulk phase, simplifying later calculations; the turbulence comes, however, at the expense of pressure drop in the catalyst bed. It will be further appreciated that, since the slow chemical step requires an energy of activation and will be temperature sensitive, fine temperature control is also a requirement for taking precise rate data.

The research being reported here made use of a laboratory-scale, gas-solids contacting scheme designed to provide conditions of rapid mass transport and good temperature control during catalytic rate studies. The experimental apparatus, a recirculation reactor with a fresh feed and product withdrawal provision, lends itself readily to the investigation of many solid-catalyzed reactions under differential rate conditions. Whereas reactor effluent was recycled at about fifty liters per minute, the fresh feed rate never exceeded one liter per minute. Hence maximum conversion across the catalyst bed, which was 5.1 cm in depth, was limited to about 2%, that is, the criterion for different conditions was 2%. Limited reaction per pass does not encumber the computation of conversions, however, which are based on the difference between fresh feed composition and reactor effluent composition. A further advantage of near-differential conversions is that temperature control is not the serious problem it might otherwise be for strongly exothermic reactions. And because of the high recycle rates, mass transfer rates are high even though the fresh feed rate is low. An additional aspect of the system is that the withdrawal product can be repeatedly

analyzed over any arbitrary length of time until steady state conditions have been reached. A final advantage of the apparatus is that rates are measured directly, eliminating the use of conversion vs. time curves to establish rates or, alternatively, eliminating the need to integrate proposed rate equations before using conversion vs. time data to evaluate them.

The reaction chosen for this study was the oxidation of ammonia with oxygen over 0.5 weight percent ruthenium supported on 1/8 inch cylindrical alumina pellets. The oxidation of ammonia was selected for the investigation because it poses experimental problems which are difficult to overcome by use of the more-conventional one-pass reactor. The reaction proceeds rapidly and is strongly exothermic, liberating 303 kcal per mole of ammonia converted to nitrogen and making it difficult both to maintain near-differential reaction conditions along the length of the catalyst bed and to operate the reactor isothermally. These are experimental problems which the stirred-flow reactor is especially well adapted to minimize. The commercial supported ruthenium catalyst was chosen for the reaction because a previous investigation using the same catalyst had shown that it induces decomposition of ammonia at temperatures as low as 340°C.[2] At these low temperatures nitrous oxide becomes a significant product of the ammonia oxidation and with the right combination of catalyst and reaction conditions might be formed in sufficiently high yields to make the reaction attractive commercially.

The reactions studied are represented in simplified fashion in Figure 1.1 and the stoichiometric equations describing the overall changes appear in Equations (1.1) and (1.2).

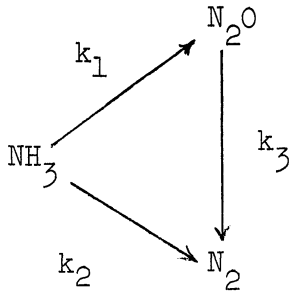

Figure 1.1. Oxidation of Ammonia to Nitrous Oxide and Nitrogen.

$$2\ NH_3 + 2\ O_2 = N_2O + 3\ H_2O \qquad (1.1)$$

$$4\ NH_3 + 3\ O_2 = 2\ N_2 + 6\ H_2O \qquad (1.2)$$

It is clear that if k_3 in Figure 1.1 is small relative to k_2, then the oxidation of ammonia with oxygen can be regarded as consisting of parallel reactions. If k_2 is small relative to k_3, on the other hand, the ammonia oxidation may be viewed as composed of consecutive reactions. Results of this work show that for the ruthenium catalyst k_3 is negligible compared to k_2 over the experimental temperature range of 246 - 345°C.

Nitrogen, nitrous oxide and water were the only reaction products found during the investigation. Partial pressures of ammonia, oxygen, nitrogen, nitrous oxide and water ranged from 1.1 to 44.1; 67.2 to 269.8; 0.1 to 13.5; 0.1 to 5.4; and 0.47 to 56.8 cm Hg, respectively. The total reaction pressure varied from 176 to 280 cm Hg (2.3 - 3.7 atmospheres). Ammonia, oxygen and water were found to influence the rates of formation of nitrogen and nitrous oxide, whereas neither nitrogen nor nitrous oxide affected the rates of reaction. Both rates were inhibited to the same

degree by increasing the water partial pressure, whereas both rates were promoted to the same extent by increasing the partial pressure of oxygen. Increasing the ammonia pressure favored the relative rate of formation of nitrous oxide. Nitrous oxide formation was more favorable at high temperatures than at low temperatures. The maximum nitrous oxide yield realized in the work was about 45%.

The experimentally measured pressure dependencies were used to develop rate equations for the oxidation of ammonia to nitrous oxide and nitrogen and to calculate the constants appearing in these equations. Temperature dependence of the constants was in turn used to evaluate apparent activation energies, heats of adsorption and entropies of adsorption. The heats of adsorption and entropies of adsorption were compared with theoretically-predicted values, giving some indication of the nature of the adsorbed species. The observed reaction rates were compared with those predicted by use of absolute rate theory and order-of-magnitude agreement resulted. Finally, a reaction mechanism consistent with the experimental observations was developed.

II SURVEY OF THE LITERATURE

This chapter first makes limited reference to the various major types of laboratory-scale reactors which have been applied to the study of gas-solid reaction systems. Then a review of previous work carried out on the ammonia oxidation reaction is presented, together with a summary of the major points of interest. Finally the use of ruthenium as a catalyst is summarized.

A. Laboratory-Scale Reactors for Gas-Solid Systems

1. Recirculation Reactors

The distinguishing characteristic of recirculation reactors is that some or all of the reactor effluent is recycled to the reactor section. When all of the effluent is recirculated, the degree of conversion is time dependent, meaning that a single run may be continued until very high conversions are attained. A series of measurements can usually be made before equilibrium is reached. If only a portion of the effluent is recirculated, the remainder is continuously withdrawn and fresh feed is added to the recycling portion to maintain the mass balance. In this case, a steady state is eventually reached so that the degree of conversion is independent of time. The fresh feed and effluent withdrawal rates can then be altered to obtain various degrees of conversion.

Butt[17] used a batch-type recirculation reactor to study the dehydration of ethanol and diethyl ether over alumina. He varied the pressure from several hundred mm Hg to atmospheric, used molten salt to maintain reaction temperatures near 300°C and recirculated the reactants at

thirty liters per minute. Gas chromatography was used for rapid sample analysis. Butt concluded that the rate of reaction was controlled by surface steps. Wicke and Hedden[57] used a closed recirculation system in the study of the Boudouard reaction ($CO_2 + C = 2\ CO$) and the oxidation of carbon to carbon dioxide. The extent of the Boudouard reaction was followed by recording the pressure increase in the system. In order to follow the second reaction, product carbon dioxide was frozen out of the recycle stream and the resulting pressure decrease was proportional to the rate of carbon oxidation.

Perkins[41] used an open recirculation system to study the propylene hydrogenation reaction over nickel-kieselguhr pellets. By keeping the fresh feed rate small relative to the recycle rate, he was able to obtain near-differential conditions with consequent fine temperature control. The recirculation pump was a self-constructed four-cylinder diaphragm type with a capacity from twenty eight to eighty four liters per minute. At the high recirculation rates used, mass transfer to the catalyst surface was shown not to be rate-controlling.

2. Mechanically Stirred Reactor with Powdered Catalyst

Trotter[52] used a thoroughly stirred, mechanically fluidized catalyst to study the kinetics of a solid-catalyzed, vapor phase reaction. His catalyst was held against a revolving porous cylindrical wall by centrifugal force. Rotating on the axis of the cylinder was an agitator fitted with wire tips extending into the catalyst bed. The purpose of this arrangement was to minimize thermal and concentration gradients in the catalyst bed. Reactants flowed inward radially through the porous cylinder wall and were removed along the axis of rotation.

3. Pulse Reactor

Kokes, Tobin and Emmett[28] suggested a micro-catalytic-chromatographic technique making use of a reactor unit attached to the top of a chromatographic column. They injected small amounts of various hydrocarbons into a hydrogen carrier gas, passed the mixture over the catalyst and thence directly into the chromatographic column for analysis. Limited data is presented in the source cited to demonstrate the potential of this pulse-reactor approach for exploratory catalytic work and for mechanism studies. The pulse-reactor approach was later applied by Giordano, Cavaterra and Zema[20] to study the oxidation of ammonia over a series of eighteen oxide catalysts. These workers determined the temperatures corresponding to 1% and 5% conversion of the pulse feed over each of the catalysts tested. They also determined the temperature at which maximum nitrous oxide yield was reached for each catalyst.

4. Coated-Wall Reactors

Smith[49] used a coated-wall reactor to determine the recombination coefficients of atoms as a function of temperature. Atoms formed by low-pressure discharge diffused through a sidearm coated with the catalytic material of interest toward a probe coated with a highly catalytic material. The temperature rise of the probe was then a measure of the extent to which atoms traversed the coated tube without recombining. Baron, Manning and Johnstone[8] used a tubular reactor coated with V_2O_5 to study the oxidation of SO_2, citing as the advantages a simple flow pattern, accurate control of catalyst temperature and catalyst surface concentration and equal accessibility of reactants to all parts of the catalyst surface.

5. Single Pass Reactors

Wynkoop[59] used a single pass reactor to study the hydrogenation of ethylene over a copper-magnesia catalyst, working with integrated rate equations but limiting conversions to about 1% and thereby approaching differential conditions. Hulburt and Srini Vasan[24] also used a one pass reactor to study the water-gas shift reaction. They worked with changes of conversion from 20% to 30% but were able to approximate differential conditions by adding product species to the feed stream. Schwab and Theophlides[46] studied the decomposition of methanol, ethanol, propanol, pentanol and other hydrocarbons under differential reaction conditions. The reactions studied involved a liquid reactant and at least one gaseous product. Reactant was then fed to the catalyst at a rate greater than 100 times the reaction rate, hence holding the reactant concentration within 1% of its input value. The reaction rate was determined by measuring the flow rate of gaseous product. Weisz and Prater[58] modified the above scheme to study the cracking of cumene to propylene and benzene over a silica-alumina catalyst, working at a conversion level less than 1% so that product adsorption competition and reverse reaction could be neglected.

B. Previous Studies of the Heterogeneous Catalytic Oxidation of Ammonia

Although the oxidation of ammonia to nitric oxide over platinum was observed by Kuhlmann[33] as early as 1839, it was not until the period 1910-1913 that Ostwald first became aware of the reaction's potential industrial significance. Until the early 1920's, research conducted on the system involved no systematic variation of temperature, feed composition and flow rate; rather, the best temperature for optimum nitric

oxide yield was randomly sought. Furthermore, the results were often contradictory and were masked by gas phase reactions believed to be occurring downstream of the catalyst bed. Andrussow,[3] working in Bodenstein's laboratory, remedied this situation by conducting experimental studies over platinum covering a temperature range from 160 - 950°C, varying flow rates by a factor of 100 and using cylinders of pre-mixed feed to insure reliable feed compositions. In attempts to establish the intermediate reaction products, Andrussow failed to find either hydrazine (N_2H_4) or hydroxylamine (NH_2OH) and therefore proposed that nitroxyl (HNO) was the primary reaction product. In further work, Andrussow[4] extended the range of experimental conditions and interpreted the results as favoring his nitroxyl hypothesis. Bodenstein[13] also analyzed Andrussow's results and proposed a reaction mechanism based on nitroxyl as the primary reaction product. Raschig,[44] however, claimed that nitroxyl, if formed, would dimerize to yield nitrous oxide; this constituted an argument against the nitroxyl theory since no nitrous oxide had at that time been identified in the reaction products. Furthermore, Raschig had found trace amounts of hydrazine while freely burning ammonia in an atmosphere of oxygen and therefore suggested that imide (NH) was the first product of reaction. Reaction of the imide with ammonia was postulated as the source of the hydrazine.

Thence followed debate concerning the merits of the two proposed mechanisms.[5,44] Some weight was lent the nitroxyl theory when von Nagel[54] oxidized ammonia over MnO_2 and found yields of up to 70% N_2O at about 300°C. Further progress was made when Bodenstein[13] and Bodenstein and

Buttner[14] studied the reaction over platinum under pressures as low as 0.01 mm Hg, using a liquid air trap to condense intermediates before they suffered significant gas-phase collisions. Condensate was found to contain hydroxylamine, which now became regarded as the primary reaction product. The experimenters last cited observed that stoichiometric excesses of oxygen and ammonia favored formation of nitric oxide and nitrogen, respectively, further supporting the hydroxylamine mechanism.

Krauss,[29] working with Bodenstein's low-pressure equipment and modifying it for analysis of non-condensed products, verified and extended Bodenstein's [15] data over a platinum catalyst, finding both nitrous acid and hydroxylamine in the reaction condensate. Krauss and Schuleit[30] later conducted further low-pressure studies on platinum and platinum alloyed with small amounts of ruthenium and rhodium, measuring the variation in yield of nitrous acid and hydroxylamine as a function of the catalyst. Krauss and Neuhaus,[31] noting von Nagel's[55] success in obtaining nitrous oxide when oxidizing ammonia over an oxide catalyst, studied the reaction over oxides of Mn, Ba, Fe and Ni and found large yields of nitrous oxide. They concluded that the relative amount of nitrous oxide formation is a function of the extent to which loosely-bound dissociated oxygen is present on the catalyst surface; they also used the mechanism developed for the reaction on platinum to explain the evidence gathered with oxide catalysts. Using a titration technique to measure the oxygen in stoichiometric excess on the several metallic oxides, they showed experimentally that the nitrous oxide yield is linearly dependent on the amount of this excess oxygen. Consistent with this observation, they also noted that as oxygen in the feed increased, higher nitrous oxide yields resulted.

In 1950 Krauss[32] advanced the opinion that the first step in the oxidation reaction is a collision of gaseous ammonia with adsorbed atomic oxygen to form hydroxylamine. Andrussow,[6] however, carried out experiments demonstrating that mass transfer to the catalyst surface must be taken into account and concluded that molecular oxygen is the main oxygen source for the reaction. Meantime Zawadzki[60] in 1950 reviewed the experimental evidence and came out in support of Raschig's imide theory. Hence considerable debate still exists concerning the mechanism of ammonia oxidation.

The major points of interest concerning the ammonia oxidation will now be summarized:

1. The leading theory attempting to explain the mechanism of ammonia oxidation is Bodenstein's hydroxylamine mechanism, which is a modification of the original Andrussow-Bodenstein nitroxyl mechanism. The reactions involved are:

$$NH_3 + O = NH_2OH \qquad (2.1)$$

$$NH_2OH + O = NHO + H_2O \qquad (2.2)$$

$$2HNO = N_2O + H_2O \qquad (2.3)$$

$$NH_2OH + O_2 = HNO_2 + H_2O \qquad (2.4)$$

$$HNO_2 + NH_3 = N_2 + 2\ H_2O \qquad (2.5)$$

$$NH_2OH + HNO = N_2 + 2\ H_2O \qquad (2.6)$$

$$NH_2OH + NH_3 = N_2 + H_2O + 2\ H_2 \qquad (2.7)$$

$$2\ HNO_2 = NO + NO_2 + H_2O \qquad (2.8)$$

$$2\ NO_2 = 2\ NO + O_2 \qquad (2.9)$$

The hydroxylamine theory is in agreement with experimental observations in these respects:

a. Hydroxylamine has been found experimentally to be an intermediate product of ammonia oxidation. This is presumeably not formed by the reaction NH + H_2O = NH_2OH because excess water has no effect on yields. Furthermore, essentially no hydrazine, which would be expected to be formed by the reaction NH + NH_3 = N_2H_4 if imide were present, was found in the low-pressure oxidation studies.

b. Equations (2.5) and (2.7) can account for the experimental observation that excess ammonia in the feed favors nitrogen formation.

c. Equations (2.4), (2.8) and (2.9) and Equations (2.2) and (2.3) can explain the experimental observation that excess oxygen in the feed favors formation of nitric oxide and nitrous oxide.

d. Equations (2.2) and (2.3) are supported by the experimentation showing that oxygen present in stoichiometric excess in metal oxides increases the nitrous oxide yield.

2. Competing with the hydroxylamine theory is the imide theory, proposed by Raschig and supported by Zawadzki:

$$NH_3 + O = NH + H_2O \qquad (2.10)$$

$$NH + O_2 = HNO_2 \qquad (2.11)$$

$$2\ HNO_2 = NO + NO_2 + H_2O \qquad (2.12)$$

$$2\ NO_2 = 2\ NO + O_2 \qquad (2.13)$$

$$NH + NH_3 = N_2H_4 \qquad (2.14)$$

$$N_2H_4 + O_2 = N_2 + 2\ H_2O \qquad (2.15)$$

$$NH + O = NHO \qquad (2.16)$$

$$2\ NHO = N_2O + H_2O \qquad (2.17)$$

The experimental observations which have been used to support this theory are:

a. Small amounts of hydrazine have been detected in the products of free combustion of ammonia in air. This hydrazine is believed to be formed by reactions (2.10) and (2.14).

b. The high efficiency of the ammonia oxidation reaction suggests that the primary step must be exothermic. The primary step in the imide scheme, as shown in Equation (2.10), will be exothermic if the imide radical is chemisorbed with an energy of about 8 kcal per mole or more.

c. Equations (2.10), (2.11), (2.12) and (2.13) account for the experimental observation that excess oxygen favors nitric oxide formation.

d. Equation (2.14) explains the experimentation which shows that excess ammonia favors nitrogen production.

3. Either of the above schemes, or various combinations of the steps listed in (2.1) through (2.17), can satisfactorily explain the reaction products observed under the various reaction conditions. No critical test has been devised to facilitate the setting down of an unequivocal reaction mechanism.

4. In the temperature range below 500°C, where significant amounts of nitrous oxide are formed over various oxide catalysts, an increasing proportion of oxygen in the feed favors the nitrous oxide yield.

5. Experimental investigation of the ammonia oxidation reaction must be designed to make careful distinction between heterogeneous, homogeneous and decomposition reactions.

6. Excluding the research reported in this present work, there is a lack of experimental observations reported in the literature for which:

a. The rate of mass transfer to the catalyst surface has been shown to be without influence on the reaction rates or product distribution,

b. the reaction conditions have been uniform within 2% over the whole length of the catalyst bed,

c. the exact dependence of rates of nitrogen and nitrous oxide formation on ammonia, oxygen, nitrogen and nitrous oxide partial pressures has been determined, and

d. the catalyst temperature has been closely controlled despite the strongly exothermic reaction.

C. Ruthenium as a Catalyst

In a recent dissertation on the chemisorption of oxygen on ruthenium dioxide, Sommerfeld[50] has surveyed the use of ruthenium as a catalyst. His survey will be drawn upon here.

Ruthenium metal has found frequent application as a hydrogenation catalyst. Parravano[1] studied the vapor phase hydrogenation of benzene over ruthenium, and Balandin and co-workers[7] have investigated liquid-phase hydrogenation of cellulose, starch and wood products using ruthenium as catalyst. Bond[11] studied acetylene and diolefin hydrogenation with a ruthenium catalyst. Rylander hydrogenated olefins[10] and ketones[16] in the presence of ruthenium. Parravano[37] has also investigated the dehydrogenation of saturated alcohols over a ruthenium catalyst.

Use of ruthenium in the Fischer-Tropsch synthesis dates back to the 1920's.[19] Ruthenium-catalyzed synthesis of lighter hydrocarbons,[25] alcohols[22] and motor fuels[27] has been studied in this country. Guyer and co-workers[23] have done recent work along this line in Switzerland.

In addition to hydrogenation reactions, ruthenium has also been used for other reactions. The aqueous decomposition of formaldehyde[35] and pyruvic acid,[36] the water gas reaction,[39] and the addition of silane compounds to unsaturated organic compounds[42] have all been studied over ruthenium. Ammonia decomposition over ruthenium has been the subject of experimentation.[2] Parravano[38] has considered the role of selective adsorption of CO by ruthenium in the polymerization of methyl methacrylate.

Finally, it should be mentioned that Rea and Bebbington[45] have published an extensive bibliography on the use of ruthenium in catalytic studies. This bibliography should be consulted for a more extensive review of the subject.

III EXPERIMENTAL EQUIPMENT

A. Description of Flow Sequence

The experimental scheme consisted of maintaining a stream of recycling reactants while continuously withdrawing a product stream from the recycle and adding fresh feed makeup. The path of flow was consequently from feed cylinders through metering devices to the recycle loop, and then from the recycle loop through a flow controller to analysis.

As depicted in Figure 3.1, provision was made for metering as many as four separate feed streams into the recycle loop, although in practice no more than two feeds were in use at one time. Downstream of the flow meter bank, the feed components entered a common line leading to the recycle loop. Once inside the loop, thorough mixing of the fresh feed and recycling effluent took place under the loop conditions of turbulent flow.

Immediately downstream of the feed entry point, the gases entered a pre-heater coil submerged with the reactor in a well-stirred molten salt bath. After coming up to the salt temperature in the coil, the gases flowed into the reactor sequence, through the catalyst bed and finally on out of the molten salt bath. From this point the bulk of the reactants then passed through a surge tank to the recycle pump, where their pressure level was raised before they retraced their path in the recycle loop. The small portion of the reactor effluent not recycled was automatically withdrawn through a back pressure regulator and was then sent to a gas bubbler where a dilute sulfuric acid solution was used to absorb unreacted ammonia

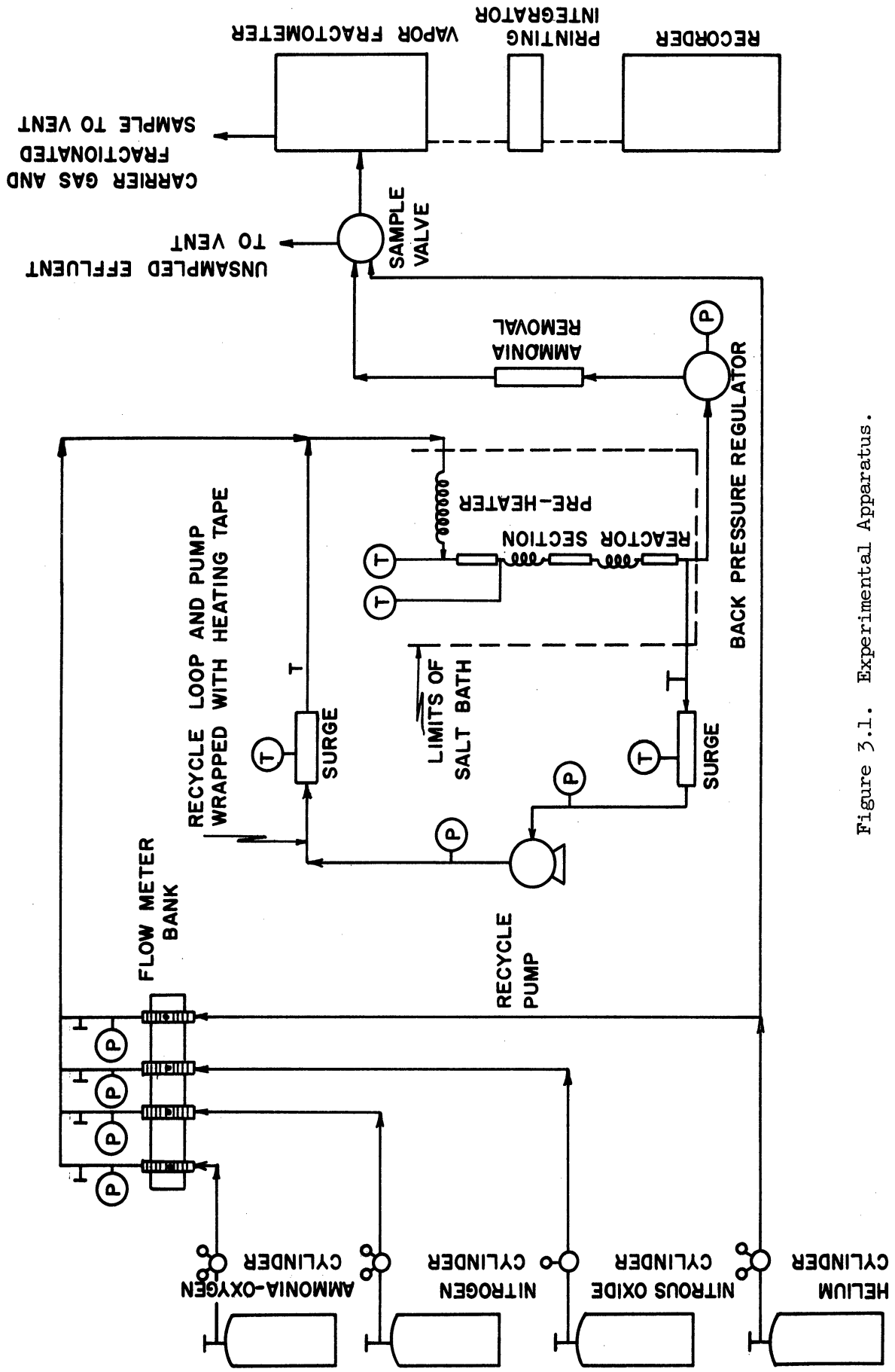

Figure 3.1. Experimental Apparatus.

and product water. The remaining gas, consisting of oxygen, nitrogen and nitrous oxide, was then sampled and analyzed quantitatively by means of gas chromatography.

B. Flow Meter Bank

Flow was metered through Matheson Universal Flowmeters, using either a sapphire or a stainless steel float. It was found that use of these floats permitted a range of flow rates satisfactory for the experimentation. Flow rates were controlled by needle valves positioned downstream of the flow meters. Gases were metered through the flow tubes at 386 cm Hg as indicated by a pressure gage placed between each tube and its flow control valve. The 386 cm Hg pressure level was chosen because it stabilized the float position, which at lower feed pressures tended to be sensitive to recycle loop pressure fluctuations. The high feed pressure also made it possible to neglect ambient pressure variations.

C. Molten Salt Bath

Stainless steel was used in construction of the molten salt bath to avoid potential corrosion problems. It was insulated with pipe insulation of the appropriate inside diameter. A heat treating salt was chosen as the bath material. It melted at 285°F and could be used at temperatures up to 1000°F. The molten salt had a low viscosity which facilitated stirring.

Two immersion heaters were used to hold the salt in a liquid state during the experimental work. One of these heaters was left on continuously; the other was used on an "on-off" basis in conjunction with a

mercury temperature sensing element and a mercury relay. Bath temperature was controlled within $\pm$ 0.1°C and did not vary from point to point within the bath.

D. Reactor

The reactor sequence used for the bulk of the experimental work consisted of three 3 inch lengths of stainless steel tubing, 3/8 inch O.D. X 0.210 inch I.D. These lengths of tubing were connected in series by two loops of 1/4 inch O.D. stainless steel tubing. The purpose of the 1/4 inch loops was to provide heat transfer area for removal of the heat released by the highly exothermic reaction.

One length of reactor is pictured in Figure 3.2. Each length was fitted at the bottom with a perforated stainless steel disc which served to support the catalyst pellets. Each disc rested on a shoulder resulting from counterboring the tubing.

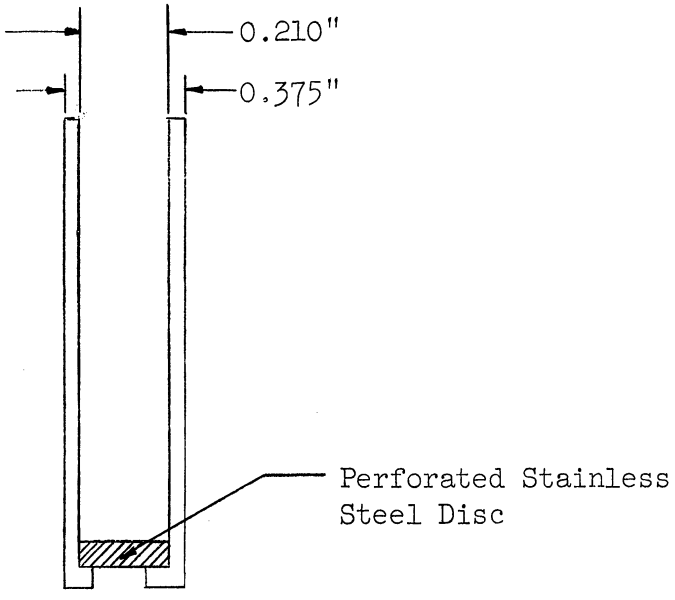

Figure 3.2. Reactor Section.

Swagelok stainless steel tube fittings were used to integrate each reactor length into the reactor sequence and recycle loop. The Swagelok fittings provided a simple and convenient means of disassembling and reassembling the tubing. Despite the many times the seals were made and broken, no leakage resulted. The Swagelok fitting used at the beginning of the reactor sequence is illustrated in Figure 3.3. Figure 3.3 demonstrates how the feed stream and thermocouple probe were introduced

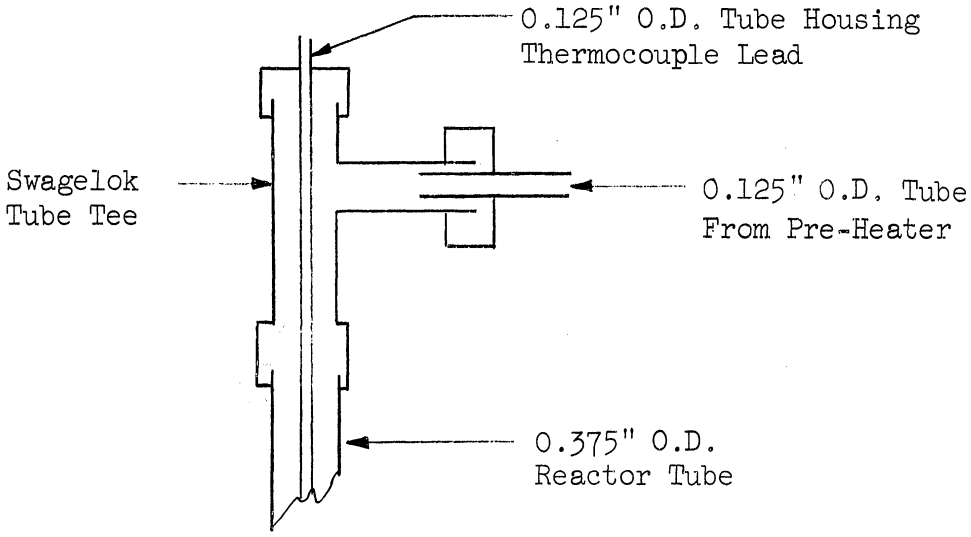

Figure 3.3. Integration of Reactor Into Recycle Loop.

to the reactor sequence via one fitting. Using a similar fitting at the bottom of the first reactor tube, it was also possible to conveniently provide a thermocouple to measure the exit gas temperature. Pellet distribution in the three reactor lengths was 17-17-16, except when only 10 pellets were used. Hence, with the partial pressures nearly constant, temperature rise of the gas stream in each length was the same. This was established experimentally. Thenceforward the temperature rise in the first section was taken as the maximum temperature rise suffered by the reactant stream.

A second reactor of smaller diameter was used to check the effect of mass transfer on the rate of reaction. Transfer of the catalyst charge from the 3/8 inch O.D. reactor to a reactor of smaller diameter was found to be the most convenient way to change the mass transfer coefficient without changing the recycle rate. Since the recycling gases removed about 90% of the heat of reaction from the catalyst sections, changing the recycle rate at a fixed feed rate might have resulted in a reaction temperature variation sufficient to mask mass transfer effects if such were present. The smaller reactor was identical to the 3/8 inch O.D. reactor sections except that it was 1/4 inch O.D. X 0.156 inch I. D. Only one small reactor section was used since mass transfer was checked using a catalyst charge of 10 pellets. Appropriate Swagelock fittings were also used to integrate the 1/4 inch O.D. reactor into the recycle loop.

E. Back Pressure Regulator

A back pressure regulator was used to withdraw reactor effluent from the recycle loop at such a rate that the pressure in the reactor remained constant. The regulator was designed to operate at pressures from 130 to 2000 cm Hg. Pressure in the isolated upper dome of the regulator was set using compressed nitrogen. Whenever pressure acting against the teflon dome diaphragm exceeded set pressure, the diaphragm would rise slightly, permitting gas to escape until pressure on the diaphragm had been reduced to set pressure. In practice, since feed was being continuously introduced to the recycle loop, the regulator diaphragm was always in a raised position. Testing showed that the regulator was able to

handle the maximum discharge rate encountered, about 900 standard cm^3 min^{-1}, at back pressures which were but insignificantly higher than set pressure.

The minimum total reaction pressure was limited to 176 cm Hg by the back pressure regulator. For the evaluation of experimental measurements, the reaction pressure was taken equal to the set pressure. Pressure drop across the reactor sequence did not exceed 1.7% of the total pressure. The loss in pressure from the reactor outlet to the back pressure regulator was negligible.

F. Recycle Pump

The equipment most fundamental to the operation of a recycle differential reactor is the recycle pump. The recycle pump had to satisfy these conditions for the investigation of the ammonia oxidation reaction:

1. The pumping rate had to be sufficiently high to eliminate the possibility that mass transfer might control the rate of reaction.

2. The recycling gases had to move through the pump without becoming contaminated.

3. The pump had to be leakproof.

4. In event of pump failure, no explosion hazards could be tolerated. This requirement was complicated by the presence of oxygen at partial pressures up to 258 cm Hg in the recycling stream.

5. The pumping head would have to be held at a temperature of 125°C to insure that no condensation of product water would take place in the pumping mechanism.

6. The pumping head would have to withstand the corrosive action of the wet ammonia recycle stream.

7. High levels of pressure operation and large pressure heads across the pump should be feasible to permit flexibility of operation.

These conditions were satisfied by obtaining a custom-made diaphragm compressor from the Lapp Insulator Company. Some of the characteristics of the compressor were:

1. Pumped gases contacted nothing but stainless steel while passing through the pump.

2. Pressures up to 3000 cm Hg could be exerted on the flexible stainless steel diaphragm at up to 360 strokes per minute. Operating pressures of about 40 atmospheres could therefore be reached if desired. Pressure heads of several hundred cm Hg across the pump were also possible.

3. A "double diaphragm" arrangement was used to transmit hydraulic pressure from a reciprocating piston to the flexing diaphragm. This made it possible to use an oxidation resistant silicone oil to actuate movement of the pumping diaphragm, reducing the explosion hazard in event of diaphragm rupture.

The compressor was therefore well suited to satisfy the recycle pump requirements.

G. Surge Cylinders

At the maximum pumping rate of 360 strokes per minute, severe pressure fluctuations in the 100 cc recycle loop were encountered. These

pressure fluctuations resulted in surging of the reactant stream through the catalyst bed and made it difficult to meter the feed stream into the recycle loop at a constant rate. Two 500 cm^3 pressure cylinders were therefore added to the recycle loop to act as surge tanks for the recycle pump. These surge tanks were used in combination with valves as shown in Figure 3.1. By maintaining a 15 cm Hg pressure differential between each surge cylinder and the reactor side of the recycle loop, pressure variations in the reactor and at the point of fresh feed entry to the loop were eliminated.

During the runs in which product water was removed from the recycling reactant gases, the surge cylinders were also used to hold the alumina pellets which acted as the water absorbent.

H. Sample Valve

After water and unreacted ammonia had been removed from the product stream, it was sent through a sample valve and a sample coil, and was then vented. Meanwhile a stream of helium, acting as the carrier gas, was also passing through a separate leg in the sample valve on its way to the separating columns in the vapor fractometer. When the sample valve was turned on the sample coil was taken out of series with the product stream and was simultaneously put into series with the helium carrier gas. Using this scheme it was possible to flush reproducible sample volumes into the fractometer separating column with no danger of contaminating the sample with air.

I. Vapor Fractometer

A Perkin-Elmer gas chromatography unit, utilizing a thermal conductivity cell as the sensing element, was used for the separation and analysis of the oxygen, nitrogen and nitrous oxide portions of the reactor effluent. Theoretically it is possible to separate and analyze these three gases in a single operation using one separation material. In practice, no single column packing could be found which gave a clean and yet rapid separation of the oxygen, nitrogen and nitrous oxide. A five Angstrom molecular sieve column could be used at room temperatures to bring about a satisfactory separation of oxygen and nitrogen, but at this low temperature nitrous oxide was retained indefinitely in the column. At the high temperature of 190°C the nitrous oxide remained in the column less than one minute but no separation of oxygen and nitrogen was possible. The decision was made to use two molecular sieves in series, one housed inside the fractometer at 190°C and the other positioned outside the fractometer at ambient temperature. A special valve was so arranged that the external column could be eliminated from the path of flow at will. One complete analysis required that two effluent samples be used. One sample was flushed into the external column to effect the separation of oxygen and nitrogen. The separated oxygen and nitrogen then moved through the internal column to the thermal conductivity cell, where their relative amounts were sensed. Next, the external column was switched out of the path of flow and a second sample was flushed directly into the internal column. This time the relative amounts of nitrous oxide and the unfractionated oxygen-nitrogen portion of the effluent were determined. From these two analyses, then, and

stoichiometric considerations, the composition of the reactor effluent could be calculated.

The two-sample approach described above assumes that the composition of both samples is the same. This assumption will be valid when the reaction system reaches steady state operation. The approach to steady state can, in fact, be measured by successive effluent analyses. Upon reaching steady state, repeated product analyses will give identical results. Such reproducible analyses were obtained with this system because feed rate, feed composition and reaction temperature were closely controlled and non-contaminated effluent samples of reproducible volume were analyzed.

J. Printing Integrator and Recorder

A recorder connected with the gas chromatography unit recorded the curves resulting from effluent analyses. A printing integrator was used for the computation of areas under the various curves. These areas were in turn used to calculate the concentration of the reactor effluent.

K. The Catalyst

The catalyst selected for this work is available commercially from Engelhard Industries, Inc. It consisted of 0.5 weight percent ruthenium supported on 1/8 inch gamma alumina pellets. Physical properties of the catalyst appear in Table III-1.

TABLE III-1

Physical Properties of Catalyst

Diameter, inches	1/8 Nominal
Length, inches	1/8 Nominal
Bulk Density, lbs./cu.ft	58
Particle Density, lbs./cu.ft	104
True Density, lbs./cu.ft	212
Internal Void Fraction	0.56
External Void Fraction	0.54

IV EXPERIMENTAL TECHNIQUES

A. Feed Composition

Most of the experimental work was conducted using a feed stream consisting of oxygen and ammonia. If these two components had been metered separately into the recycle loop, separate meter calibrations would have been required and uncertainties in metering rates would have been compounded in computation of feed composition. These considerations led to use of cylinders of pre-mixed oxygen and ammonia. Cylinders containing 5.3, 9.7 and 16.5 volume percent ammonia, the balance oxygen, were prepared. Composition of the mixtures was established by mass spectrometry and verified by a Burrell gas analysis. During the course of the experimentation, the cylinder contents were periodically analyzed by the Burrell method and it was ascertained that the compositions did not change with time.

B. Flowmeter Calibration

Rates of flow were measured with flowmeter tubes and were controlled by individual needle valves positioned downstream of each flow tube. All flows were metered at 386 cm Hg, making it possible to neglect ambient pressure variations.

The moving soap film technique was used to calibrate the flow tubes. Gas was led from the flowmeter through a water saturator into the sidearm of a calibrated burette. The gas bubbled through a soap solution in the base of the burette, forming soap films spanning the burette cross-section. The timed movement of these films was reproducible within $\pm$ 1%. Taking ambient pressure and temperature into account, the rate of flow of

the dry gas under standard conditions was easily calculated. Flow rate calibration curves for the 9.7 volume percent ammonia, balance oxygen, composition and for nitrogen, nitrous oxide and helium are presented in Figures A.1 and A.2 in Appendix A.

Float positions in the flow tubes were reproducible within ± 2%. This figure has not been corrected for the ± 1% error in timing the rate of soap film movement. Flow rates were therefore known within an error range of ± 2%. The feed composition was known within a range of ± 0.5% whenever only the premixed ammonia-oxygen was used as feed.

When the ammonia-oxygen mixtures were used for calibration of flow tubes, the ammonia portion of the mixture was absorbed in sulfuric acid downstream of the calibration burette and only the flow rate of the remaining water-saturated oxygen was measured by the soap film technique. Measured flow rates were then corrected for the known ammonia content. The solubility of ammonia in the soap solution made this approach necessary.

C. Pump Calibration

At each of the three reaction pressures, 176, 216 and 280 cm Hg, the pump capacity was measured with the pump feed surge cylinder set 15 cm Hg below reaction pressure and the pump discharge surge cylinder maintained 15 cm Hg above reaction pressure. Dry nitrogen was used to supply gas to the pump feed cylinder. Nitrogen leaving the cylinder was then saturated with water and sent through a wet test meter. Dry pumping rates corrected to standard conditions were 50, 57 and 67 liters per minute for the reaction pressures 176, 216 and 280 cm Hg, respectively.

D. Vapor Fractometer Calibration

Two cylinders of pre-mixed oxygen, nitrogen and nitrous oxide were prepared for calibration of the vapor fractometer. Analysis by mass spectrometry of the contents of the two cylinders showed them to contain 3.22 volume percent nitrogen and 3.28 volume percent nitrous oxide, balance oxygen; and 6.69 volume percent nitrogen and 6.76 volume percent nitrous oxide, balance oxygen, respectively. These two compositions covered the composition range of interest in the planned experimental work. Availability of the mixtures made it possible to easily check the vapor fractometer calibration periodically during the course of the experimentation. The calibration did not change with time.

Calibration was carried out by establishing a flow of calibrating gas through the sample valve previously described and flushing samples of this gas into the fractometer exactly as was done with the reactor effluent. When gas was flushed into the external column, areas under the resulting oxygen and nitrogen curves were measured and the percentage of the total area contributed by the nitrogen peak was computed. The ratio of percentage nitrogen in the calibrating mixture to percentage nitrogen curve area was 1.01 for both calibrating mixtures.

Similarly, when calibrating samples were flushed directly into the internal column, areas under the resulting nitrous oxide and oxygen-nitrogen curves were measured and the percentage of the total area contributed by the nitrous oxide curve was computed. The ratio of nitrous oxide in the calibrating mixture to percentage nitrous oxide curve area was a constant, 0.716, for both calibrating mixtures. It frequently happens

that the ratio of the volume percent of a gas component to the percentage curve area of that component is independent of the volume percent in the case of dilute mixtures. This linearity in the present work, where oxygen dilution did not exceed about 15%, eliminated the necessity of constructing calibration curves for the vapor fractometer. Area percentages were converted directly to volume percentages by multiplication. After computing the volume percentages of oxygen, nitrogen and nitrous oxide in this way, the ammonia and water content of the reactant stream was calculated from stoichiometric considerations as described in Appendix C.

The calibrating mixtures were used to verify that bubbling the reactor effluent through a dilute solution of sulfuric acid, as was practiced in effluent sampling, did not affect the nitrogen, nitrous oxide and oxygen portion of the effluent. Both calibrating mixtures were passed through the acid solution en route to the fractometer sample valve. The subsequent fractometer analysis showed that the calibrating mixture compositions were not affected by the sulfuric acid solution.

E. Catalytic Activity of Reactor System

Prior to taking experimental measurements, a run was carried out without adding catalyst to the reactor system. Reaction pressure was set at 280 cm Hg and a feed composition of 9.7 volume percent ammonia, the balance oxygen, was used. At feed rates of 200 cm^3 min^{-1} and reactor temperatures as high as 400°C, no product nitrogen or oxides of nitrogen were found in the reactor effluent after three hours of operation. It was concluded that the reactor system was catalytically inert for the oxygen-ammonia reactant stream and that no gas phase reaction between oxygen and ammonia would take place in the reactor.

F. Catalytic Activity of Alumina Carrier

Alumina pellets identical to those used as the carrier for production of the commercial 0.5 weight percent ruthenium catalyst were obtained from the catalyst supplier, Engelhard Industries, Inc. Fifty of these blank pellets were put in the reactor series at 200°C, other reaction conditions being identical to those described in the previous paragraph. Reaction temperature was then slowly raised and the reactor effluent was sampled periodically to check for the presence of product nitrogen and/or nitrous oxide and other oxides of nitrogen. Up to a reaction temperature of 350°C no reaction products were found. At temperatures exceeding 350°C, nitrogen began to appear in the reactor effluent. This set the upper limit on the temperature range used in the experimental work.

Using the same 50 blank alumina pellets, reactor temperature was then lowered to 345°C, the reactor system was evacuated and the vapor fractometer calibrating mixture containing 6.69 volume percent nitrogen and 6.76 volume percent nitrous oxide, the balance oxygen, was used as feed to the system under the reaction conditions described above. The object was to determine whether decomposition of the nitrous oxide would occur either thermally or as catalyzed by the alumina carrier or the reactor system. Effluent analysis showed that no nitrous oxide decomposition occurred under these conditions. The partial pressure of nitrous oxide corresponding to this run, 18.9 cm Hg, was not exceeded in any subsequent runs.

The 50 blank alumina pellets were then replaced with 50 pellets bearing 0.5 weight percent ruthenium and the calibrating mixture described above was again used as feed to the reactor system at a feed rate of about

200 cm^3 min^{-1}. No nitrous oxide decomposition was found under these conditions. Hence decomposition of nitrous oxide adsorbed from the gas phase on the ruthenium catalyst was ruled out in mechanism considerations.

G. Experimental Procedure

A fresh catalyst charge was used for each of the six reaction temperatures at which measurements were made. The total number of pellets was weighed with an analytic balance and the pellets were placed in the reactor series. No catalyst pre-treatment was followed.

When the catalyst had been loaded, a vacuum pump was used to exhaust air from the reaction system. This procedure made the initial approach to steady state operation more rapid. After the system was evacuated, feed was introduced into the recycle loop at a rapid rate until the pressure reached the level set in the back pressure regulator. The recycle pump was then turned on and the feed flow rate was adjusted to the value desired. Fifteen or more minutes later, depending on the reaction temperature and feed rate, the system was at or near steady state conditions and effluent sampling was begun.

Reaction rates at up to eight different feed rates were measured for each feed composition, reaction temperature and pressure. The order followed was one of increasing contact time. Steady state conditions at each successive flow setting therefore corresponded to an increase in extent of reaction and product concentration. After completing a series of runs, the feed valve was closed and the recycle pump was turned off. The vacuum pump was then used to remove the reactant gas from the reactor system. Then another series of runs using a different feed composition was started.

H. Reaction Products

The overall reactions which can take place in the ammonia oxidation are:

$$4\ NH_3 + 3\ O_2 = 2\ N_2 + 6\ H_2O \qquad (4.1)$$

$$2\ NH_3 + 2\ O_2 = N_2O + 3\ H_2O \qquad (4.2)$$

$$4\ NH_3 + 5\ O_2 = 4\ NO + 6\ H_2O \qquad (4.3)$$

In the commercial process, at temperatures of about 850°C, nitric oxide is formed in yields of 95% and higher. In general, as temperature is lowered the nitric oxide yield falls off and increasing quantities of nitrous oxide and nitrogen are found in the reaction products. At temperatures below about 500°C, nitrogen and/or nitrous oxide become significant and nitric oxide yield drops to low values and may even vanish.

Reaction products in the present system were investigated on a preliminary basis by using the reactor in one-pass operation. Recycling of reactor effluent was eliminated to reduce the possibility that nitric oxide, if formed, would react in the gas phase with unreacted ammonia and would therefore not be detected in the reactor effluent. Test runs used both 5.3 volume percent ammonia and 16.5 volume percent ammonia, the balance oxygen, as feed streams and involved feed rates from 50 to 1000 cm^3 min^{-1}. The catalyst bed contained 50 pellets for this test. No reddish-brown nitrogen dioxide was detected visually in the effluent until a reaction temperature of 380°C was reached. Reactor effluent was analyzed quantitatively

during the testing by flushing effluent samples into the internal column of the vapor fractometer to check for the presence of recorder peaks not attributable to nitrous oxide or oxygen-nitrogen. Only nitrous oxide and oxygen-nitrogen peaks were found at temperatures below 370°C. Even at 380°C and with the recorder operating at maximum sensitivity, only a slight tendency toward peak formation was observed when the faintly reddish-brown effluent was sampled. The retention time corresponding to the slight upward movement of the recorder pen was identical to the retention time observed when a sample of pure nitrogen dioxide was sent through the vapor fractometer.

I. Range of Variables

A temperature range from 246 - 345°C was used in this work. The upper temperature limit was fixed by the alumina carrier, which was no longer catalytically inert at temperatures above 350°C. The lower temperature was selected to provide one set of reaction rate measurements under conditions of no nitrous oxide formation.

As indicated earlier, pre-mixed feed streams having the compositions 5.3, 9.7 and 16.5 volume percent ammonia, the balance oxygen, were used for the experimentation. These mixtures allowed for variation of ammonia partial pressures over a fortyfold range under reaction conditions. A large excess of oxygen was insured under all circumstances.

Total reaction pressure varied from 176 to 280 cm Hg. The lower value was set high enough to avoid chatter in the back pressure regulator. The upper value was set low enough to permit smooth flow of fresh feed into the recycle loop. Gases were fed through the flow tubes at a constant

pressure of 386 cm Hg. Even at this pressure, one tube shattered in the preliminary work, resulting in the decision not to use the tubes at higher pressures.

In one series of runs an inert gas, helium, was added to the feed. This technique was used to lower the partial pressure of oxygen, extending the range over which this variable was studied. The presence of helium in the reactor effluent made a special vapor fractometer calibration necessary. This technique was consequently used on a limited basis.

Fresh feed rates from 205 to 925 standard cm^3 min^{-1} were used in the experimentation. Contact times were varied over a twentyfold range by using either ten or fifty pellet charges in various combinations with these fresh feed rates.

J. Stability of Catalyst

Tests were conducted to determine whether the catalytic effect of the ruthenium would be independent of time under invariant reaction conditions. Two separate catalyst loadings of 50 pellets each were tested for a period of about 24 hours per loading. The first charge was tested at 246°C, using the 9.7 volume percent ammonia, balance oxygen, feed composition. Twenty four measurements were recorded for this run. The rate of nitrogen formation, as shown in Figure 5.15, was essentially constant for the duration of the test period. The average rate of nitrogen formation was 1.88 ± 0.047 cm^3 per minute per gram of catalyst. This represents an average deviation of $\pm$ 2.5%. The maximum deviation was 9%.

The second catalyst sample was used for 24 hours at a reaction temperature of 322°C. The feed contained 16.5 volume percent ammonia, the balance oxygen. Whereas at 246°C only nitrogen and water appeared as reaction products, nitrous oxide was also formed at 322.2°C. Hence it was possible to check not only the constancy of the total reaction rate but also the consistency of the product distribution. A total of 10 measurements was recorded. The average rate of nitrogen formation, in $cm^3\ min^{-1}\ gm^{-1}$, was 11.1 $\pm$ 0.2, or 11.1 $\pm$ 1.8%; average rate of nitrous oxide formation, in the same units, was 5.7 $\pm$ 0.17, 5.7 $\pm$ 3%. The maximum nitrogen and nitrous oxide deviations were 3.6 and 5.3%, respectively. Figure 5.16 exhibits the measurements taken at 322.2°C.

K. Check on Differential Conditions

If the differential bed reactor were operating under conditions approaching differential character, then reactor effluent sampled at points upstream or downstream of the reactor would have practically the same composition. In fact, gases flowing into the reactor sequence were identical to those leaving the reactor, except that they had been diluted by the addition of fresh feed. Since gas was recycling at about 50 liters per minute and fresh feed entered the loop at a maximum of 925 $cm^3\ min^{-1}$, the maximum dilution suffered by the recycle stream was on the order of 2%.

It was decided to sample the recycle stream between the feed point and the reactor, and downstream of the reactor, to verify the above considerations experimentally. This check on the differential conditions was combined with the testing of catalyst stability already discussed. Hence, of the 34 measurements represented in Figures 5.15 and 5.16, 12

points correspond to upstream recycle sampling and the remaining 24 represent sampling downstream of the reactor section. The location of the sampling point is indicated by legend in the figures mentioned. It is seen that recycle composition is independent of location of the sampling point.

L. Data Reproducibility

It has now been established that catalytic activity is independent of time and that the reactor system operates on a differential basis. These factors must yet be considered:

1. Can data once taken be reproduced after a given catalyst sample has been used under different reaction conditions?
2. Will arbitrarily selected samples of the supported ruthenium catalyst produce the same reaction rates and the same product distribution?

The first of these considerations was checked experimentally at 322.2°C. Catalyst which had been used to take data at a reaction pressure of 216 cm Hg and a feed composition of 9.7 volume percent ammonia, balance oxygen, was removed from the reactor and exposed to the atmosphere for one hour at room temperature. Then the charge was replaced in the reactor and the 9.7 volume percent ammonia, balance oxygen, feed stream was passed over it at room temperature for 70 minutes. Finally the reactor section was resubmerged in the molten salt and runs corresponding to measurements R37-2 and R37-3 (Table B-1, Appendix B) were repeated. Results, indicated in Table IV-1, were consistent.

TABLE IV-1

REPRODUCIBILITY OF MEASUREMENTS WITH USED CATALYST

Measurement	Rate*Recorded With Fresh Catalyst		Rate*Recorded with Same Catalyst After Extended Use		Percent Deviation	
	N_2	N_2O	N_2	N_2O	N_2	N_2O
R37-2	13.5	6.56	14.0	6.45	+3.7	-1.7
R37-3	9.9	4.69	10.1	4.82	+2.0	+2.8

*Rates are in cm^3 min^{-1} gm^{-1}.

Whether different catalyst samples would yield the same reaction rates and product distribution was checked at 322°C for measurements R38-2 and R38-3. Table IV-2 displays the results. Measured rates for the second catalyst sample were somewhat lower than for the first sample but the deviation is not excessive.

TABLE IV-2

REPRODUCIBILITY OF MEASUREMENTS WITH TWO CATALYST CHARGES

Measurement	Rate*Recorded With First Catalyst Charge		Rate*Recorded With Second Catalyst Charge		Percent Deviation	
	N_2	N_2O	N_2	N_2O	N_2	N_2O
R38-2	10.2	3.97	9.42	3.71	-5.9	-6.5
R38-3	7.05	2.68	6.84	2.55	-3.0	-4.8

*Rates are in cm^3 min^{-1} gm^{-1}.

M. Reversibility of Water Adsorption

It has been noted that measurements were made in order of increasing contact time for each feed composition. The partial pressure of product water and the amount of water adsorbed on the catalyst surface under steady state conditions therefore increased as each run proceeded. If this adsorbed water remained on the catalyst surface and had a site-blocking effect, the next series of measurements might indicate deceptively low rates of reaction. This potential problem was investigated experimentally at 246°C. Using the 16.5 volume percent ammonia, balance oxygen, feed, a flow rate of 208 cm^3 per minute resulted in 38.1% ammonia conversion. Partial pressure of water in the system, as calculated from vapor fractometer measurements and stoichiometric considerations, was 25.3 cm Hg (Measurement R3-8). The flow rate was then increased to 925 cm^3 per minute. About 40 minutes later, the reaction rate previously recorded at the higher feed rate was again reached as the steady state value. This higher feed rate corresponded to a water partial pressure of 11.7 cm Hg (Measurement R3-4). Hence at the lowest reaction temperature studied, water apparently readily desorbed from the catalyst surface even under continuing reaction conditions.

An identical test was conducted at 322°C. Water pressure corresponding to a feed rate of 35.5 cm^3 per minute using the 16.5 volume percent ammonia, balance oxygen, feed was 56.8 cm Hg (Measurement R39-5). After recording this measurement, the flow was increased to a value of 290 $cm^3\ min^{-1}$, corresponding to a previously recorded steady state water partial pressure of 21.3 cm Hg (Measurement R39-1). The rate of reaction

recorded at the lower contact time was again measured as the steady state value. Product distribution between nitrogen and nitrous oxide was also the same. This further substantiated the conclusion that water desorbed readily from catalyst sites contributing to the reaction.

As a final precaution, the high contact time conditions for the 16.5 volume percent ammonia, balance oxygen, feed were re-established and partial pressure of water was again brought to the steady state, 56.8 cm Hg level. Then a vacuum was pulled on the system for 10 minutes. Measurement R38-4 for the 5.3 volume percent ammonia, balance oxygen, feed was next re-measured. The two measured values for measurement R38-4 differed by 3.6%. It is apparent that the relatively high concentrations of water vapor over the catalyst had not influenced the catalytic activity.

N. Removal of Water from the Recycle Stream

For several series of runs it was desired to remove product water from the recycle gas stream. Alumina pellets, already shown experimentally to be catalytically inert below 350°C in terms of ammonia oxidation, were chosen for this purpose. These pellets were placed in the surge cylinder downstream of the reactor. During water removal runs, the cylinder was kept at ambient temperature to increase alumina's water absorptive capacity.

It was assumed that water would be formed in the system at the rate of 150 cm^3 min^{-1}. At room temperature, alumina can absorb 10% of its own weight of water and yet reduce water partial pressure to zero. Hence 43 grams of alumina would be necessary to absorb water under the assumed condition for 30 minutes. Ten times this weight of alumina was used.

As the next step, experimentation was conducted to establish the time required for 500 grams of alumina to become saturated with ammonia and oxygen at the approximate pressure levels to be used. Conditions for measurement R1-4 were re-established, with the exception that 500 grams of alumina were introduced into the feed line between the flow meters and the recycle loop. The steady state reaction rate expressed by measurement R1-4 would not be established until the alumina pellets ceased to absorb gas from the feed. Fifty minutes after the feed was turned on, the steady state reaction rate previously recorded was again measured as the steady state value. This indicated that no more than 50 minutes would be required to saturate the alumina with respect to ammonia and oxygen at ambient temperature.

Before each series of water absorption runs was started, fresh feed was introduced to the system at the maximum flow rate and with all operating conditions satisfied except that the reactor was not immersed in the molten salt. Purpose of this procedure was to saturate the alumina pellets with ammonia and oxygen. One hour after startup, the reactor was then lowered into the salt bath and the series of data points was measured in the usual way.

If during a series of water-removal runs the alumina absorbed an amount of water exceeding about 10% of the weight of the alumina, not all water would be removed from the recycling stream. In this circumstance, the assumption of negligible water partial pressure might be violated. It was therefore necessary to test the recycle for water content on the downstream side of the absorbent. This was carried out by withdrawing

reactor effluent on the upstream side of the reactor and passing the effluent through shielded glass tubing immersed in an ice bath. Observations were made throughout the course of each series of runs. No condensate was observed in the glass tubing during the water absorption runs. The vapor pressure of liquid water at 0°C is 0.47 cm Hg, meaning that the partial pressure of water in the recycle stream did not exceed this value. The value of 0.47 cm Hg is sufficiently low so that the additive term in the denominator of the Langmuir adsorption isotherm representing competition from water for adsorption sites can be neglected.

It is noted that, unless unchanging values of oxygen, ammonia, nitrogen and nitrous oxide partial pressures were established in the recycle stream, analyses of the reactor effluent would not have been reproducible. The analyses indicated that steady state conditions were reached. The alumina did not create a problem by acting indefinitely as either a sink or source for reactants or for nitrogen or nitrous oxide.

O. Presence of Hydrogen

The molecular sieve used for the oxygen-nitrogen separation in the vapor factometer was also capable of separating hydrogen from air. It was therefore possible during the standard effluent analysis procedure to observe whether hydrogen appeared as a reaction product. Hydrogen was at no time detected during the effluent analyses.

As a further check for hydrogen, the reactor was used on a one-pass basis at the lowest and highest temperature levels of experimentation. Again no hydrogen was found in the effluent.

V EXPERIMENTAL RESULTS

A. Influence of Ammonia Pressure on Total Rate of Ammonia Oxidation

Figures 5.1, 5.2 and 5.3 display most of the measurements which show the influence of ammonia partial pressure on the total rate of ammonia reaction. The logarithm of the total reaction rate, $cm^3\ min^{-1}\ gm^{-1}$, is plotted vs. the partial pressure of ammonia in the reactant stream with temperature as a parameter. For these measurements, only ammonia and oxygen were used as feed. All products of the reaction were left in the recycle. The oxygen partial pressure for any given curve is constant within a few percent because of the relatively low percentages of ammonia in the feed. The measurements are seen to be consistent with other measurements made in each series of runs. The rate decreases regularly with decreasing ammonia partial pressure and increases with rising temperature.

Figure 5.1 shows measurements made at four temperatures. For each of the four curves shown, the 5.3 volume percent ammonia, balance oxygen, feed was used. Reaction pressure was also constant for all Figure 5.1 measurements at 280 cm Hg. Adjacent to each curve is the reaction temperature and a reference to the data tables in Appendix B. The uppermost curve, for example, corresponds to a reaction temperature of 345°C and presents measurements appearing under R-48 in Appendix B. Considerations analogous to these for Figure 5.1 also apply to Figures 5.2 and 5.3.

B. Influence of Nitrogen on Rate of Product Formation

At three of the six temperatures investigated, a series of runs for which nitrogen was added directly to the feed was carried out. It was

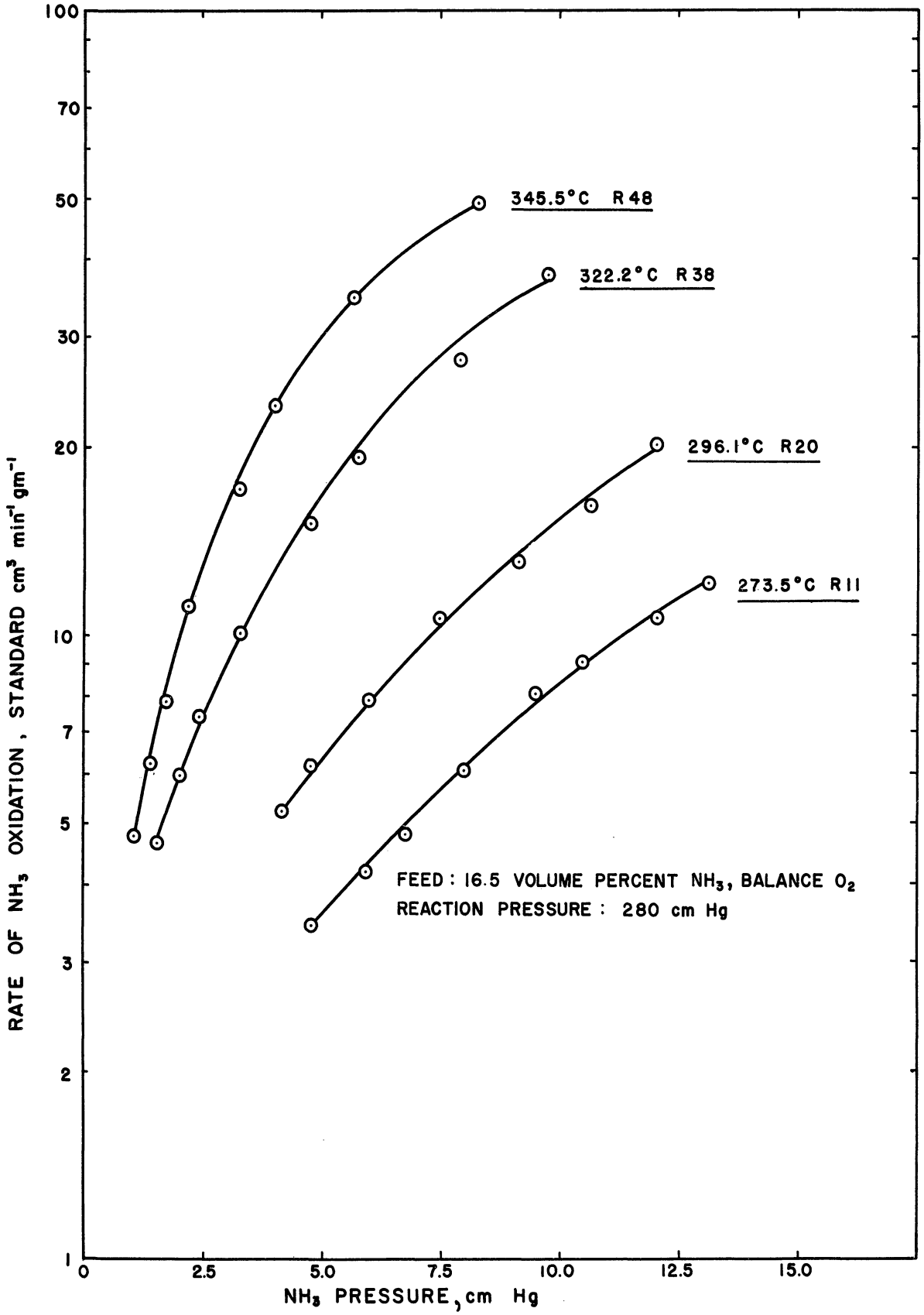

Figure 5.1. Influence of Ammonia on Total Rate of Ammonia Oxidation, Pressure 280 cm Hg, 5.3 Volume Percent Ammonia in Feed.

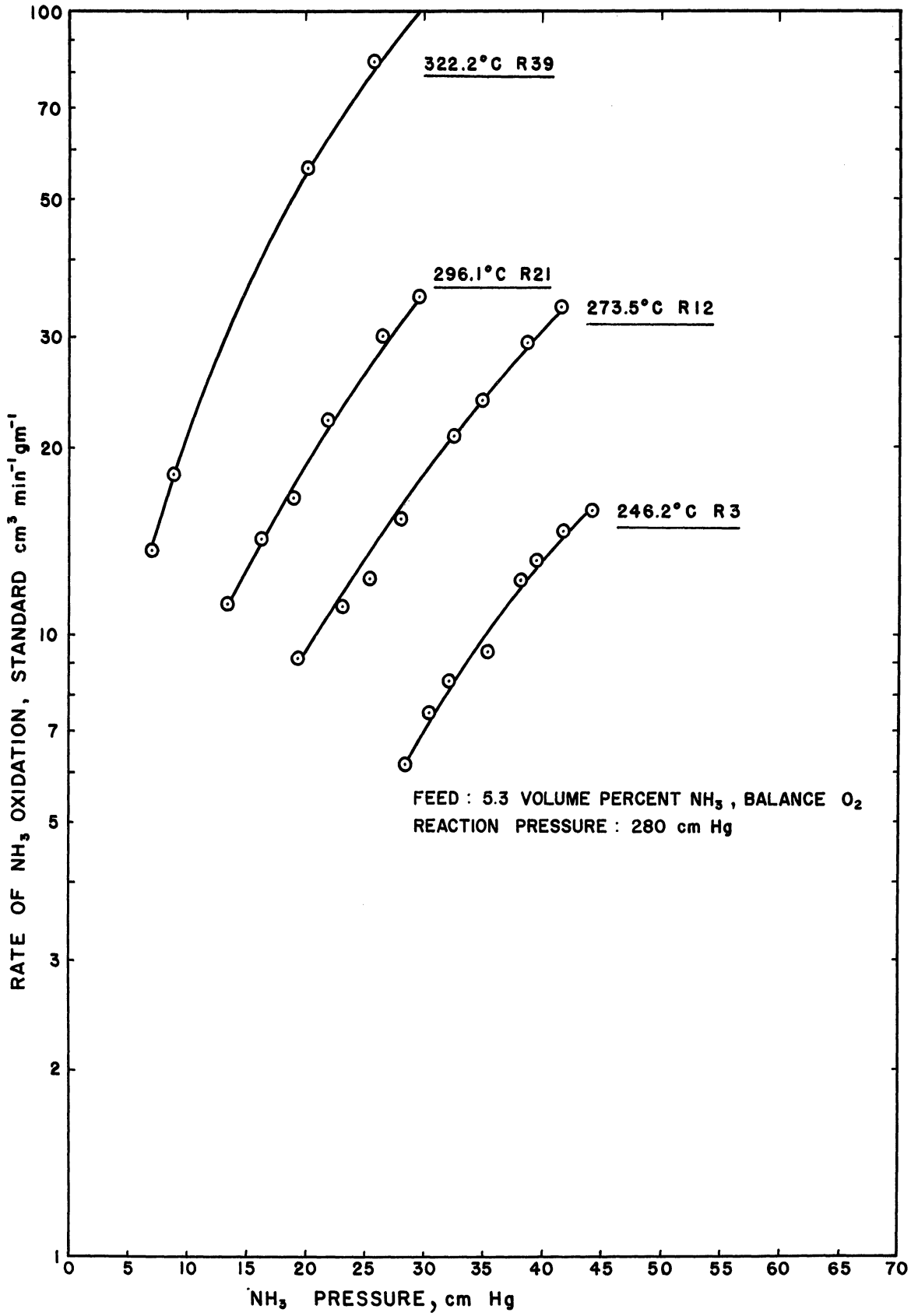

Figure 5.2. Influence of Ammonia on Total Rate of Ammonia Oxidation, Pressure 280 cm Hg, 16.5 Volume Percent Ammonia in Feed.

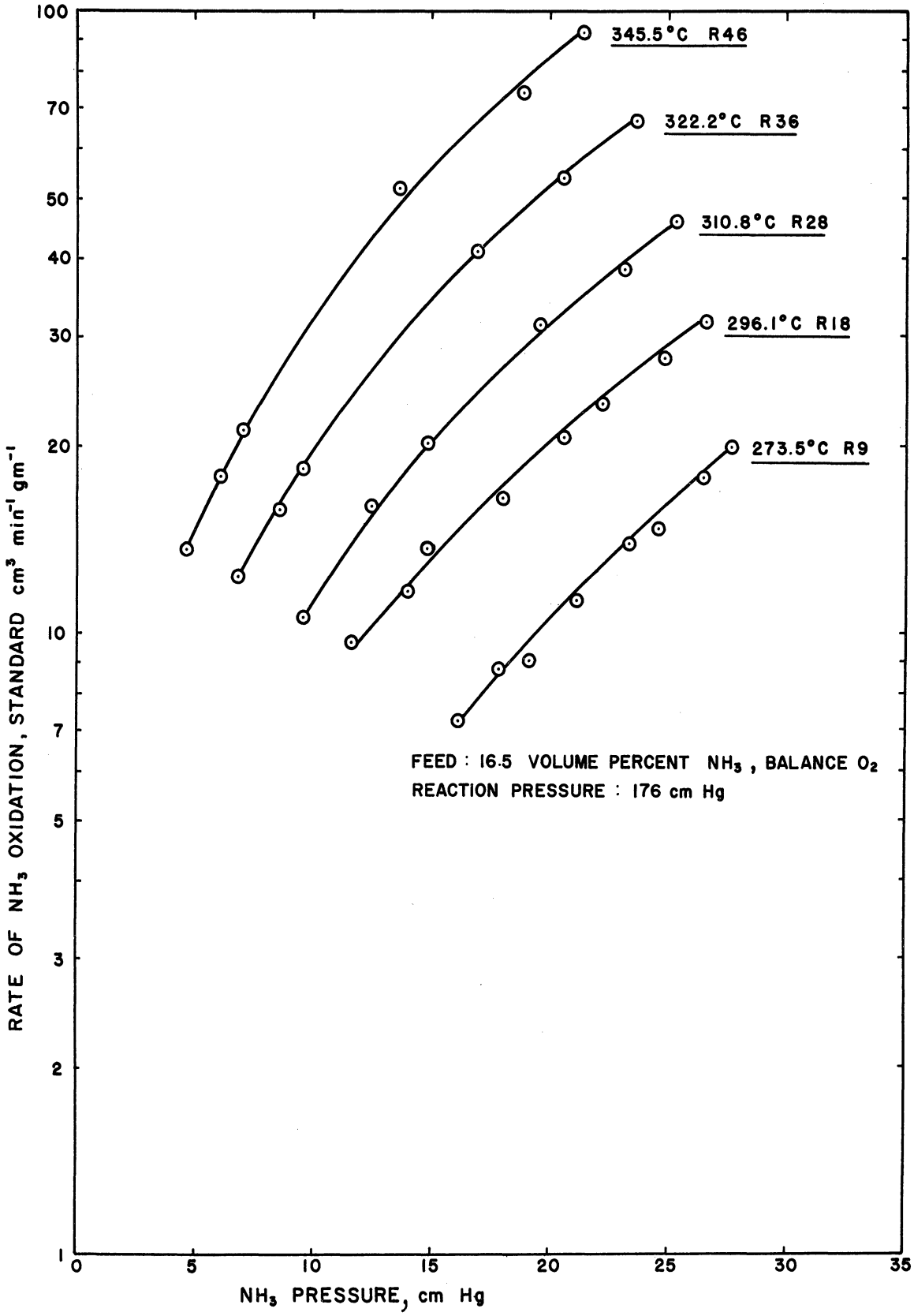

Figure 5.3. Influence of Ammonia on Total Rate of Ammonia Oxidation, Pressure 176 cm Hg, 16.5 Volume Percent Ammonia in Feed.

taken as a working postulate for these runs that nitrogen would have no influence on the rate of ammonia oxidation. This postulate was tested by comparing reaction rates measured under two sets of reaction conditions which were identical in all respects except that nitrogen was added to the feed in one case and not in the other. When nitrogen was added to the feed, the reaction pressure was raised accordingly so that the partial pressure of the added nitrogen would not change the partial pressures of the other gases in the reaction system. If the working postulate that the added nitrogen acts as an inert is valid, then identical rates of reaction will be measured under both sets of conditions.

Figures 5.4, 5.5 and 5.6 show the results of such measurements taken at 296, 310 and 345°C, respectively. Measured values of the rates of formation of nitrogen and nitrous oxide have been plotted separately in these figures. Three types of points are associated with each of the two curves shown in each figure: measurements for conditions of no nitrogen added to the feed; measurements for conditions involving addition of nitrogen to the feed; and measurements for conditions involving addition of nitrous oxide to the feed, to be discussed next. Significance of the data is indicated for each figure by legend.

C. Influence of Nitrous Oxide on Rate of Product Formation

The experimental scheme just discussed to investigate the influence of nitrogen on reaction rates and product distribution was also used to determine whether nitrous oxide affected the rates of reaction. The working postulate was that nitrous oxide added directly to the feed would

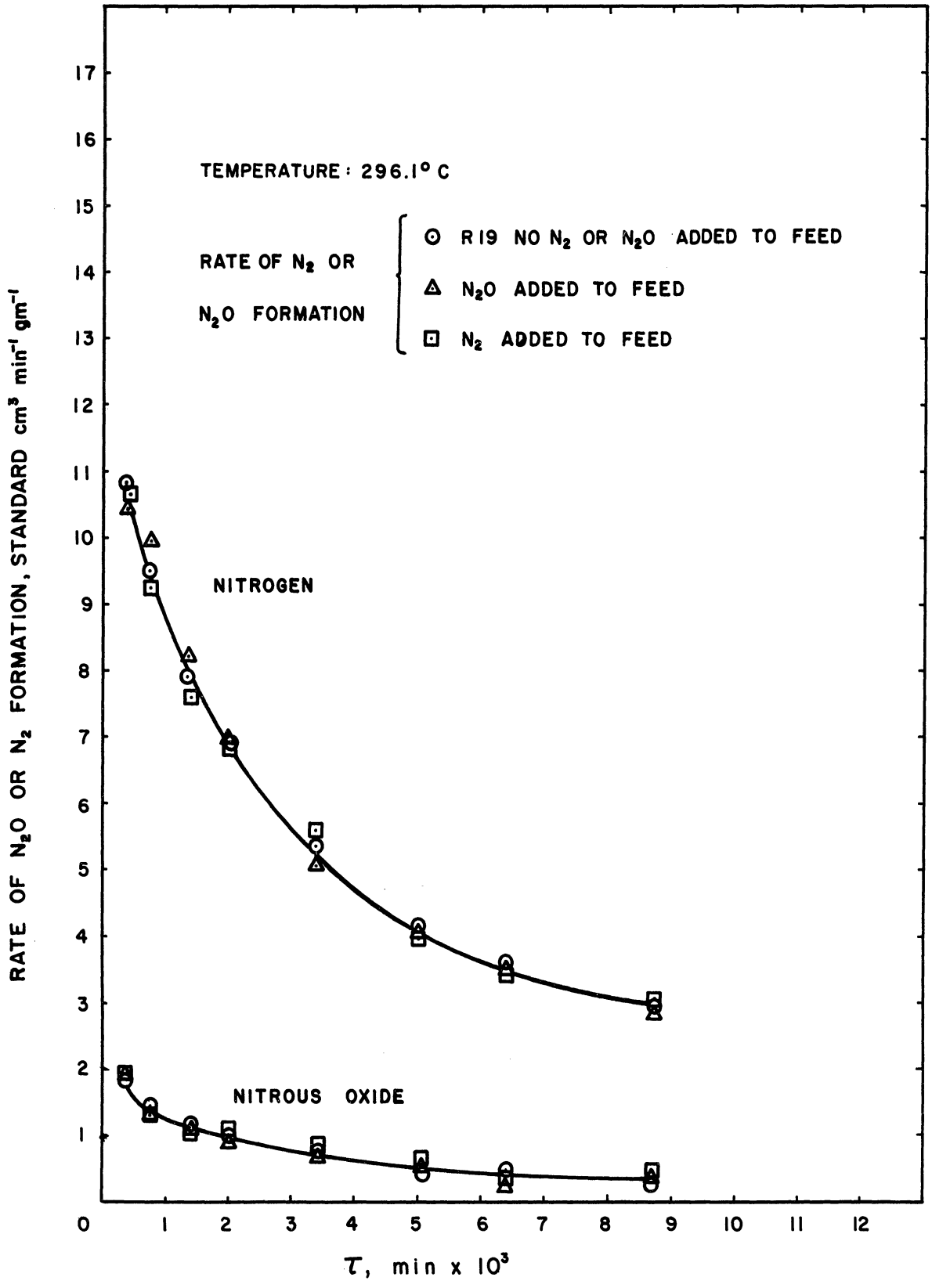

Figure 5.4. Influence of Nitrogen and Nitrous Oxide on Rate of Product Formation at 296°C.

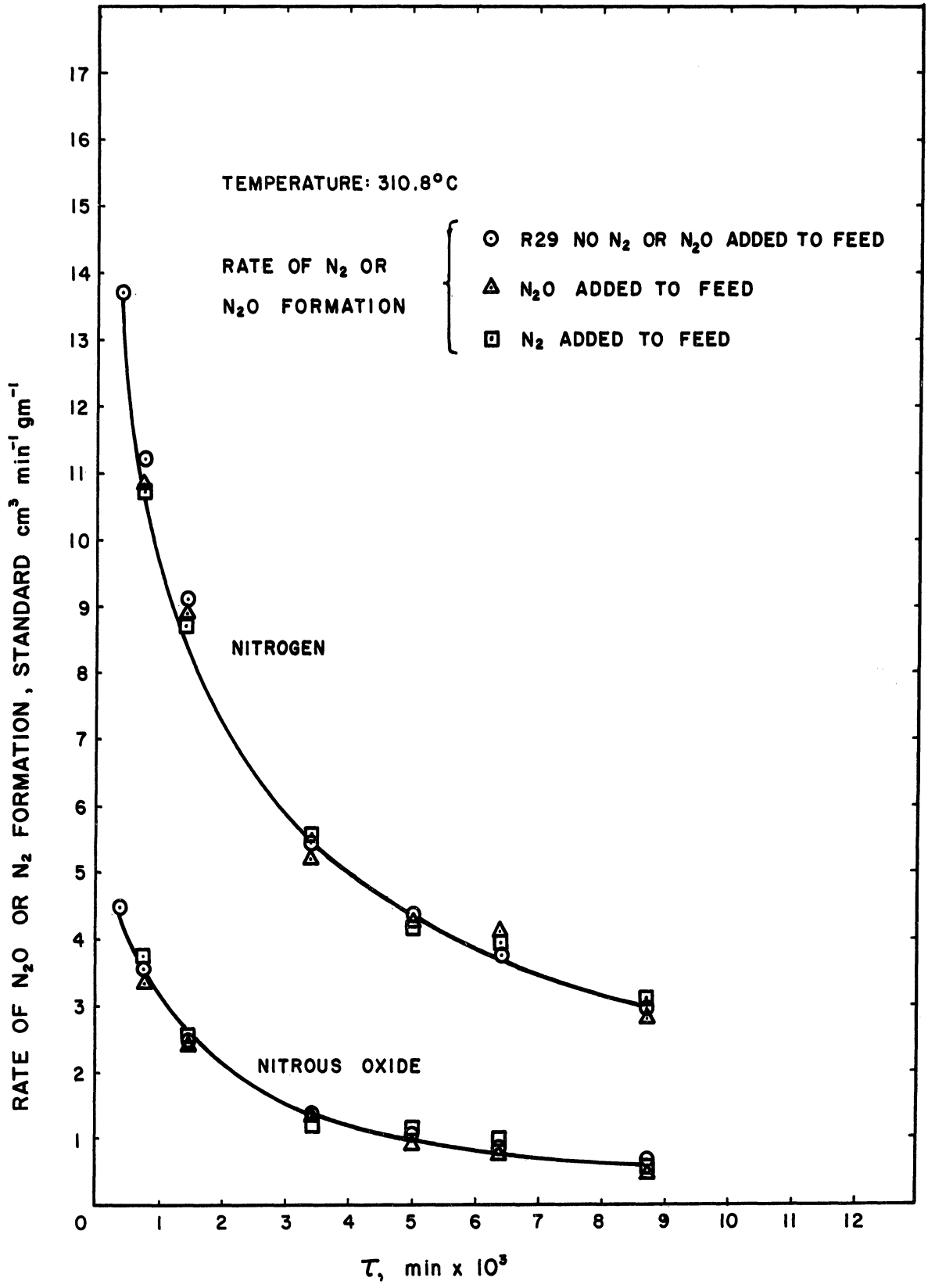

Figure 5.5. Influence of Nitrogen and Nitrous Oxide on Rate of Product Formation at 310°C.

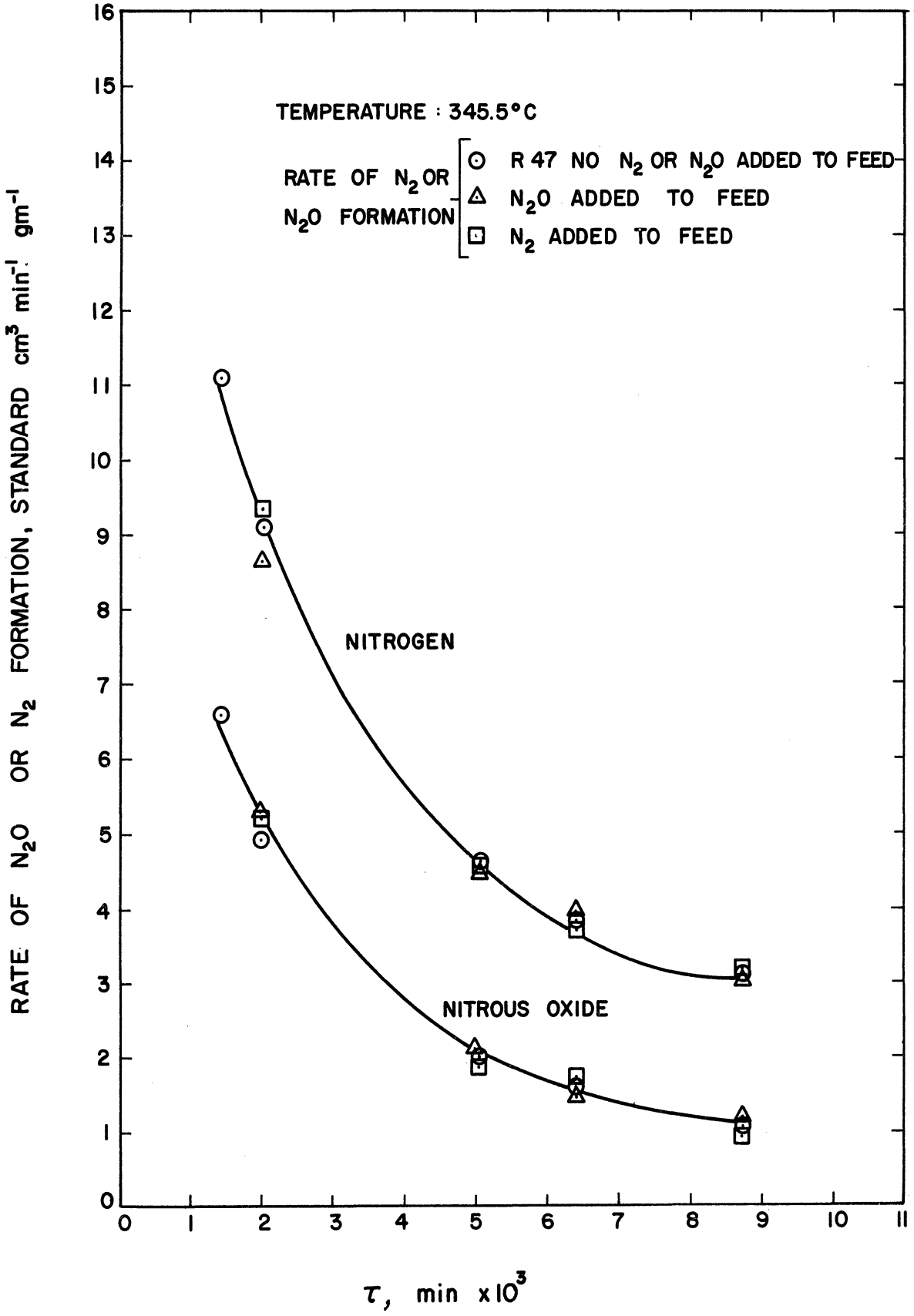

Figure 5.6. Influence of Nitrogen and Nitrous Oxide on Rate of Product Formation at 345°C.

behave as an inert in the reaction system. Presence of the added nitrous oxide in the reaction system was compensated by raising the reaction pressure an appropriate amount. Measurements taken under these conditions were then compared with measurements taken under conditions otherwise identical except that no added nitrous oxide was present in the reactant stream. Figures 5.4, 5.5 and 5.6 display the results recorded at temperatures of 296, 310 and 345°C, respectively. These are the same figures that were used to exhibit the measurements for which nitrogen was added to the feed. The legend on each figure explains the reaction conditions under which each measurement was made.

D. Influence of Ammonia on Rate of Product Formation

The influence of ammonia on the rates of formation of nitrogen and nitrous oxide was investigated under conditions of constant oxygen partial pressure and constant water partial pressure. It was indicated earlier that oxygen partial pressure remained nearly constant for any given feed composition and reaction pressure. Water partial pressure was maintained at a very low level in the reactant stream by using alumina to remove product water from the recycle.

Measurements made to study the ammonia influence are displayed in Figures 5.7 and 5.8. Figure 5.7 shows the effect of ammonia on the rate of nitrogen formation; Figure 5.8 shows the effect of ammonia on the rate of nitrous oxide formation. In both figures, the logarithm of the pertinent rate of formation is plotted against the logarithm of the partial pressure of ammonia in the reactant stream. Measurements for all six temperatures studied in the experimental work are included. Appropriate legends

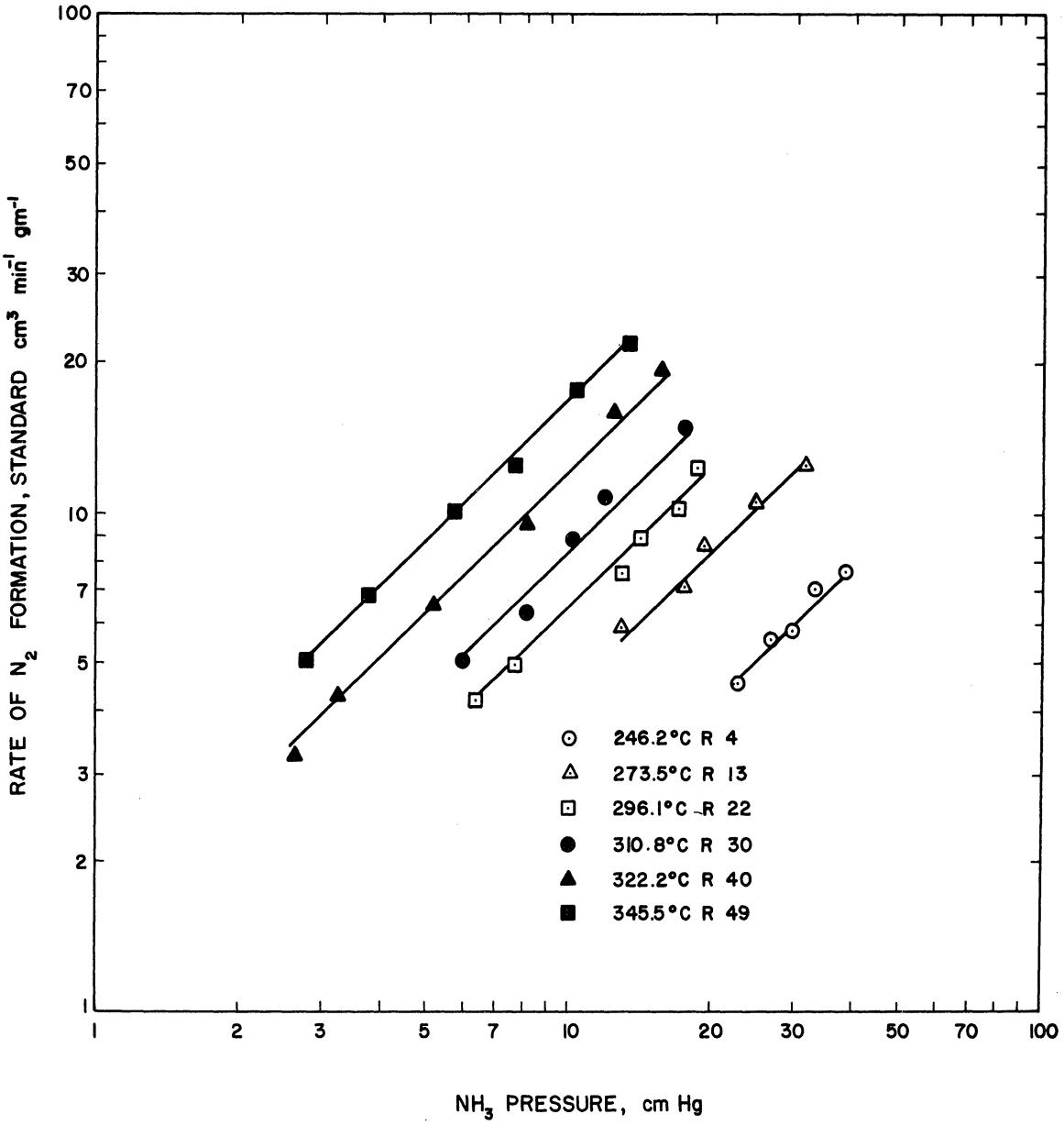

Figure 5.7. Influence of Ammonia on Rate of Nitrogen Formation. (Water Removed from Recycle)

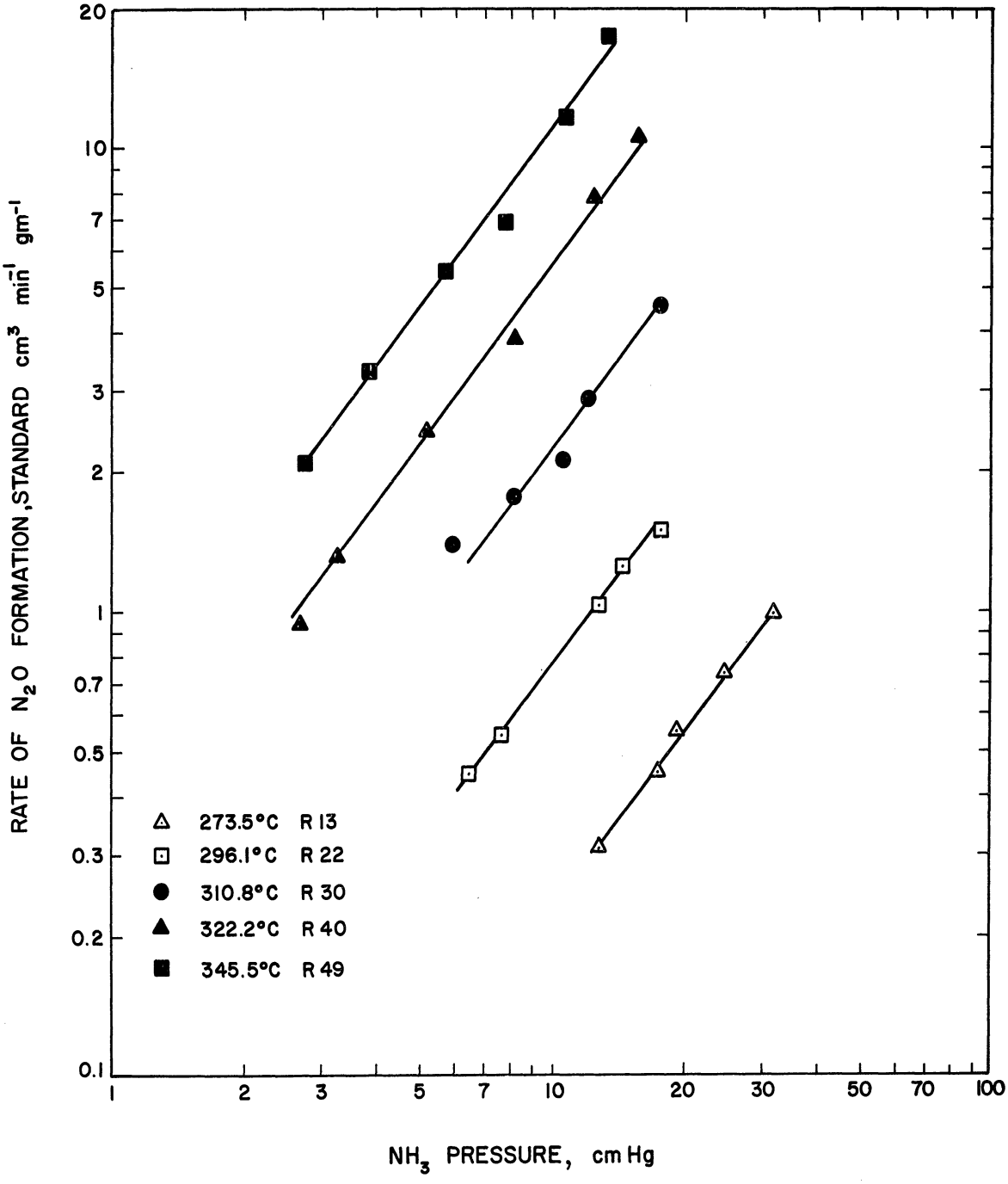

Figure 5.8. Influence of Ammonia on Rate of Nitrous Oxide Formation. (Water Removed from Recycle)

on each figure indicate the various temperatures and reference the measurements as tabulated in Appendix B. The ammonia pressure in this work varied from 1.1 to 44.1 cm Hg.

E. Influence of Oxygen on Rate of Product Formation

The effect of oxygen on the rate of formation of nitrogen and nitrous oxide was determined by taking measurements for which water was eliminated as a variable. The water partial pressure was held at a negligibly low value by absorbing water from the recycle stream with alumina. Various combinations of reaction pressure and feed composition were used to vary the oxygen partial pressure from about 70 to 265 cm Hg. The influence of ammonia on these measurements was taken into account by making use of information developed from Figures 5.7 and 5.8. After making quantitative allowance for the ammonia partial pressure, rates of product formation under the various reaction conditions were then related directly to the partial pressure of oxygen in the reactant stream.

Figures 5.9 and 5.10 show the measurements taken to investigate the oxygen influence. Figure 5.9 shows the effect of oxygen on the rate of nitrogen formation; Figure 5.10 indicates the influence of oxygen on the rate of nitrous oxide formation. In both figures, the logarithm of a function of reaction rate and ammonia partial pressure has been plotted vs. the logarithm of the partial pressure of oxygen in the reactant stream. Measurements for all six temperatures studied in the experimentation are included. A legend on each figure indicates the various temperatures and references the measurements as tabulated in Appendix B.

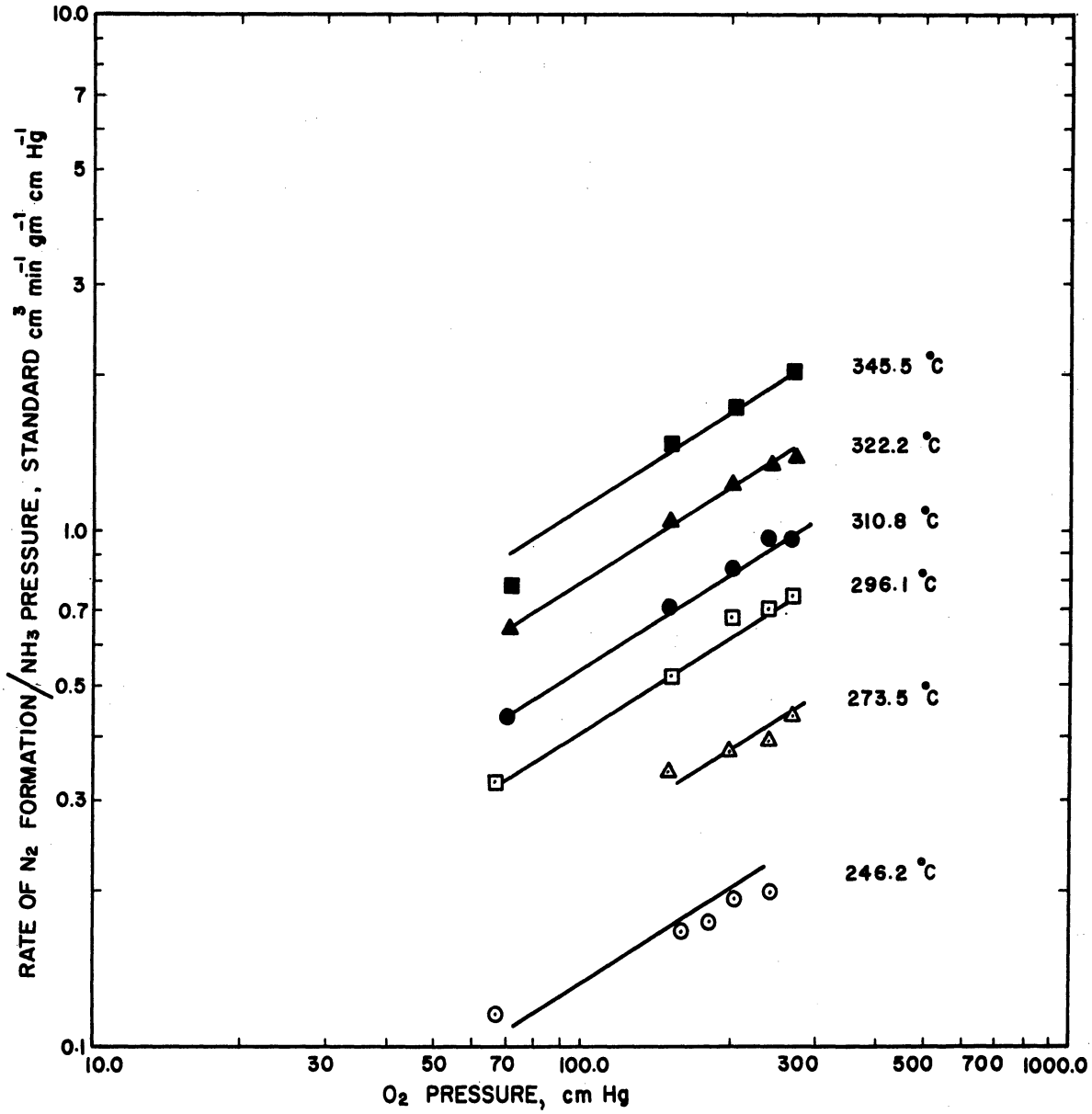

Figure 5.9. Influence of Oxygen on Rate of Nitrogen Formation. (Water Removed from Recycle)

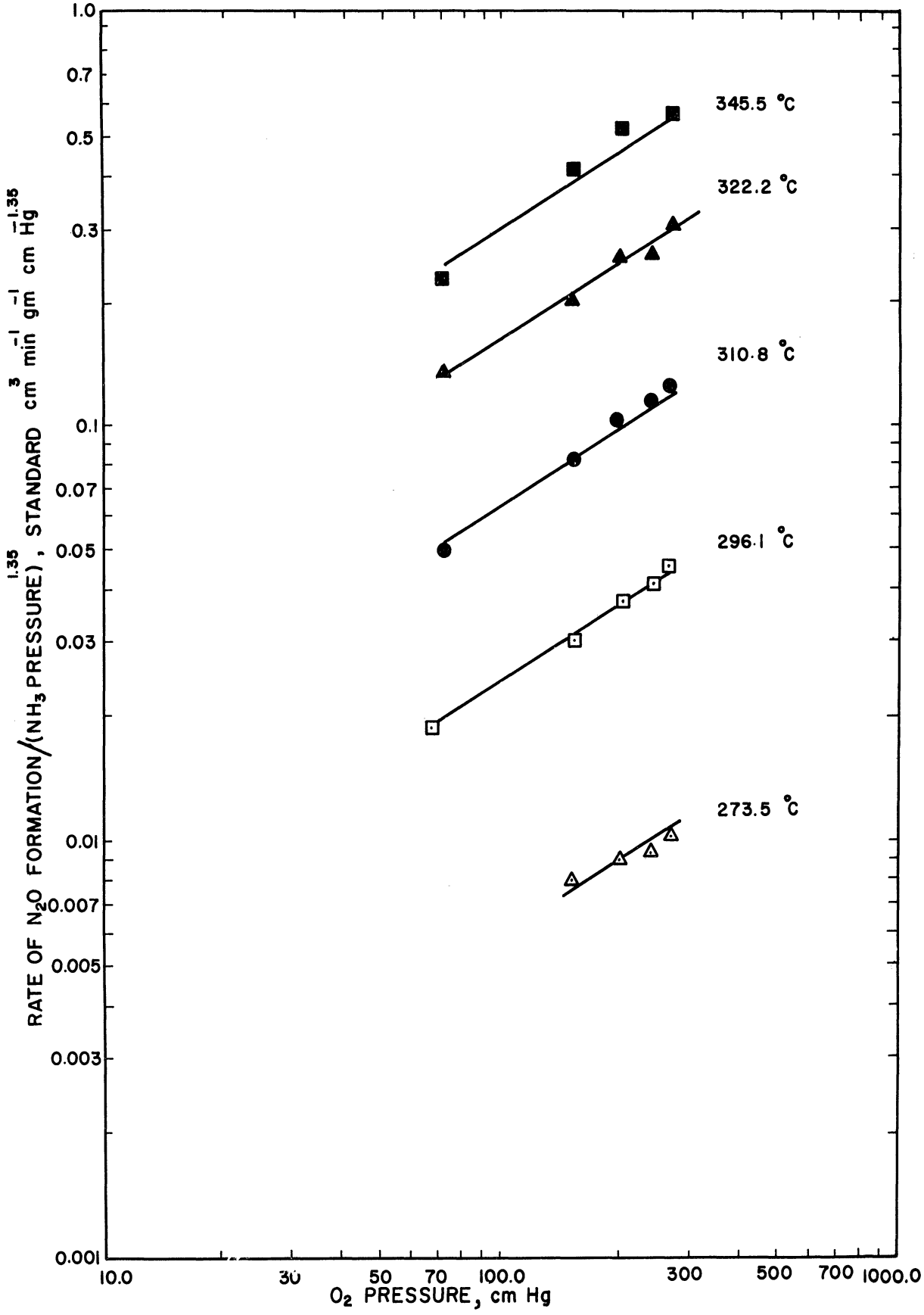

Figure 5.10. Influence of Oxygen on Rate of Nitrous Oxide Formation. (Water Removed from Recycle)

F. Influence of Water on Rate of Product Formation

Oxygen partial pressure in the reactant stream was approximately constant for each feed composition and reaction pressure. For a given temperature, feed composition and reaction pressure, then, the rate of product formation measured at various feed rates can be related solely to the partial pressures of ammonia and water in the reactant stream. The quantitative influence of ammonia on these rates can be taken into account, however, by using information developed from Figures 5.7 and 5.8. This is done by normalizing the rate of formation of the pertinent reaction product with respect to ammonia, i.e., by dividing the rate of formation by the partial pressure of ammonia raised to the proper power. Suitable plotting of this normalized rate vs. the partial pressure of water then indicates the extent to which water influences the rate of product formation.

Plots of the logarithms of such normalized rates of product formation vs. the logarithm of water partial pressure are shown in Figures 5.11 and 5.12. Figure 5.11 shows measurements of the rate of formation of nitrogen; Figure 5.12 shows measurements of the rate of formation of nitrous oxide. In both cases, linear relationships result. The measurements used for Figures 5.11 and 5.12 are simply replots of some of the measurements shown in Figures 5.1, 5.2 and 5.3. One curve has been drawn in each of the two Figures 5.11 and 5.12 for each of the six temperatures investigated. Most of the other measurements made during this experimentation could also be replotted in the manner shown. The data displayed are completely representative. The slopes of the straight lines are independent of reaction temperature, feed composition and reaction pressure.

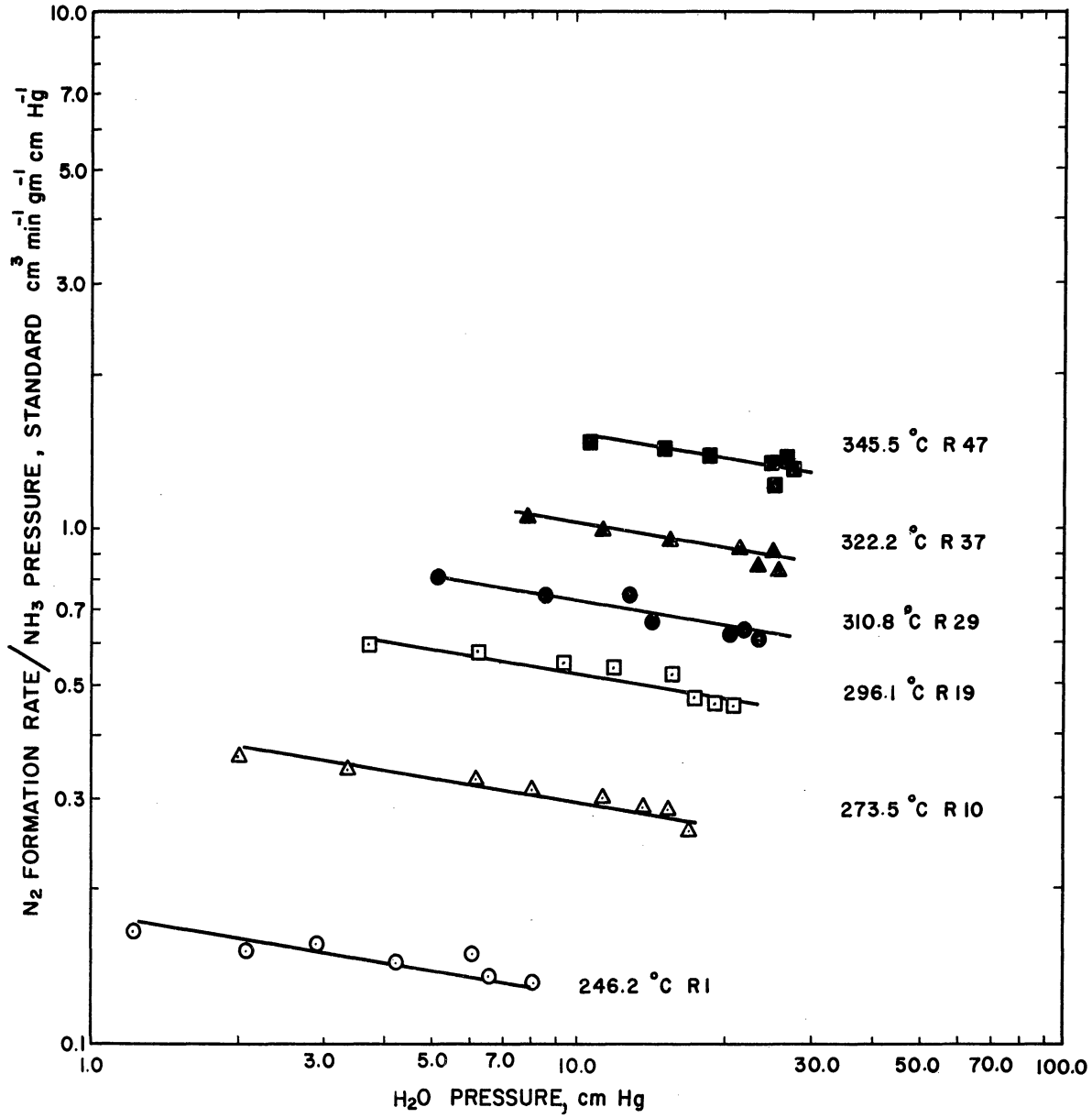

Figure 5.11. Influence of Water on Rate of Nitrogen Formation.

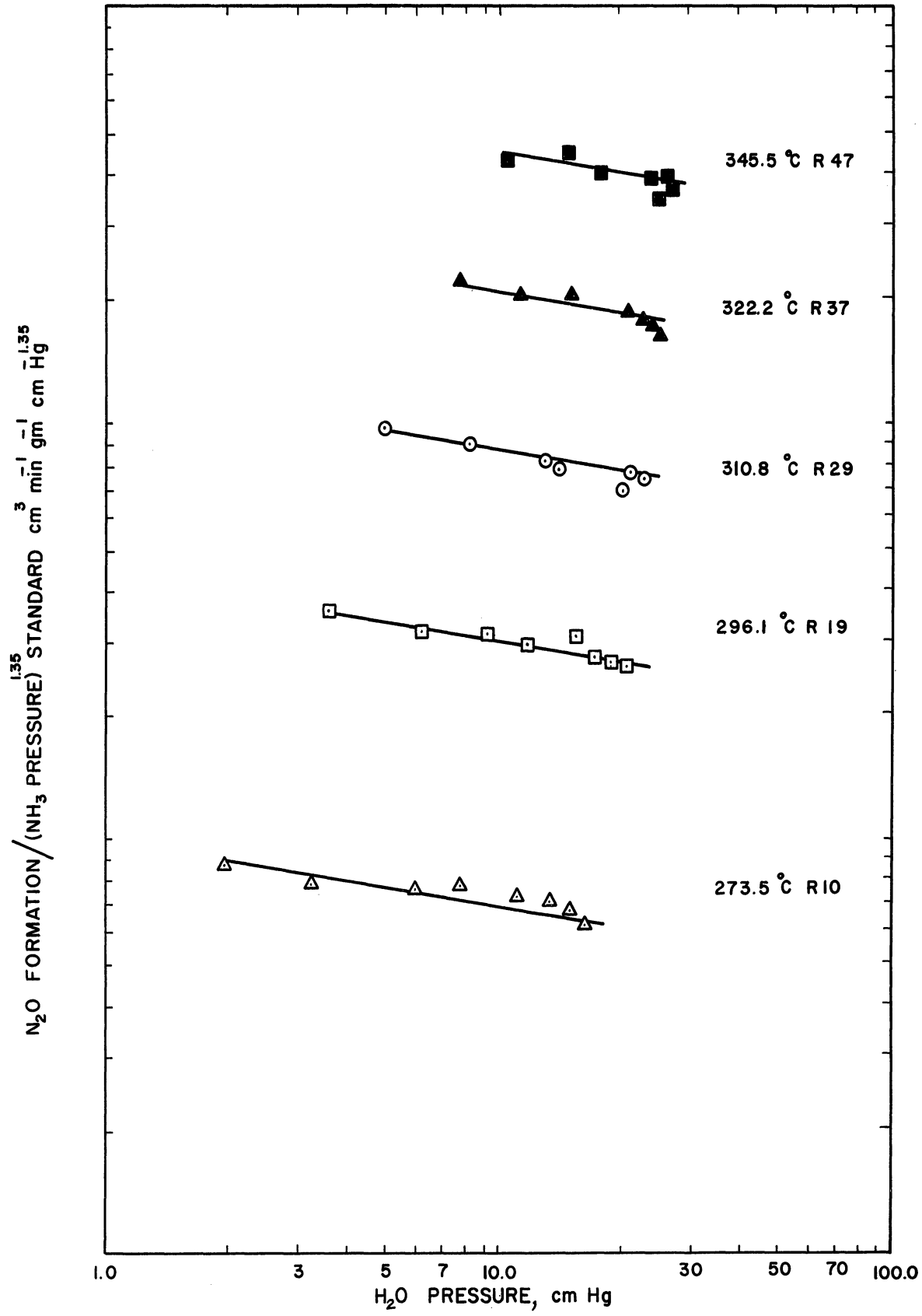

Figure 5.12. Influence of Water on Rate of Nitrous Oxide Formation.

The approach described in the two preceding paragraphs is an indirect one. The influence of water on the rate of ammonia oxidation was also investigated directly by establishing reaction conditions for which the partial pressures of oxygen and ammonia were held approximately constant while the partial pressure of water was varied. Due to experimental difficulties, however, measurements were made for only two values of water partial pressure at any given ammonia and oxygen partial pressure. These measurements are displayed in Figure 5.13. Two curves have been drawn for each of the three temperatures investigated. The reaction conditions corresponding to the measured values are described on the figure itself. Results are in agreement with the results presented in Figures 5.11 and 5.12, i.e., other conditions being equal, an increase in the partial pressure of water in the reactant stream inhibits the rates of formation of both nitrogen and nitrous oxide.

G. Influence of Mass Transfer on Rate of Product Formation

The influence of mass transfer on the rate of ammonia oxidation was checked by varying the mass transfer coefficient under otherwise identical reaction conditions. The mass transfer coefficient was changed by changing the cross sectional area of the reactor. This procedure was carried out at a temperature of 345°C. If mass transfer was without influence on the rate of reaction at this temperature, then it would also be without influence at the lower reaction rates corresponding to the lower temperatures of experimentation.

It is shown in Appendix D that the mass transfer coefficient k is inversely proportional to the diameter of the reactor when other conditions are constant, that is

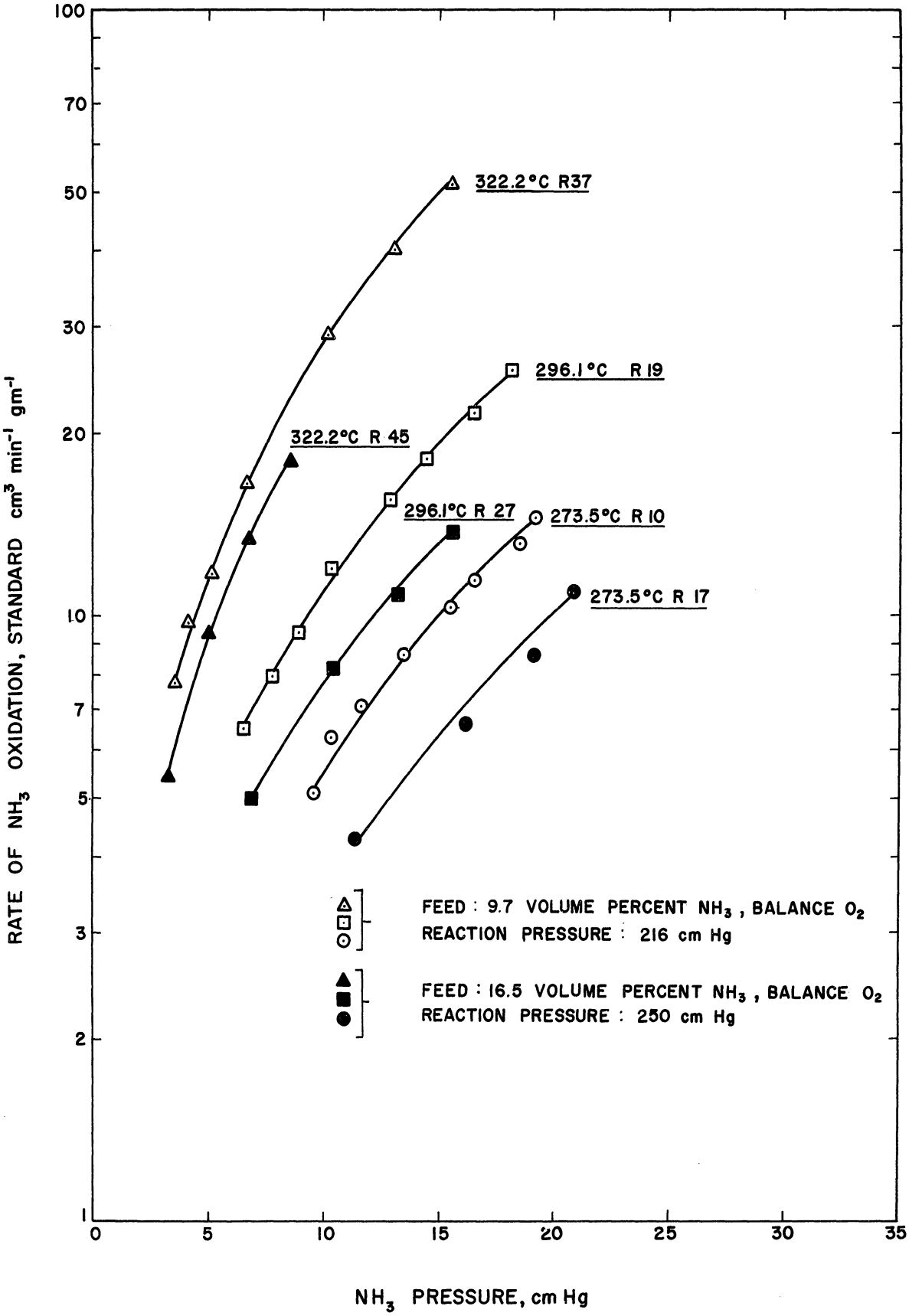

Figure 5.13. Rate of Ammonia Oxidation vs. Ammonia Pressure. (Water Pressure Controlled)

$$k \alpha 1/D \qquad (5.1)$$

The mass transfer coefficient was increased by 35% in this work by substituting an 0.156 inch diameter reactor for the 0.210 inch diameter reactor used during most of the experimentation. Figure 5.14 shows the measurements for which the mass transfer coefficient was varied. The total rate of formation of nitrogen and nitrous oxide is plotted vs. contact time. Measurements are shown for each of three feed compositions. Three feed rates were used for each feed composition. The measured rates of product formation are seen to be independent of the rate of mass transfer to the catalyst surface.

H. Stability of Catalyst and Check on Differential Conditions

Figures 5.15 and 5.16 display the data taken to determine whether catalytic activity was a function of time and whether differential conditions existed in the reactor. Under the reaction conditions indicated on the two figures cited, reaction rates were measured over a time interval of 24 hours. Effluent was sampled both upstream and downstream of the catalyst section. The measurements show that composition was independent of the sampling point and independent of time.

I. Influence of Ammonia on Relative Rate of Nitrous Oxide Formation

Information derived from Figures 5.9 and 5.10, and from Figures 5.11 and 5.12, indicates that the rates of nitrous oxide and nitrogen formation have identical dependence on the partial pressure of oxygen and water at all temperatures investigated. This suggests that for any of the measurements taken in this work, the ratio of the rate of formation

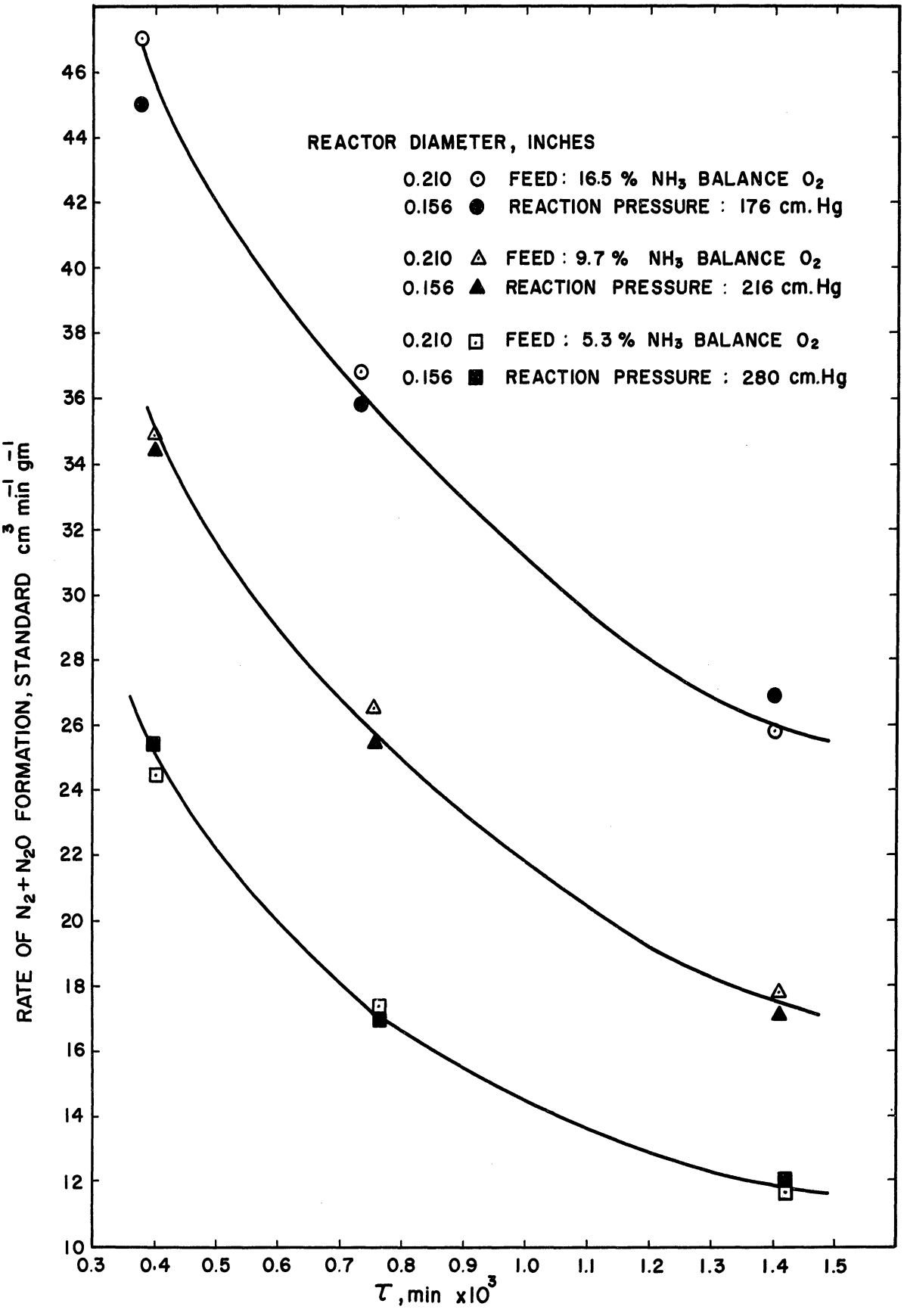

Figure 5.14. Influence of Mass Transfer on Rate of Ammonia Oxidation.

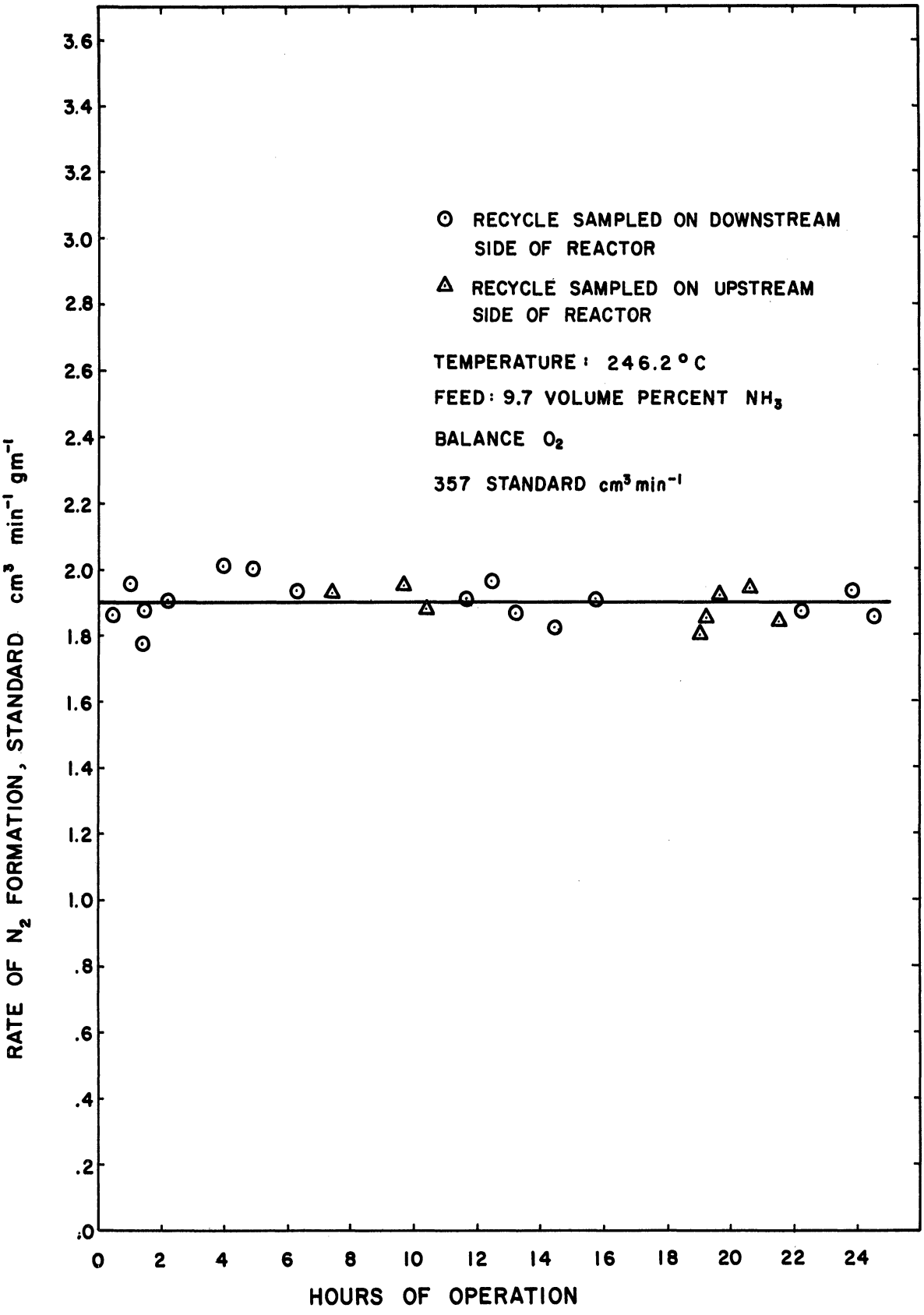

Figure 5.15. Stability of Catalyst and Check on Differential Conditions at 246°C.

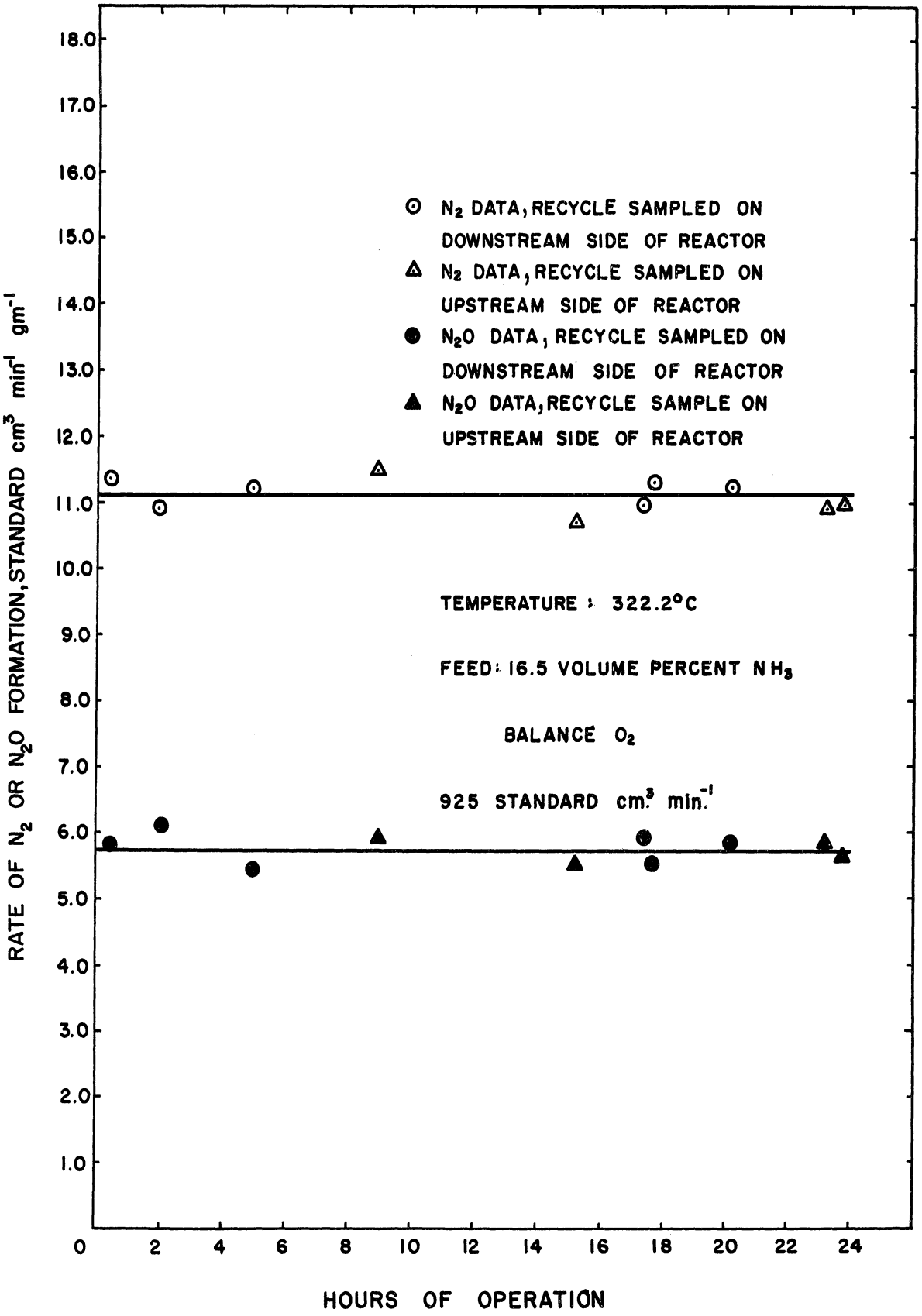

Figure 5.16. Stability of Catalyst and Check on Differential Conditions at 322°C.

of nitrous oxide to that of nitrogen should depend only on the partial pressure of ammonia. This dependence should be quantitatively predictable from the measurements shown in Figures 5.7 and 5.8.

Figure 5.17 is a plot of the logarithm of the ratio of nitrous oxide and nitrogen rates of formation vs. the partial pressure of ammonia in the reactant stream. Experimental values are shown for each of the five temperatures at which both nitrous oxide and nitrogen appeared as reaction products. At each temperature, data from two arbitrarily selected sets of feed composition and reaction pressure have been included. This is a replotting of a portion of the measurements presented in Figures 5.1, 5.2 and 5.3. The information used is completely representative. It is evident from the figure that the logarithm of the ratio of rates of formation of nitrous oxide and nitrogen is approximately linearly dependent on the partial pressure of ammonia.

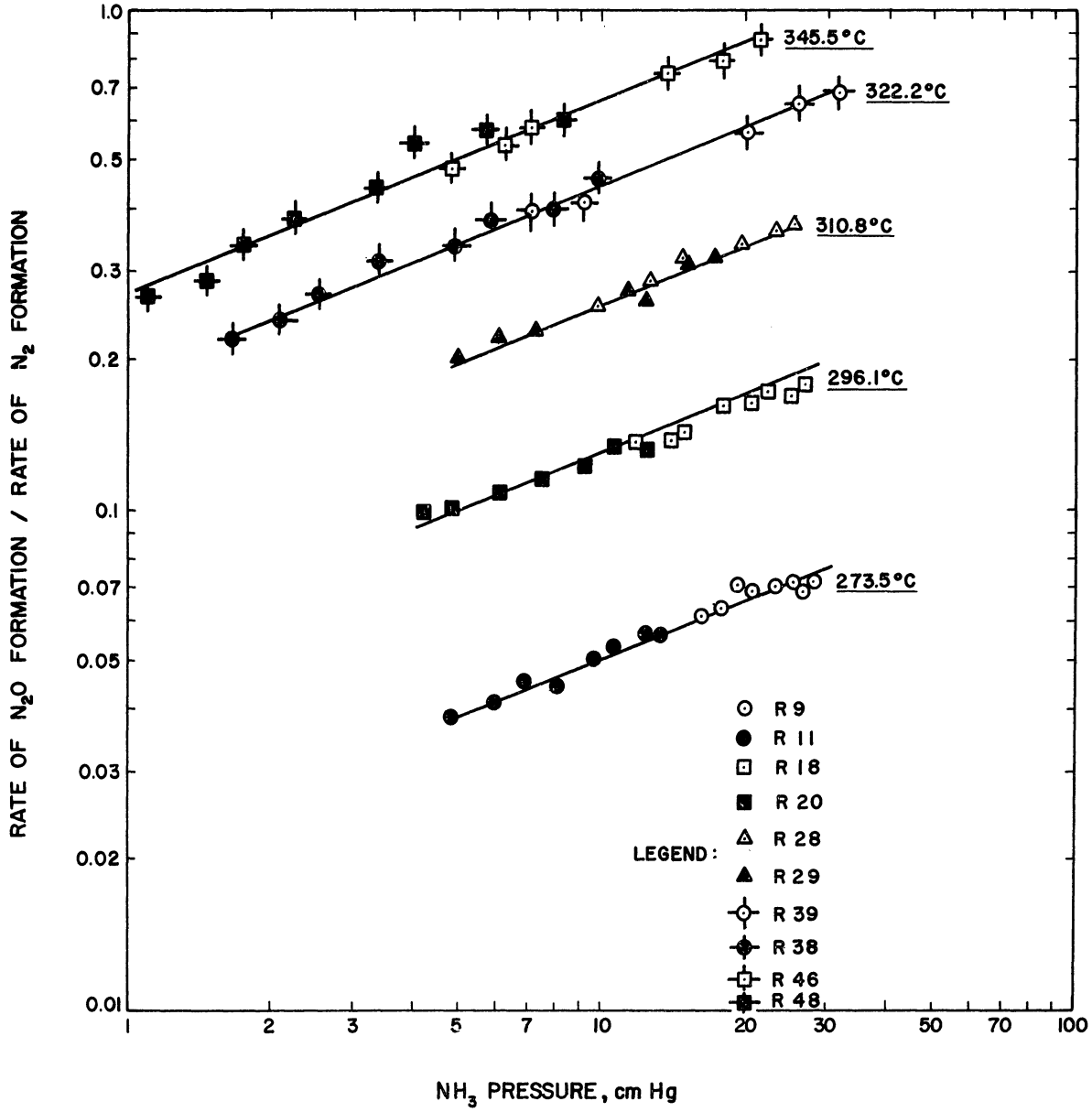

Figure 5.17. Influence of Ammonia on Relative Rate of Nitrous Oxide Formation.

VI DISCUSSION OF RESULTS

A. Influence of Partial Pressures on Reaction Rates

Several conclusions can be drawn immediately from the results presented in Chapter V. Inspection of Figures 5.4 through 5.6 shows that the rate of nitrogen formation is independent of nitrogen partial pressure within experimental error. The rate of nitrous oxide formation is also seen to be independent of nitrogen partial pressure. Partial pressure of nitrogen introduced in the feed was as great as 7.7 cm Hg and in several instances exceeded the partial pressure of product nitrogen. These results justify the assumption that nitrogen is without influence on nitrogen and nitrous oxide rates of formation. Inspection of Figures 5.4 through 5.6 also indicates that the rates both of nitrogen and nitrous oxide formation are independent of nitrous oxide partial pressure, even though the partial pressure of added nitrous oxide was as high as 9.2 cm Hg.

Figures 5.7 and 5.8 show that the logarithms both of the rates of formation of nitrogen and nitrous oxide are linearly dependent on the partial pressure of ammonia. The slopes of the straight lines correlating the measurements are independent of temperature. The slope of the straight lines corresponding to nitrogen formation rates is 1.0. This means that the rate of nitrogen formation is proportional to the first power of ammonia partial pressure. The slope of the measurements corresponding to nitrous oxide formation rates has the value 1.35, indicating that the rate of nitrous oxide formation is proportional to the 1.35 power of ammonia partial pressure.

It will be shown shortly that the ratio of nitrous oxide to nitrogen formed in the reaction is independent of the partial pressures both of oxygen and water in the reactant stream. This same ratio should, then, be proportional to the ammonia partial pressure raised to the 0.35 power, consistent with the slopes of 1.35 and 1.0 just discussed. These statements are tested in Figure 5.17, where the logarithm of the ratio of measured nitrous oxide and nitrogen rates is plotted versus ammonia partial pressure. The measurements shown have been randomly selected and are completely representative. The data are reasonably fitted with straight lines of slope 0.35, substantiating the conclusion regarding the influence of ammonia partial pressure on the rate of reaction.

The measurements exhibited in Figures 5.9 and 5.10 indicate that the logarithms of rates of formation of nitrogen and nitrous oxide are linearly dependent on the partial pressure of oxygen. The straight lines corresponding to this linear dependence have a slope of 0.71, independent of temperature. This value of the slope applies to both nitrogen and nitrous oxide rate data. Hence the rates of nitrogen and nitrous oxide formation depend to the same extent on the partial pressure of oxygen. Or, to express the result in another way, the ratio of nitrous oxide to nitrogen formed in the reaction is independent of the oxygen partial pressure in the reactant stream. Figure 5.17 substantiates this conclusion.

Variation of the rate of oxidation of ammonia as a function of water pressure can be displayed by isothermal measurements for which water pressure is varied while the partial pressures of ammonia and oxygen are held constant. Limited measurements of this type are shown for temperatures

of 273.5, 296.1 and 322.2°C in Figure 5.13. The upper curve for each temperature corresponds to a feed of 9.7 volume percent ammonia, balance oxygen, and a reaction pressure of 216 cm Hg. Oxygen pressure for this data is 183 ± 10 cm Hg. While using a feed containing less oxygen, namely 16.5 volume percent ammonia, balance oxygen, it was possible, by a suitable increase in the reaction pressure, to also set the oxygen partial pressure for this feed at the 183 cm Hg level. Use of appropriately high contact times for the 16.5 volume percent ammonia feed resulted in a lowering of ammonia pressure to the level encountered in the 9.7 volume percent ammonia feed case. Data for the two combinations of feed composition and reaction pressure can then be compared in a manner making the water effect explicit.

The lower curve for each temperature in Figure 5.13 shows data corresponding to the 16.5 volume percent ammonia feed case. For any fixed value of the abscissa, say 17 cm Hg, the lower curve and upper curve isothermal rates were then measured under essentially identical conditions of ammonia and oxygen partial pressures. But since the extent of ammonia reaction in the lower curve case was greater, water pressure in the reactant stream was also greater. For any given abscissa value in Figure 5.13, the water pressure for the lower and upper curves differs by 31 cm Hg. This is true, independent of choice of abscissa, because the difference in water pressure depends only on the constant values of the ammonia mole fraction in the two feeds used.

It is evident in Figure 5.13 that water retards the rate of reaction. In all cases, rate curves corresponding to higher water pressures

are below those for which water pressure was not as great. The influence of water, however, becomes less pronounced as temperature increases. This evidence suggests that water decreases the reaction rate by occupying surface sites which would otherwise participate in the reaction. Such a conclusion is consistent with the fact that the water effect becomes less pronounced with increasing temperature.

Figures 5.11 and 5.12 demonstrate that the logarithms of rates of formation of nitrogen and nitrous oxide are linearly dependent on the partial pressure of water. Both for nitrogen and nitrous oxide rate measurements, the straight lines correlating the data are independent of temperature and have a slope of -0.15. Hence water retards the rates of nitrogen and nitrous oxide formation to the same extent. This means that the ratio of nitrous oxide to nitrogen formed in the reaction is independent of the water concentration in the reactant stream. This conclusion is verified in Figure 5.17.

B. Influence of Mass Transfer on Reaction Rate

Figure 5.14 indicates that the rates of formation of nitrogen and nitrous oxide are independent of mass transfer effect under the conditions used for this experimentation. Measurements shown in the figure correspond to widely varying Modified Reynolds Numbers. Rates measured under the otherwise identical reaction conditions are nonetheless independent of the Reynolds number within experimental error.

C. Formulation of Reaction Mechanism

A satisfactory reaction mechanism should account for the experimentally observed pressure dependencies of the reaction rate in terms of the steps occurring on the catalyst surface. The frequency of oxygen participation in steps prior to and including the controlling step, for example, should be consistent with the oxygen pressure dependence shown in Figures 5.9 and 5.10. Suppose the oxygen concentration on the catalyst surface can be represented by a Langmuir adsorption isotherm:

$$\theta_o = \frac{b_{O_2}^{1/2} \; p_{O_2}^{1/2}}{1 + b_{O_2}^{1/2} \; p_{O_2}^{1/2} + b_{H_2O} \; p_{H_2O}} \qquad (6.1)$$

Equation (6.1) allows for site competition from water molecules and assumes dissociative adsorption of oxygen. Terms representing competition of oxygen with nitrous oxide and nitrogen for adsorption sites are not included because experimental measurements showed that these later two species were without influence on the reaction rate. The denominator term in Equation (6.1) representing competition from ammonia for sites has been assumed negligible compared to the other denominator terms; justification for this simplifying assumption is found in Figures 5.7 and 5.8, where the measured relationships are approximately linear rather than curved as they would be if ammonia played a significant role in the denominator of the oxygen surface concentration expression. Either ammonia adsorption was weak relative to that of oxygen and water, or ammonia did not compete for adsorption on the same sites as those attracting oxygen and water.

Since water was removed from the recycle stream for the measurements shown in Figures 5.9 and 5.10, Equation (6.1) becomes

$$\theta_o = \frac{b_{O_2}^{1/2} p_{O_2}^{1/2}}{1 + b_{O_2}^{1/2} p_{O_2}^{1/2}} \cong B_{O_2} P_{O_2}^{n} \qquad \text{where } n < 1/2 \qquad (6.2)$$

Equation (6.2) approximates dissociatively adsorbed oxygen concentration on the catalyst surface as a constant times the oxygen pressure raised to a power less than 1/2. It is recalled that the slope in Figures 5.9 and 5.10 is 0.71. This suggests that dissociatively adsorbed oxygen must enter the reaction mechanism at least twice up to and including the controlling step.

The role of adsorbed ammonia in the steps leading to nitrogen formation should be consistent with the above conclusion concerning the participation of oxygen in the reaction. Consider a scheme in which atomic oxygen reacts with molecular ammonia to form imide (NH) and water. The imide in turn can dimerize to form nitrogen and hydrogen. Taking the dimerization reaction as controlling, the supposition that dissociatively adsorbed oxygen enters the scheme twice is then satisfied. A Langmuir adsorption isotherm expressing the concentration of adsorbed ammonia is shown in Equation (6.3).

$$\theta_{NH_3} = \frac{b_{NH_3} p_{NH_3}}{1 + b_{NH_3} p_{NH_3}} \qquad (6.3)$$

Equation (6.3) postulates that oxygen and water do not compete with ammonia for adsorption on those sites attracting ammonia. Nitrogen and nitrous oxide have been neglected in the denominator of Equation (6.3) for the same reason that they were neglected in Equation (6.1). Use of Equation (6.3) leads to a second order dependence of the nitrogen rate on ammonia pressure, however, which is inconsistent with the measurements shown in Figure 5.7. A first order dependence, in agreement with the experimental results, does occur if this approximation is made:

$$\theta_{NH_3} \cong B_{NH_3} P_{NH_3}^{1/2} \qquad (6.4)$$

It is now our task to find a sequence of surface steps which results in formation of nitrous oxide. Dissociatively adsorbed oxygen should enter this sequence twice, consistent with Figure 5.10; and ammonia should enter the sequence in a manner consistent with the ammonia influence expressed in Figure 5.8. For the first step, it is postulated that molecularly adsorbed ammonia reacts with two dissociatively adsorbed oxygens to form nitroxyl (HNO) and water. The double-participation of oxygen in this step satisfies the oxygen pressure dependence shown in Figure 5.10. Some nitrogen-containing species which exists independent of the concentration of dissociatively adsorbed oxygen should now react with the nitroxyl formed in the first step to yield nitrous oxide and perhaps other species. It is postulated that this reaction involves collision of a gas phase ammonia with the nitroxyl. The factor involving ammonia which then enters the nitrous oxide formation is

$$\frac{b_{NH_3} p_{NH_3}}{1 + b_{NH_3} p_{NH_3}} \cdot p_{NH_3} = \frac{b_{NH_3} p_{NH_3}^2}{1 + b_{NH_3} p_{NH_3}} \qquad (6.5)$$

Equation (6.5) indicates a second order dependence of the rate of formation of nitrous oxide on ammonia, inconsistent with the experimental measurements. Making the approximation shown in Equation (6.6),

$$\frac{b_{NH_3} p_{NH_3}^2}{1 + b_{NH_3} p_{NH_3}} \cong B'_{NH_3} P_{NH_3}^{1.35} \qquad (6.6)$$

the dependence of the rate of formation of nitrous oxide is in agreement with that determined experimentally and shown in Figure 5.8.

D. Rate Equations Corresponding to Proposed Mechanism

Referring to Figure 6.1, the rate of formation of nitrogen, controlled by Reaction 10, is

$$r_{N_2} = k_{N_2} (\theta_{NH})^2 \qquad (6.7)$$

The surface concentration of imide is developed from the reaction

$$NH_{3(ads)} + {}^{O}{}_{(ads)} = {}^{NH}{}_{(ads)} + H_2{}^{O}{}_{(gas)} \qquad (6.8)$$

which is assumed to proceed by the mechanism shown in Figure 6.1.

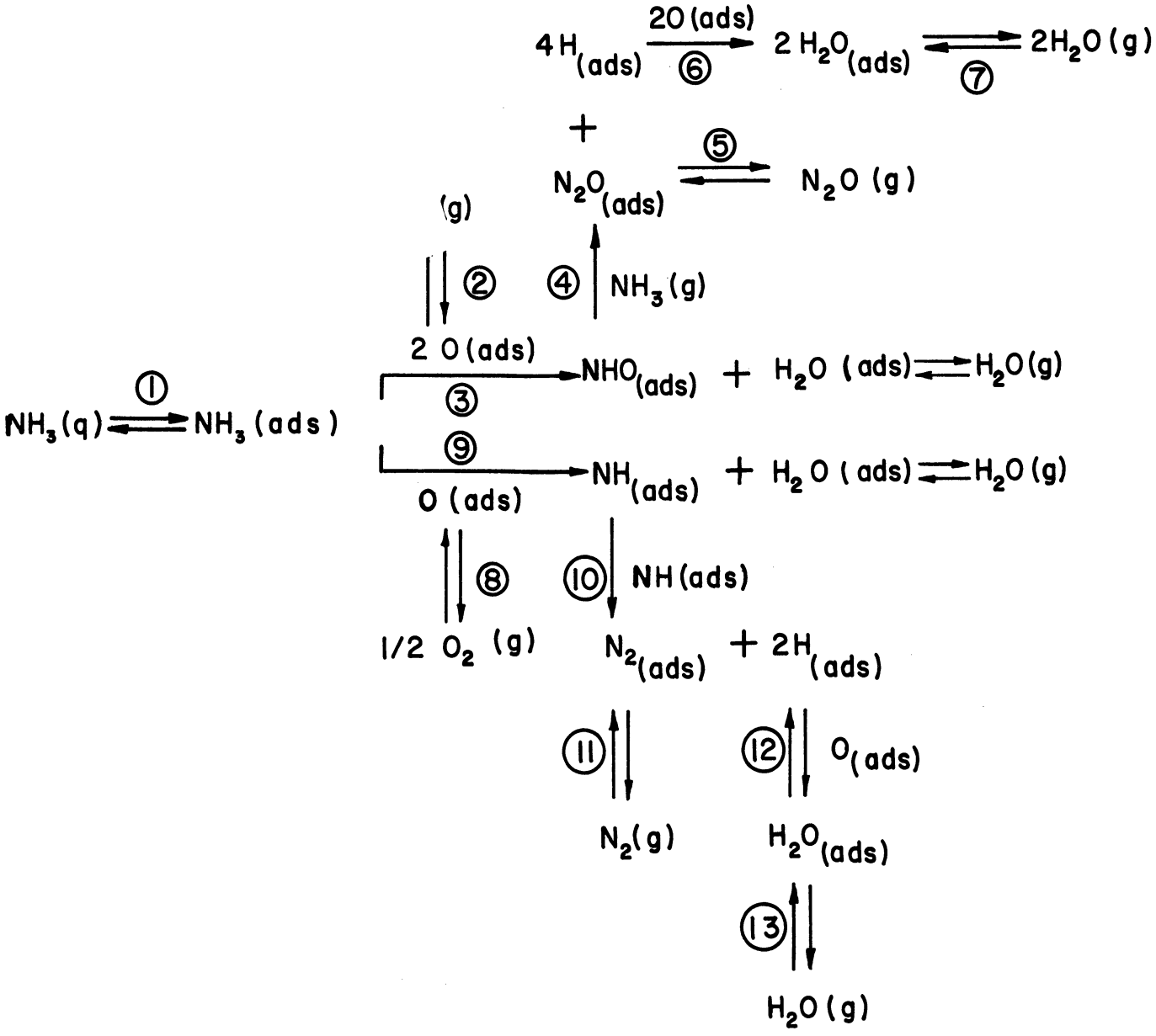

Figure 6.1. Illustration of Steps in Proposed Reaction Mechanism.

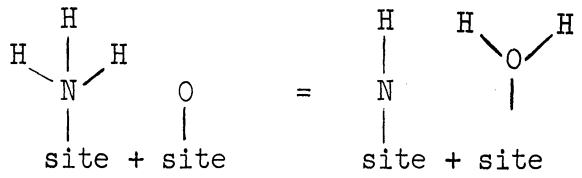

Figure 6.2. Mechanism for Reaction Between Adsorbed Ammonia and One Dissociatively Adsorbed Oxygen.

Reaction (6.8) is assumed to be at equilibrium and the reverse reaction is assumed to proceed independent of the concentration of adsorbed water, analogous to a pseudo monomolecular reaction.

$$K_{NH} = \frac{\theta_{NH}}{\theta_{NH_3}\ \theta_O} \quad ; \quad \text{or} \quad \theta_{NH} = K_{NH}\ \theta_{NH_3}\ \theta_O \tag{6.9}$$

Substituting Equation (6.9) into Equation (6.7),

$$r_{N_2} = k_{N_2}\ K_{NH}^2\ \theta_{NH_3}^2\ \theta_O^2 \tag{6.10}$$

Substituting expressions (6.4) and (6.2) for θ_{NH_3} and θ_O, respectively, Equation (6.10) becomes

$$r_{N_2} = \frac{K_{N_2}\ p_{O_2}\ p_{NH_3}}{(1 + b_{O_2}^{1/2}\ p_{O_2}^{1/2} + b_{H_2O}\ p_{H_2O})^2} \tag{6.11}$$

where

$$K_{N_2} = k_{N_2}\ K_{NH}^2\ B_{O_2}^2\ B_{NH_3}^2$$

The rate of nitrous oxide formation, assumed to be controlled by reaction 4, Figure 6.1, is

$$r_{N_2O} = k_{N_2O}\, p_{NH_3}\, \theta_{NHO} \tag{6.12}$$

The surface concentration of nitroxyl is determined by the reaction

$$NH_{3(ads)} + 2O_{(ads)} = NHO_{(ads)} + H_2O_{(gas)} \tag{6.13}$$

which is assumed to proceed by the mechanism shown in Figure 6.3.

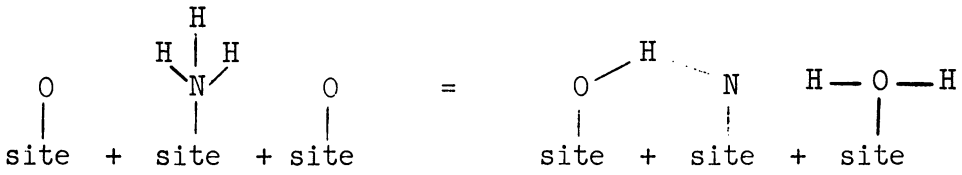

Figure 6.3. Mechanism for Reaction Between Adsorbed Ammonia and Two Dissociatively Adsorbed Oxygens.

Reaction (6.13) is also assumed to be at equilibrium and the reverse reaction is assumed to proceed independent of the concentration of adsorbed water, analogous to a pseudo monomolecular reaction.

$$K_{NHO} = \frac{\theta_{NHO}}{\theta_{NH_3}\,(\theta_O)^2} \quad ; \quad \text{or} \quad \theta_{NHO} = K_{NHO}\,\theta_{NH_3}\,\theta_O^2 \tag{6.14}$$

Substituting Equation (6.14) into Equation (6.12),

$$r_{N_2O} = k_{N_2O} K_{NHO} P_{NH_3} \theta_{NH_3} \theta_O^2 \qquad (6.15)$$

Substitution of expressions (6.3) and (6.2) for θ_{NH_3} and θ_O, respectively, in Equation (6.15) gives

$$r_{N_2O} = \frac{k_{N_2O} K_{NHO} B_{O_2} b_{NH_3} p_{NH_3} p_{O_2}}{(1 + b_{NH_3} p_{NH_3})(1 + b_{O_2}^{1/2} p_{O_2}^{1/2} + b_{H_2O} p_{H_2O})^2} \qquad (6.16)$$

Equation (6.6) is now used to substitute $B'_{NH_3} P_{NH_3}^{1.35}$ into Equation (6.16), yielding the final rate equation for the rate of nitrous oxide formation

$$r_{N_2O} = \frac{K_{N_2O} p_{NH_3}^{1.35} p_{O_2}}{(1 + b_{O_2}^{1/2} p_{O_2}^{1/2} + b_{H_2O} p_{H_2O})^2} \qquad (6.17)$$

where

$$K_{N_2O} = k_{N_2O} K_{NHO} B_{O_2} B'_{NH_3}$$

E. Evaluation of Constants in Rate Equations

The measurements obtained at each temperature were treated mathematically in a series of hand calculations to establish approximate values for the constants in Equations (6.11) and (6.17). Appendix C contains the details of the determination of the constants at 273°C. The final data fit was carried out by writing a computer program which would accept values of $b_{O_2}^{1/2}$ and b_{H_2O} and find the best K_{N_2} and K_{N_2O} by least squares methods. Table E in the Appendix lists the constants as a function of

temperature and shows the average percentage deviation between calculated and experimental rates.

F. Theoretical and Experimental Heats of Adsorption

The experimental heats of adsorption λ are related to the adsorption equilibrium constant b and absolute temperature T by the equation:

$$b = b_o \exp(\lambda/RT) \tag{6.18}$$

where b_o is constant. Plotting the logarithm of b against $1/T$ should give a straight line with slope equal to λ/R. Such plots for $b_{O_2}^{1/2}$ and b_{H_2O} have been shown in Figure 6.4. The adsorption heats for oxygen and water resulting from this figure are:

$$(\lambda_{O_2})_{exptl} = 11.3 \text{ kcal gm mole } O_2^{-1} \tag{6.19}$$

$$(\lambda_{H_2O})_{exptl} = 9.17 \text{ kcal gm mole } H_2O^{-1} \tag{6.20}$$

No completely satisfactory method has yet been developed for estimating theoretically the heat of adsorption. The method commonly employed is to postulate an adsorption mechanism and then express the heat effect accompanying the mechanism as a difference of bond energies. Estimation of bond energies involves knowledge of the dipole moments of the surface bonds, for which few data are available. Dipole moments approximated from differences in electronegativities have shown wide deviation from known dipole moments. The measured dipole moment for the O-Ni bond,

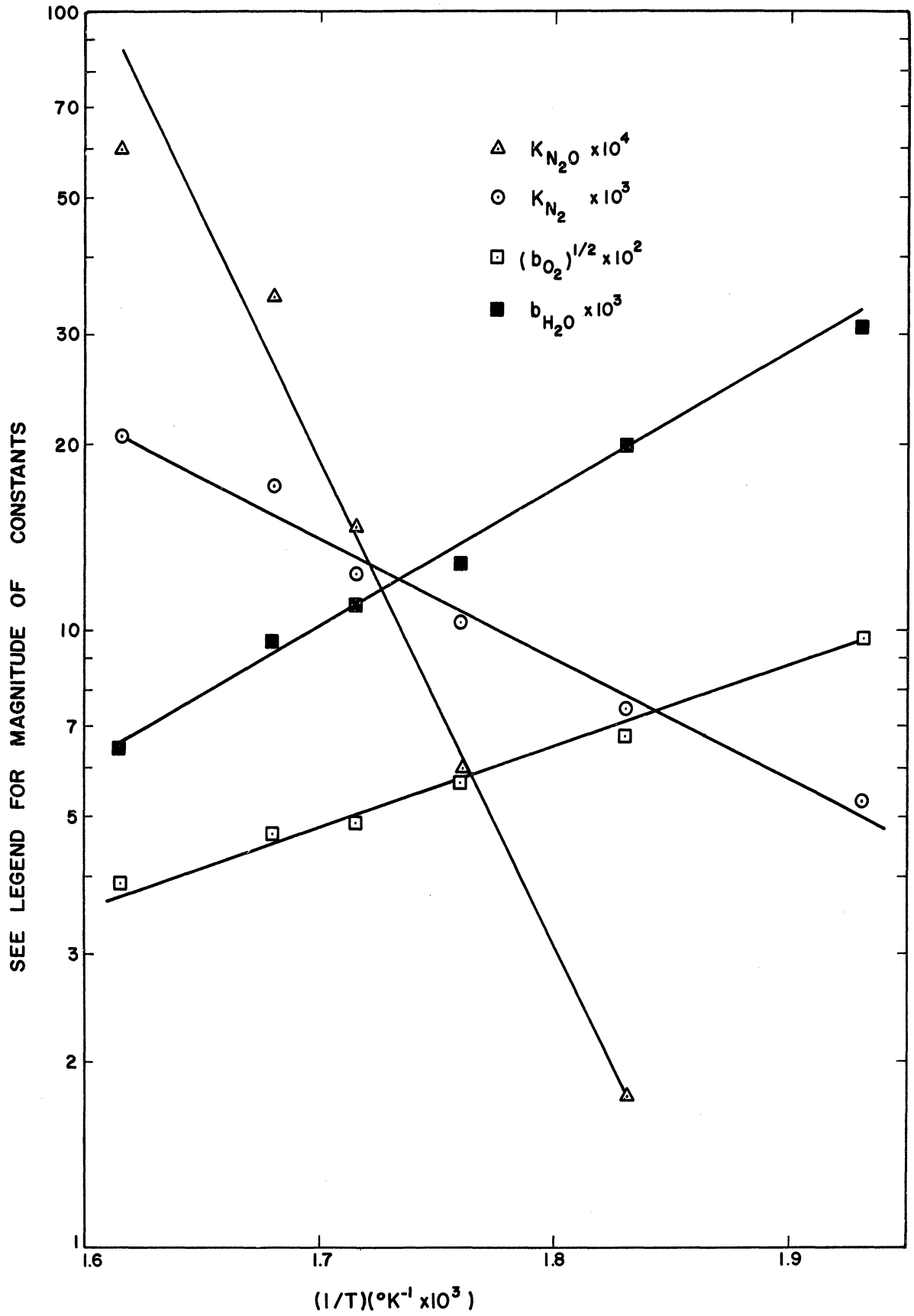

Figure 6.4. Temperature Dependence of Rate Equation Constants.

for example, is 0.78[51] whereas the dipole moment as estimated from electronegativity differences is 1.7, or 218% higher than the measured value. A further objection to using a difference of bond energies to approximate the heat of adsorption is that this procedure fails to take into account repulsive forces that may exist between neighboring adsorbed particles and also makes no allowance for heterogeneity of surface sites. Theoretically estimated heats of adsorption should therefore always be compared at best with differential adsorption heats determined experimentally at very low coverages. Figure 6.5 shows the adsorption mechanisms postulated for adsorption of oxygen and water. The notation "(Ru - Site)" indicates the state of ruthenium as deposited on the alumina carrier and functioning as an adsorption site.

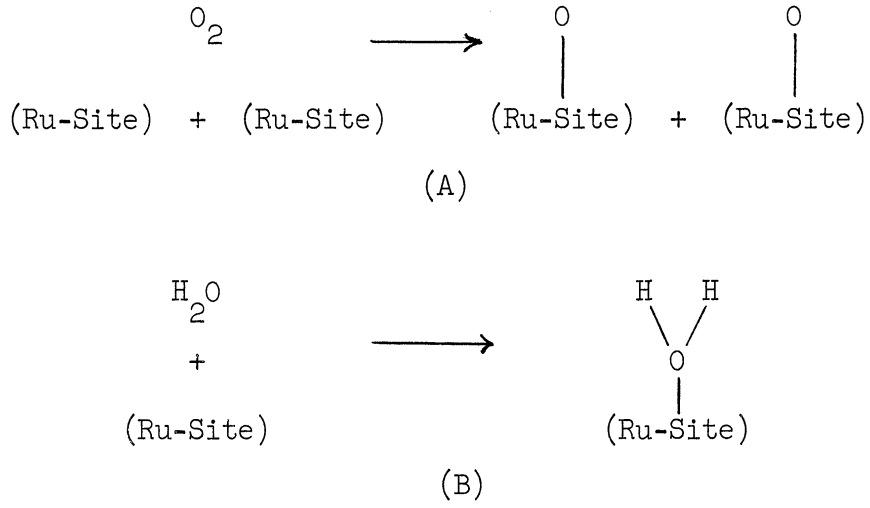

Figure 6.5. Mechanism 1 for Adsorption of Oxygen and Water on Ruthenium.

Energy equations corresponding to these mechanisms are:

$$(\lambda_{O_2})_{theo} = 2\,E\,[(Ru\text{-}Site)\text{-}O] - E\,[O_2] \qquad (6.21)$$

$$(\lambda_{H_2O})_{theo} = E\,[(Ru\text{-}Site)\text{-}OH_2] \qquad (6.22)$$

The energy terms represented in (6.21) and (6.22) are estimated by using the Pauling[40] equation for single bond energies. After application of the Pauling equation as discussed by Trapnell[51], (6.21) and (6.22) become

$$(\lambda_{O_2})_{theo} = E\,[Ru{=}Ru] + 46.12\,\mu^2 \qquad (6.23)$$

$$(\lambda_{H_2O})_{theo} = E\,[Ru\text{-}Ru] + 23.06\,\mu^2 \qquad (6.24)$$

E [Ru=Ru] is taken as one third the heat of sublimation of ruthenium and the dipole moment μ is assumed to be roughly equal to the difference in electronegativities of ruthenium and the adsorbed species. Electronegativity values are obtained from Pauling's table. Upon substitution of the appropriate values into Equations (6.23) and (6.24), there results:

$$(\lambda_{O_2})_{theo} = 131.3 \text{ kcal gm mole}^{-1} \qquad (6.25)$$

$$(\lambda_{H_2O})_{theo} = 65.7 \text{ kcal gm mole}^{-1} \qquad (6.26)$$

A sample calculation of $(\lambda_{O_2})_{theo}$ has been included in Appendix C.

An adsorption mechanism alternate to that in Figure 6.5 could also be assumed for adsorption on the ruthenium surface. In contrast to the mechanism depicted in Figure 6.5, the alternate mechanism would assume rupture of ruthenium surface bonds upon adsorption. This situation is pictured in Figure 6.6.

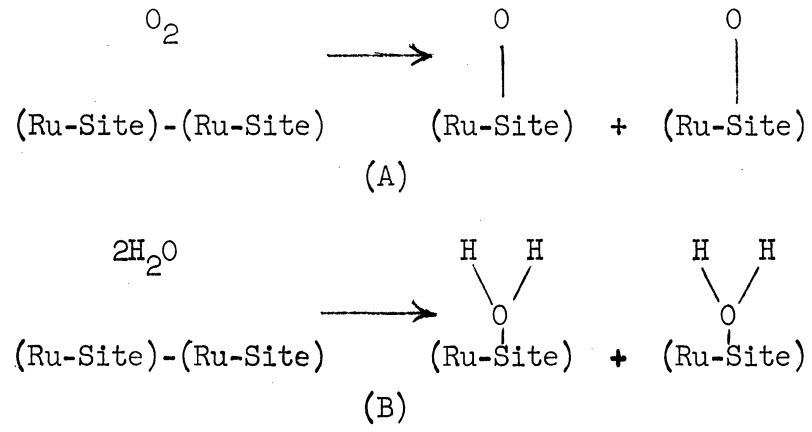

Figure 6.6. Mechanism 2 for Adsorption of Oxygen and Water on Ruthenium.

One surface bond would have to rupture to accomodate two oxygen atoms; the rupture of one surface bond would accomodate two water molecules. Adsorption heats corresponding to this alternate mechanism would be less than those given by Equations (6.25) and (6.26) by an amount equal to the appropriate metal bond energy. Using the previous assumption that rupture of one metal bond requires energy equal to one sixth the heat of sublimation, the theoretical adsorption heats are:

$$(\lambda_{O_2})_{theo} = 104.6 \text{ kcal gm mole}^{-1} \qquad (6.27)$$

$$(\lambda_{H_2O})_{theo} = 52.3 \text{ kcal gm mole}^{-1} \qquad (6.28)$$

In practice, adsorption might not result in complete bond ruptures as shown in Figure 6.6 but it would also probably not be completely without effect on the interaction between adjacent ruthenium surface atoms as supposed in Figure 6.5. An intermediate effect would lead to a theoretical adsorption heat between the values listed in Equations (6.25) and (6.26), (6.27) and (6.28).

Theoretical adsorption heats corresponding to either assumed adsorption mechanism are clearly much higher than the experimentally determined values. There is one order of magnitude discrepancy between the experimentally calculated and theoretical λ_{O_2} values; the discrepancy between experimental and theoretical λ_{H_2O} is half an order of magnitude. The limitations of the method used to estimate the theoretical values of the heat of adsorption have already been indicated, including its failure to account for possible repulsion of adjacent adsorbed molecules and possible heterogeneity of adsorption sites. A sample calculation in Appendix C shows that for typical reaction conditions encountered in the experimentation, approximately 35% surface coverage by atomic oxygen is in effect. Hence direct comparison of experimental and theoretical heats of adsorption is probably not strictly valid. A further point to bear in mind is that the experimental adsorption heats calculated here result from experimental measurements of rates of reactions and not from direct adsorption experimentation.

It is instructive to consider how marked the relationship between the heat of adsorption and the extent of surface coverage can be. Measurements taken by Sommerfeld[50] on the chemisorption of oxygen on ruthenium dioxide show a marked decrease in adsorption heat with increasing surface coverage. Sommerfeld found the heat of adsorption at 1% surface coverage to be 122.2 kcal gm mole^{-1}. At 11% surface coverage the adsorption heat had decreased to 12.2 kcal gm mole^{-1}. Here is an example, then, of variation in adsorption heat of one order of magnitude.

G. Theoretical and Experimental Adsorption Equilibrium Constant b_o ; Entropies of Adsorption

Values of the constant b_o appearing in Equation (6.18) can be computed when experimental values of b are known at two temperatures. The b_o value can also be estimated theoretically by two possible routes, using either a statistical approach or a kinetic approach. Results based on either approach are in order of magnitude agreement with each other. The kinetic consideration is the one used here.

At equilibrium, the rates of adsorption and desorption of a gas from a solid surface are equal. The rate of adsorption is taken equal to the rate of collision of gas phase molecules with the adsorbing surface. This rate, expressed as moles colliding per unit surface per unit time, is readily calculated from the kinetic theory of gases as

$$\frac{dn}{dt} = \frac{P}{\sqrt{2\pi MRT}} \qquad (6.29)$$

At equilibrium, the rate given in Equation (6.29) must equal the number of moles of adsorbed gas escaping from unit surface in unit time. Before a molecule can escape from the surface, it must possess a vibrational mode which involves at least as much energy as the heat of adsorption λ . The term $\exp(-\lambda/RT)$ gives the fraction of adsorbed molecules which possess this required energy. The product $\theta \exp(-\lambda/RT)$ then gives the fraction of surface covered with molecules satisfying the escape energy requirement. If the frequency of the pertinent vibration is v , the rate of change of covered surface per unit time due to escape from the surface is then

$$\frac{d\theta}{dt} = v\theta e^{-\lambda/RT} \tag{6.30}$$

The expression

$$n = \frac{\theta d}{V_m} \tag{6.31}$$

relates the thickness d of an adsorbed layer and the molecular volume V_m to the total moles adsorbed per unit surface at fractional coverage θ. Combination of (6.31) and (6.30) yields

$$\frac{dn}{dt} = \frac{vd\theta}{V_m} e^{-\lambda/RT} \tag{6.32}$$

Equating the rates given in (6.29) and (6.32),

$$\frac{P}{\sqrt{2\pi MRT}} = \frac{vd\theta}{V_m} e^{-\lambda/RT}, \quad \text{or}$$

$$\frac{\theta}{p} = \frac{V_m}{vd\sqrt{2\pi MRT}} e^{\lambda/RT} \tag{6.33}$$

But from the Langmuir adsorption isotherm.

$$\theta = \frac{bp}{1 + bp}, \quad \text{or}$$

$$b = \frac{\theta}{p(1-\theta)} \cong \frac{\theta}{p} = b_o e^{\lambda/RT} \tag{6.34}$$

The approximation made in (6.34) is quite good at low surface coverage and can be justified in this case even for intermediate coverage because an order of magnitude calculation is our concern here. Comparison of Equations (6.33) and (6.34) shows that

$$b_o = \frac{V_m}{vd\sqrt{2\pi MRT}} \qquad (6.35)$$

Evaluation of Equation (6.35) at 300°C for oxygen and water gives the values listed in Table VI-1.

TABLE VI-1

EXPERIMENTAL AND THEORETICAL VALUES OF b_o

	b_o Experimental mm Hg^{-1}	b_o Theoretical mm Hg^{-1}
Oxygen	$1.48 \cdot 10^{-8}$	$1.73 \cdot 10^{-8}$
Water	$3.99 \cdot 10^{-7}$	$1.49 \cdot 10^{-8}$

The experimental values of b_o as calculated from

$$\ln b = \frac{\lambda}{RT} + \ln b_o \qquad (6.36)$$

are also listed in Table IV-1. Appendix C contains sample calculations of both the experimental and theoretical b_o values for oxygen.

The theoretical and experimental b_o values for oxygen check very closely, whereas the experimental value for water is an order of magnitude higher than the theoretical value. Such deviation is not unusual. Kemball[26] suggests that in such cases the translational motion perpendicular to the surface is replaced by a vibration of lower frequency than

would ordinarily be expected. A smaller v appearing in the denominator of Equation (6.35) would have the effect of increasing the theoretical b_o value, tending to bring it into agreement with the experimental value.

The question may be posed, why do the b-values yield adsorption heats differing widely from theoretically-predicted values and yet give b_o's in close agreement with theory. The answer is that adsorption heats are directly proportional to the slope of the logarithm of b vs. 1/T plot, whereas the b_o's are computed from the intercept of this plot. Theory predicts straight lines having the same intercepts as found experimentally but with slopes greater than those found experimentally.

Experimental values of the entropy of adsorption are calculated by means of the thermodynamic relations

$$\Delta S = \frac{\Delta H - \Delta G}{T} \tag{6.37}$$

and

$$-\Delta G = RT \ln K_p \tag{6.38}$$

whence

$$\Delta S = \frac{\Delta H}{T} + R \ln K_p \tag{6.39}$$

where K_p is defined by the relation

$$K_p = \frac{\theta}{p(1-\theta)} \tag{6.40}$$

and is identical with the constant b in Langmuir's equation under the usual assumptions of monolayer adsorption, homogeneity of surface sites

and heat of adsorption independent of surface coverage. Application of Equation (6.39) to the cases for oxygen and water, using the experimental adsorption heats given by Equations (6.18) and (6.19), gives:

$$(\Delta S)_{O_2} \text{ exptl} = -23.1 \text{ e.u.} \tag{6.41}$$

$$(\Delta S)_{H_2O} \text{ exptl} = -13.6 \text{ e.u.} \tag{6.42}$$

We have assumed the validity of the Langmuir adsorption isotherm thus far. This requires, however, that the adsorbed species present on the surface are immobile. Postulating that oxygen and water lose three degrees of translational freedom upon adsorption, the loss in entropy expected to accompany the adsorption process is given by

$$(\Delta S)_{theo} = -{}_3S_{trans} + S_{config} \tag{6.43}$$

where ${}_3S_{trans}$ is the translational entropy of a perfect gas of molecular weight M at atmospheric pressure in three dimensions,

$${}_3S_{trans} = R\ln M^{3/2}T^{5/2} - 2.3 \tag{6.44}$$

and S_{config} is configurational entropy arising because the immobile adsorbed species may be distributed over the surface in a number of different ways.[26] For single site adsorption, as postulated for water,

$$S_{config} = R(x\ln x - (x - 1)\ln(x-1)) \tag{6.45}$$

and for dissociative adsorption, as postulated in the case of oxygen,

$$S_{config} = 2R\ 2(x-1/4)\ln(x-1/4) + \ln 2 - x\ln x - (x-1)\ln(x-1) \quad (6.46)$$

where $x = 1/\theta$. Applying these equations in the case of oxygen and water at 600°K, the entropies of adsorption expected if the adsorbed species are immobile and θ is taken as 1/2 appear in Table VI-2 together with the experimental values previously presented.

TABLE VI-2

EXPERIMENTAL AND THEORETICAL VALUES OF ADSORPTION ENTROPY

	$(\Delta S)_{exptl}$, e.u.	$(\Delta S)_{theo}$, e.u.
Oxygen	-23.1	-24.9
Water	-13.6	-35.2

A sample calculation is given for the case of oxygen in Appendix C.

The experimental entropies in Table VI-2 are larger than the corresponding theoretical entropies by 1.8 e.u. and 21.6 e.u. for oxygen and water, respectively. These values can be brought into closer agreement by consideration of S_{vib} , the entropy associated with the vibrational mode which has replaced the degree of translation perpendicular to the adsorbent surface. This vibrational entropy is given by

$$S_{vib} = R\left[\frac{h\nu}{kT}\left(e^{h\nu/kT}-1\right) - \ln\left(1-e^{-h\nu/kT}\right)\right] \quad (6.47)$$

If the frequency ν of the vibrational mode is sufficiently large, the vibrational entropy approaches zero and is usually neglected. In some cases of adsorption, however, the translational motion perpendicular to the surface may be replaced by a vibration of such low frequency that S_{vib} as calculated from (6.47) becomes significant. Kemball[26] has calculated values of the vibrational entropy from (6.47). His results show that at 600°K, if the pertinent vibrational frequency for oxygen is $3.1 \cdot 10^{12}$ sec^{-1}, a value for S_{vib} of approximately 1.8 e.u. results. This value makes the theoretical entropy of adsorption for oxygen equal to the experimental value.

The difference of 21.6 e.u. between the experimental entropy change for water and the value which is expected to result if immobile adsorption occurs can also be accounted for by the vibrational frequency consideration. If the vibrational frequency of the water molecule is approximately 10^9 sec^{-1}, the term S_{vib} amounts to 21 e.u. Hence immobile adsorption of water could occur in spite of the low experimental value for the entropy of adsorption.

H. Apparent and True Activation Energies

The energy of activation ΔE associated with a chemical reaction is found from the relationship:

$$\Delta E = -R \frac{d(\ln k)}{d(1/T)} \qquad (6.48)$$

where k is the rate constant corresponding to the reaction. When a series of steps is involved in a reaction, then the true activation energy is the

one corresponding to the assumed slow step. If the rate constant involved in the slow step were known, determination of the activation energy from Equation (6.48) would pose no problem. This rate constant is not, however, directly measured; rather all overall rate constant which includes the controlling rate constant as a factor is computed from the experimental data. This overall constant is the K_{N_2} and K_{N_2O} appearing in rate Equations (6.16) and (6.17), respectively, and tabulated in Appendix E. When Equation (6.27) is used with the overall rate K constant in place of k, the resulting ΔE is referred to as the apparent activation energy, as distinguished from the true activation energy. Apparent activation energies computed from the temperature dependence of K_{N_2} and K_{N_2O} are:

$$(\Delta E)_{N_2,\ \text{apparent}} = 8.83 \text{ kcal (mole)}^{-1} \tag{6.49}$$

$$(\Delta E)_{N_2O,\ \text{apparent}} = 34.9 \text{ kcal (mole)}^{-1} \tag{6.50}$$

The factors making up the overall rate constants are exhibited in Equations (6.51) and (6.52):

$$K_{N_2} = B_{NH_3}^2 \, B_{O_2}^2 \, K_{NH}^2 \, k_{N_2} \tag{6.51}$$

$$K_{N_2O} = B'_{NH_3} \, B_{O_2}^2 \, K_{NHO} \, k_{N_2O} \tag{6.52}$$

k_{N_2} and k_{N_2O} are the rate constants corresponding to the assumed slow steps; K_{NH} and K_{NHO} are the equilibrium constants for Steps 10 and 4, respectively, in the reaction mechanism, Figure 6.1. Taking logarithms on both sides in Equations (6.51) and (6.52), differentiating with respect to reciprocal absolute temperature, rearranging and introducing the gas constant R :

$$(\Delta E)_{N_2,\text{true}} = -R\frac{d\ln k_{N_2}}{d(1/T)} = -R\frac{d\ln K_{N_2}}{d(1/T)} + 2R\frac{d\ln B_{NH_3}}{d(1/T)} + 2R\frac{d\ln B_{O_2}}{d(1/T)} + 2R\frac{d\ln K_{NH}}{d(1/T)} \quad (6.53)$$

(1) (2) (3) (4) (5)

$$(\Delta E)_{N_2O,\text{true}} = -R\frac{d\ln k_{N_2O}}{d(1/T)} = -R\frac{d\ln K_{N_2O}}{d(1/T)} + R\frac{d\ln B'_{NH_3}}{d(1/T)} + 2R\frac{d\ln B_{O_2}}{d(1/T)} + R\frac{d\ln K_{NHO}}{d(1/T)} \quad (6.54)$$

(1) (2) (3) (4) (5)

Terms in Equations (6.53) and (6.54) have been numbered to facilitate reference to them. Terms 1 are the desired true activation energies. Terms 2 are the known apparent activation energies. Terms 3 involve the unknown heat of adsorption of ammonia on the catalyst surface. Terms 4 involve the known heat of adsorption of oxygen. Terms 5 express the unknown temperature dependence of the equilibrium constants for Steps 4 and 10 in Figure 6.1.

The heat of adsorption of ammonia could be computed theoretically by the method used to calculate the theoretical adsorption heats of oxygen and water. In view of the large differences between the theoretical and experimental values for both oxygen and water, however, the use of such a calculated value in Equations (6.53) and (6.54) comes into serious question. Terms 5 must also remain unknown until measurements are available for the heat effect accompanying formation of imide and water, and nitroxyl and water, from adsorbed ammonia and atomic oxygen. Hence there is insufficient information for estimation of the true activation energies of the reaction.

I. Absolute Rate Theory

Van Reijen and Schuit[53] have shown how absolute rate theory can be used in conjunction with a power rate law fit of kinetic data to predict the pre-exponential factor arising in the power rate law expression. They start on the basis that all adsorbed species are in equilibrium with the gas phase and proceed to represent the surface concentrations as a function of adsorption heats and differences of the free energy functions of the gaseous and adsorbed species. This representation is taken from statistical mechanical considerations. Next they assume that the free energy function of the adsorbed species is negligible and make the approximation that the temperature dependence of kT/h, gaseous free energy functions, adsorption heats and surface coverage has negligible effect on the activation energy of the reaction. From the power rate law data fit,

$$r = k_o \, p_A^m \, p_B^n \exp(-E/RT) \tag{6.55}$$

they observe that

$$E = -R \left[\frac{d\ln r}{d(1/T)} \right] \tag{6.56}$$

and

$$m = \left[\frac{d\ln r}{d\ln p_A} \right]_{T, p_B \text{ constant}} \tag{6.57}$$

They finally insert the surface concentration expression and Equations (6.56) and (6.57) into the rate expression derived by Laidler[34] in application of Eyring's[18] absolute rate theory, giving the final expression of interest:

$$(k_o)_{theo} = (kT/h)\exp(m\phi_{A/R})\exp(n\phi_{B/R}) \qquad (6.58)$$

In the case of ammonia oxidation, Equations (6.55) and (6.58) take the form

$$r_{N_2} = k_{o_{N_2}} p_{NH_3}^{a} p_{O_2}^{b} p_{H_2O}^{c} \exp [E_{N_2}/RT] \qquad (6.59)$$

$$r_{N_2O} = k_{o_{N_2O}} p_{NH_3}^{d} p_{O_2}^{e} p_{H_2O}^{f} \exp [E_{N_2O}/RT] \qquad (6.60)$$

$$(k_o)_{N_2 theo} = (kT/h)\exp[(a\phi_{NH_3} + b\phi_{O_2} + c\phi_{H_2O})/R] \qquad (6.61)$$

$$(k_o)_{N_2O theo} = (kT/h)\exp[(d\phi_{NH_3} + e\phi_{O_2} + f\phi_{H_2O})/R] \qquad (6.62)$$

It is observed that a distinction has been made between the oxygen and water exponents in Equations (6.59) and (6.60), even though Figures 5.9, 5.10, 5.13 and 5.14 demonstrate that both nitrogen and nitrous oxide formation rates are dependent in the same manner on oxygen and water partial pressures. It would be expected to follow in the rate fit that $b = e$ and $c = f$.

Equations (6.59) and (6.60) cannot be applied to data for which water was removed from the recycle stream, since the right hand side of the equations would then be zero and zero rates would be predicted. Disregarding, then, that portion of the data, the remaining data can be represented when the terms in the power rate law have these numerical values as determined by a least squares fit:

$$
\begin{aligned}
&a = 1. \\
&d = 1.35 \\
&b = e = .458 \\
&c = f = -.396 \\
&E_{N_2} = 12.6 \text{ kcal gm mol}^{-1} \\
&E_{N_2O} = 35. \text{ kcal gm mol}^{-1} \\
&(k_o)_{N_2 \text{ exptl}} = 2.01 \cdot 10^2 \text{ molecules site}^{-1} \text{ sec}^{-1} \\
&(k_o)_{N_2O \text{ exptl}} = 1.47 \cdot 10^9 \text{ molecules site}^{-1} \text{ sec}^{-1}
\end{aligned}
\qquad (6.63)
$$

Eighty six percent of the data for which the partial pressure of water is not zero are represented within $\pm$ 7% by the values listed in (6.63). The other 14% of the measurements correspond to low water partial pressures. As water pressure approaches zero, the power rate law becomes less capable of fitting the data. Only water pressures greater than about 5 cm Hg are included in the 86% of data predictable from the power rate law.

The activation energy E appearing in Equation (6.55) is calculated from Equation (6.56). A sample calculation of E is included in Appendix C for the nitrogen rate measurements.

The pre-exponential factors appearing in (6.59) and (6.60) can be computed from any arbitrarily-chosen rate measurement. A more representative value of these factors is, however, that value corresponding to a least squares fit of the data to Equations (6.59) and (6.60). The least squares fit actually determines values of the product of k_o and the exponential term. These values are shown in Table VI-1 as a function of temperature.

TABLE VI-3

EXPERIMENTAL PRE-EXPONENTIAL FACTORS IN POWER RATE LAW

Temp°C	$(k_o)_{N_2}\exp(-E_{N_2}/RT)$	$(k_o)_{N_2O}\exp(-E_{N_2O}/RT)$
246.2	.03[1]	
273.5	.0712	.00177[2]
296.1	.137	.00828
310.8	.191	.0228
322.2	.30	.057
345.5	.444	.126

[1]Units: $cm^3 min^{-1} gm^{-1} cm\ Hg^{-1.062}$
[2]Units: $cm^3 min^{-1} gm^{-1} cm\ Hg^{-1.412}$

A sample calculation of $(k_o)_{N_2\ exptl}$ is included in Appendix C. The free energy functions for ammonia, oxygen and water appearing in Equations (6.61) and (6.62) are listed in Appendix F. Using the values for a, b and c listed in (6.63) and the free energy function data given in Appendix F, these values result for the theoretical pre-exponential factors:

$$(k_o)_{N_2\ theo} = 9.1 \cdot 10^2 \text{ molecules site}^{-1} \text{ sec}^{-1} \qquad (6.64)$$

$$(k_o)_{N_2O\ theo} = 0.97 \cdot 10^9 \text{ molecules site}^{-1} \text{ sec}^{-1} \qquad (6.65)$$

A sample calculation of $(k_o)_{N_2\ theo}$ is presented in Appendix C. The theoretical k_o values are seen to be within an order of magnitude of the values listed in (6.63). Hence measured rates are in good agreement with rates predicted by van Reijen and Schuit's application of absolute rate theory.

VII SUMMARY AND CONCLUSIONS

These results have been obtained in this study:

1. An experimental system facilitating precise rate measurements was built and used to determine the partial pressure and temperature dependence of the oxidation of ammonia over supported ruthenium. Reaction conditions were essentially uniform over the whole length of the catalyst bed. Conversion per pass was at all times under two percent. Pressure drop across the catalyst bed was negligible relative to total reaction pressure. The drop in ammonia pressure between the bulk gas and the catalyst surface was calculated to be less than 1.5%. The temperature difference between the catalyst surface and the entering gas stream did not exceed 3°C in the worst case. At the highest temperature studied, 345°C, measured reaction rates remained the same even after the mass transfer coefficient was increased by approximately 35%, demonstrating that mass transfer was not the rate-determining step.

2. Rates of formation of both nitrogen and nitrous oxide were found to depend on the partial pressures of ammonia, oxygen and water and to be independent of nitrogen and nitrous oxide. Increasing water pressure inhibited both rates to the same extent, whereas increasing oxygen pressure promoted both rates

to the same extent. Increasing ammonia pressure favored the relative rate of formation of nitrous oxide. The maximum nitrous oxide yield was about 45%.

3. From the observed rate dependencies two rate equations, expressing formation rates of nitrogen and nitrous oxide, respectively, were developed. The constants appearing in these equations were evaluated as a function of temperature. Logarithmic plots of the various constants vs. reciprocal absolute temperature yielded straight line relationships. The rate equations fit the data with a deviation of $\pm$ 3.2%.

4. Apparent activation energies, heats of adsorption and entropies of adsorption were evaluated from the temperature dependence of the rate equation constants. The two latter effects were compared with theoretically-estimated adsorption heats and entropies. The adsorption heat of oxygen was low, in line with speculation that oxidation catalysts hold chemisorbed oxygen loosely. The entropies of adsorption of oxygen and water correspond to immobile adsorption of these species if the degree of translation normal to the solid surface is replaced with a vibrational mode having a low frequency.

5. A reaction mechanism consistent both with the observed pressure dependencies and with the interrelationship of these dependencies was developed.

6. The data were fit with a power rate law and the resulting pre-exponential factor was compared with a calculated pre-exponential factor based on absolute rate theory. Order of magnitude agreement resulted.

The results of this study are seen as a unique contribution to the literature on the subject of ammonia oxidation. The exact dependence of the rate of ammonia oxidation on the partial pressures of oxygen, ammonia, water, nitrous oxide and nitrogen had not been previously determined. Such factors as temperature, partial pressures and mass transfer were not this carefully controlled to facilitate taking precise rate measurements. Rate equations expressing formation rate of products had also not been previously presented. Further work on this system should include studies of the adsorption of the various species on the catalyst surface. Continued studies over the ruthenium catalyst with a different range of ammonia and oxygen partial pressures might lead to changed reaction rate behavior which in turn might be related to the reaction mechanism. Low pressure studies conducted in conjunction with a mass spectrometer could conceivably yield useful information concerning reaction intermediates. Study of the reaction over the various oxides of ruthenium might also provide information with which to speculate with more certitude about the reaction mechanism.

APPENDICES

APPENDIX A

CALIBRATION OF FLOW METERS

The flow meters used in this work have been described on page 20 and their calibration has been detailed on page 30. Figure A.1 shows the results of such calibration for Matheson Tube 203, using both a stainless steel and a sapphire float and a feed composition of 9.7 volume percent ammonia, balance oxygen. Data used in the figure, as well as data for the other two ammonia-oxygen feed compositions used, appear in Table A-1.

TABLE A-1

FLOWMETER CALIBRATION MEASUREMENTS

Tube Reading/Feed:	1[a]	2[b]	3[c]
9[d]	205	206	208
11[d]	277	281	290
13[d]	355	357	363
15[d]	434	440	450
17[d]	523	529	544
7[e]	253	254	256
9[e]	367	366	369
11[e]	471	475	490
13[e]	590	598	610
15[e]	712	725	742
17[e]	889	899	925

a: 5.3 Volume Percent NH_3, Balance O_2
b: 9.7 Volume Percent NH_3, Balance O_2
c: 16.5 Volume Percent NH_3, Balance O_2
d: Sapphire Float
e: Stainless Steel Float

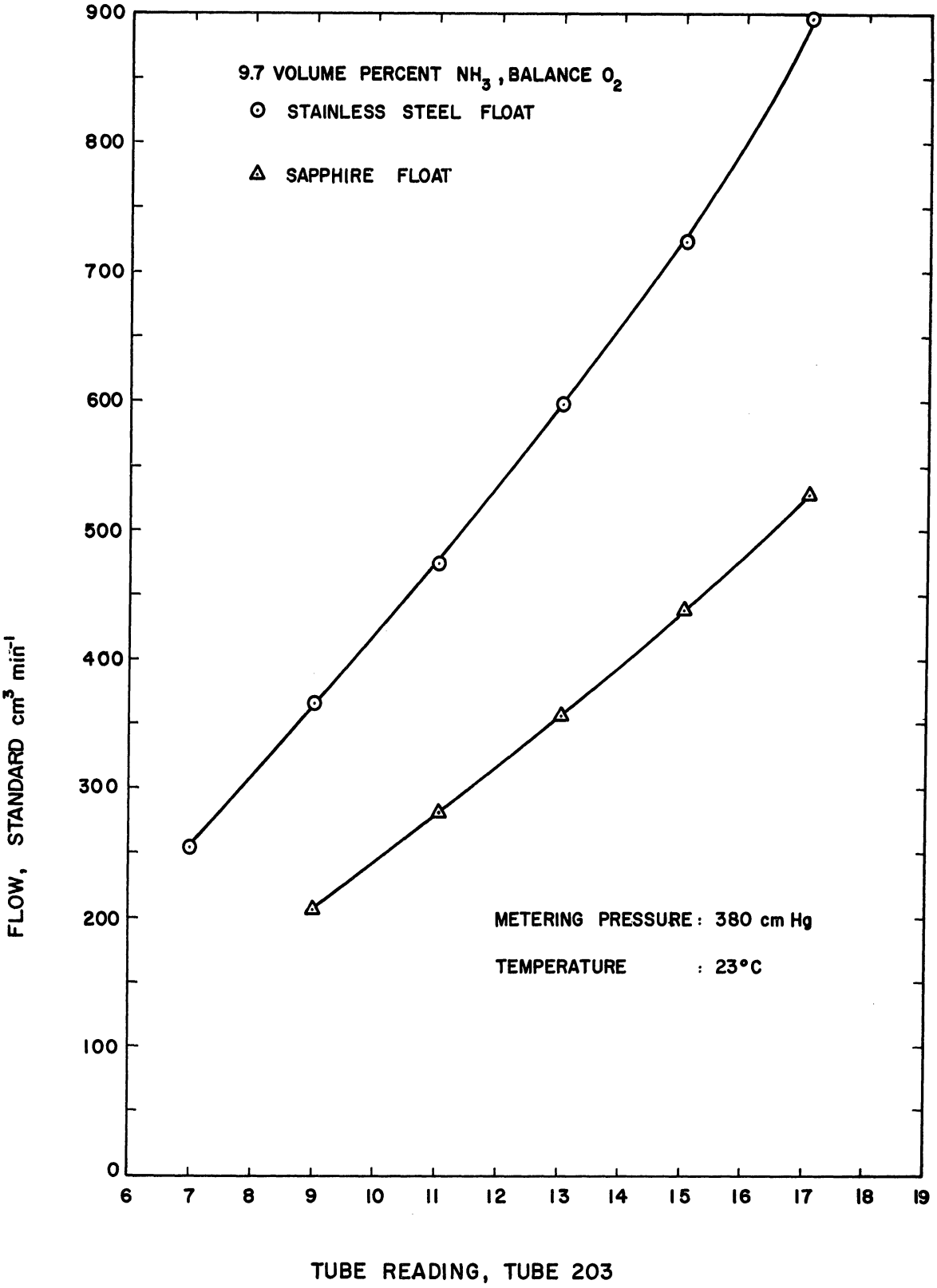

Figure A.1. Flowmeter Calibration Curve for 9.7 Volume Percent Ammonia, Balance Oxygen, Feed.

Nitrogen, nitrous oxide and helium were also used as a portion of the feed stream in a limited number of runs. Calibration data for these three gases over a range of tube readings is shown in Figure A.2. In practice, only one feed rate was used for each of these gases: 7.1 std. cm^3 min^{-1} N_2; 8.75 std. cm^3 min^{-1} N_2O; and 275 std. cm^3 min^{-1} He.

Conversion of the raw rates to standard conditions is trivial and will not be shown here.

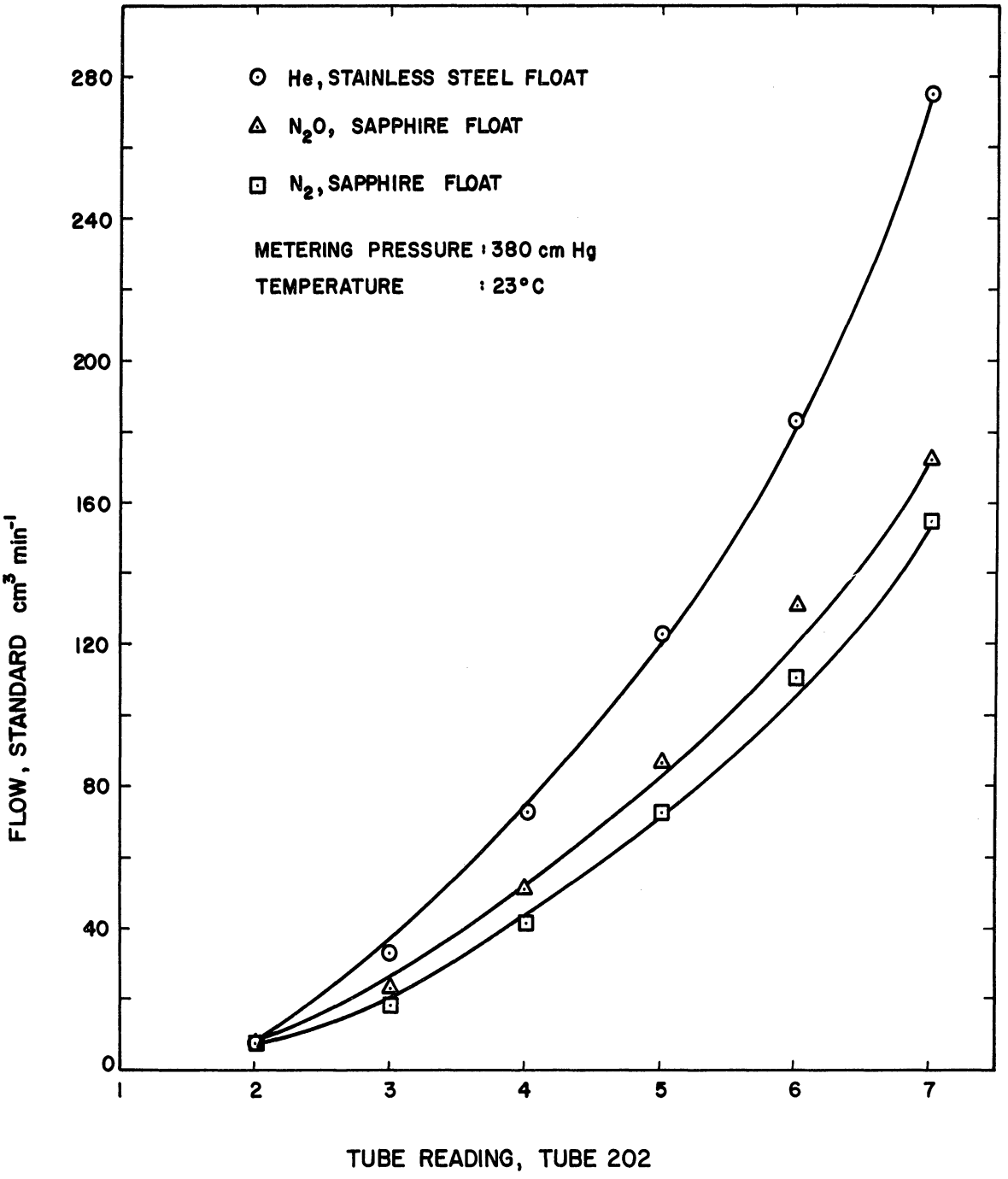

Figure A.2. Flowmeter Calibration Curves for Helium, Nitrogen and Nitrous Oxide.

APPENDIX B

EXPERIMENTAL DATA

In this appendix are presented the experimental values of partial pressures of ammonia, oxygen and water, and the values of the rate of formation of nitrogen and nitrous oxide. The rates of formation of nitrogen and nitrous oxide as calculated from the constants used to fit the experimental measurements are also listed, together with the percentage deviation between experimental and predicted values.

TABLE B-1

EXPERIMENTAL VALUES OF PARTIAL PRESSURES
AND RATES OF PRODUCT FORMATION

Measurement No.	Contact Time, min · 10^3	P_{NH_3}, cm Hg	P_{O_2}, cm Hg	P_{H_2O}, cm Hg	$Rate_{N_2}$ (Data), $cm^3\ min^{-1}\ gm^{-1}$	$Rate_{N_2}$ (Calc), $cm^3\ min^{-1}\ gm^{-1}$	% Dev	$Rate_{N_2O}$ (Data), $cm^3\ min^{-1}\ gm^{-1}$	$Rate_{N_2O}$ (Calc), $cm^3\ min^{-1}\ gm^{-1}$	% Dev
	Run No. R1, T = 246.2°C, P = 176 cm Hg, Feed 9.7 Volume Percent NH_3, Balance O_2									
1	0.112	16.5	158.1	0.7	2.78	2.75	1.1			
2	0.212	16.2	158.1	1.2	2.63	2.66	-1.1			
3	0.394	15.7	158.1	2.0	2.36	2.52	-6.3			
4	0.560	15.0	157.1	2.9	2.36	2.35	0.4			
5	0.952	14.2	156.0	4.2	2.00	2.13	-6.1			
6	1.42	13.0	155.5	6.0	1.90	1.86	2.1			
7	1.79	12.6	155.0	6.6	1.67	1.77	-5.7			
8	2.44	11.5	154.0	8.1	1.50	1.56	-3.8			
	Run No. R2, T = 246.2°C, P = 216 cm Hg, Feed 5.3 Volume Percent NH_3, Balance O_2									
1	0.0815	11.1	204.6	0.5	2.05	2.09	-1.9			
2	0.154	10.7	204.1	1.4	1.86	1.96	-5.1			
3	0.286	10.0	203.6	2.0	1.91	1.81	5.5			
4	0.408	9.7	203.1	2.6	1.68	1.72	-2.3			
5	0.695	8.6	202.0	3.7	1.58	1.48	6.6			
6	1.02	7.9	201.5	5.2	1.36	1.31	3.8			
7	1.31	7.5	200.5	5.7	1.16	1.22	-4.9			
8	1.77	6.7	199.9	6.9	1.04	1.07	-2.8			
	Run No. R3, T = 246.2°C, P = 280 cm Hg, Feed 16.5 Volume Percent NH_3, Balance O_2									
1	0.0605	44.1	231.5	2.9	7.91	8.20	-3.5			
2	0.114	41.9	231.0	5.3	7.38	7.36	0.3			
3	0.218	39.7	227.9	9.1	6.59	6.36	3.6			
4	0.302	38.0	226.3	11.7	6.14	5.72	7.3			
5	0.515	35.6	223.2	14.9	4.64	4.97	-6.6			
6	0.772	32.1	221.1	20.0	4.19	4.01	4.2			
7	0.965	30.4	218.6	23.9	3.74	3.49	7.1			
8	1.35	28.4	216.0	25.3	3.05	3.15	-3.2			
	Run No. R4, T = 246.2°C, P = 280 cm Hg, Feed 16.5 Volume Percent NH_3, Balance O_2									
1	0.302	38.0	236.1	0.0	7.57	7.67	-1.3			
2	0.515	33.0	238.2	0.0	7.01	6.69	4.8			
3	0.772	29.5	240.3	0.0	5.81	5.99	-3.0			
4	0.965	26.6	240.3	0.0	5.54	5.40	2.6			
5	1.35	22.7	241.8	0.0	4.57	4.63	-1.3			
	Run No. R5, T = 246.2°C, P = 176 cm Hg, Feed 9.7 Volume Percent NH_3, Balance O_2									
1	0.560	15.3	160.2	0.0	2.55	2.61	-2.3			
	Run No. 6, T = 246.2°C, P = 276 cm Hg, Feed 5.3 Volume Percent NH_3, Balance O_2									
1	0.560	9.7	205.7	0.0	1.86	1.84	1.1			
	Run No. R7, T = 246.2°C, P = 216 cm Hg, Feed 16.5 Volume Percent NH_3, Balance O_2									
1	0.667	31.4	182.4	0.0	5.47	5.68	-3.7			
	Run No. R8, T = 246.2°C, P = 74.5 cm Hg, Feed 9.7 Volume Percent NH_3, Balance O_2									
1	0.830	7.0	67.2	0.0	0.81	0.78	3.8			
	Run No. R9, T = 273.5°C, P = 176 cm Hg, Feed 16.5 Volume Percent NH_3, Balance O_2									
1	0.103	27.6	145.7	2.2	9.22	8.67	6.4	0.660	0.656	0.6
2	0.195	26.5	144.7	3.9	8.36	8.01	4.2	0.577	0.598	-3.5
3	0.372	24.8	142.6	6.4	6.82	7.04	-3.2	0.495	0.513	-3.5
4	0.515	23.4	141.6	8.4	6.52	6.36	2.6	0.461	0.454	1.5
5	0.877	21.2	139.5	11.6	5.29	5.36	-1.3	0.366	0.370	-1.1
6	1.32	19.2	137.5	14.4	4.20	4.54	-7.5	0.303	0.303	0.0
7	1.65	17.8	135.9	16.5	4.09	4.02	1.7	0.259	0.261	-0.8
8	2.29	16.1	134.4	19.0	3.36	3.46	-2.9	0.205	2.217	-5.5
	Run No. R10, T = 273.5°C, P = 216 cm Hg, Feed 9.7 Volume Percent NH_3, Balance O_2									
1	0.0772	19.4	193.8	2.0	6.90	7.13	-3.2	0.472	0.476	-0.8
2	0.146	18.6	192.2	3.4	6.22	6.63	-6.2	0.409	0.437	-6.4
3	0.272	16.7	190.7	6.2	5.40	5.63	-4.1	0.335	0.357	-6.1
4	0.374	15.6	190.2	7.9	4.87	5.07	-3.9	0.310	0.314	1.3
5	0.655	13.5	188.6	11.3	4.09	4.09	0.0	0.239	0.241	-0.8
6	0.970	11.7	187.1	13.7	3.37	3.39	-0.6	0.193	0.190	1.6
7	1.24	10.4	185.5	15.2	3.01	2.90	3.8	0.156	0.156	0.0
8	1.68	9.5	184.0	16.9	2.44	2.57	-5.0	0.126	0.134	-6.0

TABLE B-1 (CONT'D)

Measurement No.	Contact Time, min · 10^3	P_{NH_3}, cm Hg	P_{O_2}, cm Hg	P_{H_2O}, cm Hg	$Rate_{N_2}$ (Data), $cm^3\ min^{-1}\ gm^{-1}$	$Rate_{N_2}$ (Calc), $cm^3\ min^{-1}\ gm^{-1}$	% Dev	$Rate_{N_2O}$ (Data), $cm^3\ min^{-1}\ gm^{-1}$	$Rate_{N_2O}$ (Calc), $cm^3\ min^{-1}\ gm^{-1}$	% Dev
	Run No. R11, T = 273.5°C, P = 280 cm Hg, Feed 5.3 Volume Percent NH_3, Balance O_2									
1	0.0602	13.2	263.6	2.4	5.74	5.62	2.1	0.322	0.327	-1.5
2	0.114	12.1	262.0	3.9	4.99	5.02	-0.6	0.277	0.284	-2.4
3	0.212	10.5	261.0	6.3	4.31	4.12	4.6	0.231	0.224	3.1
4	0.301	9.5	261.0	7.9	3.82	3.63	5.2	0.195	0.188	3.7
5	0.513	8.0	258.4	10.1	2.89	2.93	-1.4	0.132	0.143	-7.7
6	0.755	6.8	256.9	12.0	2.29	2.42	-5.4	0.106	0.112	-5.4
7	0.967	5.9	255.8	13.3	1.99	2.04	-2.5	0.0832	0.0896	-3.8
8	1.31	4.8	255.3	14.8	1.66	1.63	2.0	0.0637	0.0666	-4.3
	Run No. R12, T = 273.5°C, P = 280 cm Hg, Feed 16.5 Volume Percent NH_3, Balance O_2									
1	0.0578	41.8	228.9	6.4	15.4	15.4	0.0	1.35	1.34	0.7
2	0.109	38.9	226.9	10.5	13.5	13.3	1.5	1.15	1.13	1.8
3	0.209	35.0	218.1	16.3	10.9	10.5	3.8	0.915	0.866	5.7
4	0.289	32.5	221.2	20.2	9.7	9.3	4.3	0.791	0.740	7.0
5	0.492	28.1	216.0	26.3	7.1	7.1	0.0	0.581	0.542	7.2
6	0.738	25.7	212.9	29.5	5.7	6.1	-6.5	0.431	0.453	-4.6
7	0.925	23.1	211.4	33.3	5.2	5.2	0.0	0.362	0.370	-2.1
8	1.28	19.5	208.3	38.4	4.3	4.0	7.5	0.282	0.270	4.5
	Run No. R13, T = 273.5°C, P = 280 cm Hg, Feed 16.5 Volume Percent NH_3, Balance O_2									
1	0.289	31.6	238.3	0.0	12.4	13.4	-7.4	1.01	1.06	-4.7
2	0.492	24.6	238.3	0.0	10.5	10.5	0.0	0.746	0.762	-2.1
3	0.738	19.2	241.3	0.0	8.59	8.22	4.5	0.559	0.546	2.4
4	0.925	17.5	242.9	0.0	7.12	7.51	-5.2	0.461	0.483	-4.5
5	1.28	12.9	244.4	0.0	5.89	5.57	5.4	0.322	0.323	0.3
	Run No. R14, T = 273.5°C, P = 280 cm Hg, Feed 5.3 Volume Percent NH_3, Balance O_2									
1	0.513	7.33	267.7	0.0	3.28	3.29	-0.3	0.151	0.156	-3.2
	Run No. R15, T = 273.5°C, P = 216 cm Hg, Feed 9.7 Volume Percent NH_3, Balance O_2									
1	0.656	12.9	199.0	0.0	4.80	5.02	-4.4	0.285	0.291	-2.0
	Run No. R16, T = 273.5°C, P = 176 cm Hg, Feed 16.5 Volume Percent NH_3, Balance O_2									
1	0.878	20.4	149.9	0.0	6.97	6.85	1.8	0.476	0.465	2.4
	Run No. R17, T = 273.5°C, P = 251 cm Hg, Feed 16.5 Volume Percent NH_3, Balance O_2									
1	1.04	20.8	190.7	29.0	5.17	4.68	10.5	0.332	0.320	3.7
2	1.43	19.2	188.6	32.3	4.05	4.08	-0.7	0.259	0.271	-4.4
3	2.92	16.2	185.0	36.3	3.15	3.21	-1.9	0.182	0.201	-9.5
4	8.38	11.4	181.9	43.2	2.04	2.02	1.0	0.110	0.112	-1.8
	Run No. R18, T = 296.1°C, P = 176 cm Hg, Feed 16.5 Volume Percent NH_3, Balance O_2									
1	0.988	26.6	144.7	3.5	13.5	13.5	0.0	2.44	2.39	2.0
2	0.186	24.8	142.6	6.3	11.9	12.0	-0.8	2.05	2.07	-0.9
3	0.357	22.3	140.6	9.9	9.86	10.1	-2.3	1.71	1.68	1.8
4	0.495	20.7	139.0	12.3	8.85	8.98	-1.4	1.46	1.45	0.7
5	0.840	18.0	137.0	16.2	7.09	7.31	-3.0	1.16	1.13	2.7
6	1.26	14.9	133.9	20.7	5.96	5.60	6.4	0.862	0.807	6.8
7	1.58	14.0	132.8	21.7	5.10	5.17	-1.3	0.709	0.730	-2.9
8	2.20	11.7	130.7	25.2	4.24	4.07	4.2	0.581	0.539	7.8
	Run No. R19, T = 296.1°C, P = 216 cm Hg, Feed 9.7 Volume Percent NH_3, Balance O_2									
1	0.074	18.2	192.2	3.7	10.9	10.9	0.0	1.78	1.68	+6.0
2	0.140	16.7	190.7	6.3	9.52	9.58	-0.6	1.43	1.44	-0.7
3	0.261	14.6	189.1	9.4	7.91	7.97	-0.8	1.16	1.14	1.8
4	0.370	13.0	187.6	11.9	6.86	6.79	1.0	0.952	0.934	1.9
5	0.628	10.3	181.9	15.9	5.32	5.03	5.8	0.716	0.639	11.0
6	0.930	9.0	183.5	17.5	4.16	4.33	-3.9	0.529	0.525	0.8
7	1.18	7.8	182.4	19.4	3.59	3.63	-1.1	0.420	0.418	0.5
8	1.61	6.5	181.4	21.0	2.92	2.96	-1.4	0.326	0.319	2.2
	Run No. R20, T = 296.1°C, P = 280 cm Hg, Feed 5.3 Volume Percent NH_3, Balance O_2									
1	0.0578	12.1	262.5	3.7	8.92	8.58	3.9	1.19	1.15	3.5
2	0.109	10.7	260.5	6.1	7.05	7.32	-3.8	0.960	0.942	1.9
3	0.203	9.2	258.4	9.0	5.81	6.04	-3.8	0.724	0.738	-1.9
4	0.289	7.5	257.1	10.8	4.76	4.78	-0.4	0.555	0.542	2.4
5	0.492	6.0	255.8	12.9	3.54	3.70	-4.3	0.386	0.389	-0.8
6	0.724	4.8	255.6	14.9	2.79	2.89	-3.4	0.281	0.281	0.0
7	0.928	4.2	255.3	15.9	2.39	2.48	-3.6	0.236	0.230	2.6
8	1.25	3.2	252.2	17.3	1.87	1.83	2.2	0.158	0.161	-1.8
	Run No. R21, T = 296.1°C, P = 280 cm Hg, Feed 16.5 Volume Percent NH_3, Balance O_2									
1	0.109	29.8	219.1	23.8	14.6	14.7	-0.7	2.80	2.70	3.7
2	0.203	26.9	216.5	28.1	12.6	12.5	0.8	2.29	2.21	3.6
3	0.492	22.0	212.4	35.1	9.26	9.27	-0.1	1.67	1.53	9.1
4	0.724	19.1	206.7	39.0	7.09	7.56	-5.9	1.20	1.19	0.8
5	0.927	16.5	205.2	42.7	6.22	6.24	-0.3	0.915	0.930	-1.6
6	1.25	13.9	203.1	46.7	4.95	4.97	-0.4	0.660	0.699	-5.0

TABLE B-1 (CONT'D)

Measurement No.	Contact Time, min · 10^3	P_{NH_3}, cm Hg	P_{O_2}, cm Hg	P_{H_2O}, cm Hg	$Rate_{N_2}$ (Data), $cm^3\ min^{-1}\ gm^{-1}$	$Rate_{N_2}$ (Calc), $cm^3\ min^{-1}\ gm^{-1}$	% Dev	$Rate_{N_2O}$ (Data), $cm^3\ min^{-1}\ gm^{-1}$	$Rate_{N_2O}$ (Calc), $cm^3\ min^{-1}\ gm^{-1}$	% Dev
	Run No. R22, T = 296.1°C, P = 216 cm Hg, Feed 9.7 Volume Percent NH_3, Balance O_2									
1	0.74	18.5	196.3	0.0	12.1	11.8	2.5	1.89	1.84	2.7
2	0.140	17.1	198.4	0.0	10.2	10.9	-6.4	1.54	1.66	-7.2
3	0.261	14.3	197.4	0.0	8.81	9.13	-3.5	1.30	1.30	0.0
4	0.370	12.9	198.4	0.0	7.57	8.29	-8.7	1.03	1.14	-9.6
5	0.930	7.7	202.6	0.0	4.91	5.00	-1.8	0.555	0.573	-3.2
6	1.18	6.3	203.1	0.0	4.23	4.08	3.7	0.446	0.436	2.3
	Run No. R23, T = 296.1°C, P = 176 cm Hg, Feed 16.5 Volume Percent NH_3, Balance O_2									
1	1.58	12.2	153.4	0.0	6.34	6.78	-6.5	0.877	0.912	-3.8
	Run No. R24, T = 296.1°C, P = 280 cm Hg Feed 16.5 Volume Percent NH_3, Balance O_2									
1	0.472	16.3	242.4	0.0	11.7	11.6	+.9	1.78	1.73	2.9
	Run No. R25, T = 296.1°C, P = 280 cm Hg, Feed 5.3 Volume Percent NH_3, Balance O_2									
1	0.109	10.5	266.1	0.0	7.91	7.90	+0.1	1.07	1.01	6.0
	Run No. R26, T = 296.1°C, P = 176 cm Hg, Feed 9.7 Volume Percent NH_3, Balance O_2									
1	0.762	6.9	67.2	0.0	2.24	2.30	-2.6	0.255	0.253	0.8
	Run No. R27, T = 296.1°C, P = 251 cm Hg, Feed 16.5 Volume Percent NH_3, Balance O_2									
1	0.985	15.6	185.0	37.3	6.04	5.88	2.7	0.885	0.863	2.5
2	1.37	13.3	183.5	40.5	4.80	4.77	0.6	0.709	0.662	7.1
3	2.80	10.5	180.9	44.5	3.64	3.57	2.0	0.461	0.467	-0.1
4	4.39	6.9	176.2	49.7	2.24	2.17	3.2	0.251	0.239	5.0
5	8.03	4.8	174.7	52.7	1.55	1.46	6.1	0.144	0.143	0.7
	Run No. R28, T = 310.8°C, P = 176 cm Hg, Feed 16.5 Volume Percent NH_3, Balance O_2									
1	0.0965	25.3	143.7	5.5	16.8	16.6	1.2	6.26	6.13	2.1
2	0.183	23.2	141.6	8.7	14.0	14.4	-2.8	5.17	5.17	0.0
3	0.348	19.7	138.0	13.5	11.7	11.3	3.5	4.01	3.83	4.7
4	0.822	14.8	133.9	20.7	7.61	7.61	0.0	2.40	2.33	3.0
5	1.23	12.4	131.3	24.1	6.19	6.04	2.5	1.79	1.74	2.9
6	2.15	9.7	128.2	28.1	4.24	4.41	-3.8	1.10	1.17	-6.0
	Run No. R29, T = 310.8°C, P = 216 cm Hg, Feed 9.7 Volume Percent NH_3, Balance O_2									
1	0.072	17.3	192.2	5.1	13.8	13.6	1.5	4.46	4.40	1.4
2	0.136	15.2	190.2	8.5	11.2	11.4	-1.7	3.53	3.54	0.3
3	0.254	12.4	187.1	12.6	9.11	8.79	3.6	2.46	2.53	-2.8
4	0.360	11.3	185.5	14.3	7.42	7.79	-4.7	2.05	2.17	-5.5
5	0.905	7.2	182.4	20.6	4.35	4.56	-4.6	1.01	1.09	-7.3
6	1.15	6.0	181.0	21.7	3.73	3.71	0.6	0.836	0.827	1.1
7	1.57	4.9	179.3	23.7	2.98	2.95	1.0	0.622	0.613	1.5
	Run No. R30, T = 310.8°C, P = 216 cm Hg, Feed 9.7 Volume Percent NH_3, Balance O_2									
1	0.072	17.5	196.3	0.0	14.8	14.9	-0.7	4.61	4.84	-4.7
2	0.254	11.8	198.4	0.0	10.7	10.2	4.9	2.92	2.88	1.4
3	0.360	10.2	199.4	0.0	8.77	8.83	-6.8	2.34	2.37	-1.3
4	0.612	8.1	201.0	0.0	6.30	6.99	-9.9	1.62	1.62	0.0
5	0.905	5.9	201.6	0.0	4.99	5.11	-2.3	1.10	1.13	-2.6
	Run No. R31, T = 310.8°C, P = 280 cm Hg, Feed 5.3 Volume Percent NH_3, Balance O_2									
1	0.193	6.93	267.7	0.0	6.64	7.06	-5.9	1.72	1.65	4.2
	Run No. R32, T = 310.8°C, P = 176 cm Hg, Feed 16.5 Volume Percent NH_3, Balance O_2									
1	0.483	17.7	150.9	0.0	12.6	12.9	-2.3	3.97	4.21	-5.7
	Run No. R33, T = 310.8°C, P = 280 cm Hg, Feed 16.5 Volume Percent NH_3, Balance O_2									
1	0.102	29.4	240.3	0.0	28.7	28.2	1.8	10.9	11.0	-0.9
	Run No. R34, T = 310.8°C, P = 176 cm Hg, Feed 16.5 Volume Percent NH_3, Balance O_2									
1	0.725	3.6	70.8	0.0	1.54	1.58	-2.5	0.274	0.294	-6.8
	Run No. R35, T = 310.8°C, P = 251 cm Hg, Feed 16.5 Volume Percent NH_3, Balance O_2									
1	0.962	12.9	185.0	41.4	6.67	6.51	2.5	2.02	1.90	6.3
2	1.34	10.8	183.5	44.2	5.25	5.25	0.0	1.44	1.44	0.0
3	2.73	8.2	180.9	48.0	3.94	3.78	4.2	0.949	0.940	1.0
4	4.28	5.3	176.2	52.2	2.34	2.32	0.9	0.517	0.496	4.2
5	7.83	3.6	174.1	54.3	1.53	1.53	0.0	0.270	0.286	-5.6

TABLE B-1 (CONT'D)

Measurement No.	Contact Time, min · 10^3	P_{NH_3}, cm Hg	P_{O_2}, cm Hg	P_{H_2O}, cm Hg	$Rate_{N_2}$ (Data), $cm^3\ min^{-1}\ gm^{-1}$	$Rate_{N_2}$ (Calc), $cm^3\ min^{-1}\ gm^{-1}$	% Dev	$Rate_{N_2O}$ (Data), $cm^3\ min^{-1}\ gm^{-1}$	$Rate_{N_2O}$ (Calc), $cm^3\ min^{-1}\ gm^{-1}$	% Dev
	Run No. R36, T = 322.2°C, P = 176 cm Hg, Feed 16.5 Volume Percent NH_3, Balance O_2									
1	0.0947	23.6	141.6	8.1	20.8	21.3	-2.3	12.6	13.1	-3.8
2	0.179	20.6	139.0	12.0	17.1	17.6	-2.8	9.86	10.2	-1.6
3	0.342	16.9	135.4	17.8	13.1	13.3	-1.5	7.42	7.23	1.2
4	1.21	9.7	128.2	28.2	6.45	6.59	-2.1	2.83	2.95	-4.1
5	1.51	8.7	127.1	29.7	5.59	5.77	-3.1	2.30	2.48	-7.2
6	2.10	6.8	126.1	32.6	4.46	4.34	2.8	1.71	1.71	0.0
	Run No. R37, T = 322.2°C, P = 216 cm Hg, Feed 9.7 Volume Percent NH_3, Balance O_2									
1	0.0705	15.7	189.7	7.9	16.6	17.2	-3.5	9.07	9.09	-0.2
2	0.133	13.2	187.1	11.5	13.5	13.8	-2.2	6.56	6.88	-4.6
3	0.248	10.3	182.4	15.5	9.90	10.1	-2.0	4.69	4.61	1.7
4	0.600	6.5	180.9	21.5	6.64	5.92	2.0	2.29	2.30	-0.4
5	0.885	5.1	179.8	23.6	4.39	4.58	+4.1	1.59	1.64	-3.1
6	1.13	4.3	178.8	24.7	3.73	3.78	-1.3	1.22	1.27	-4.1
7	1.54	3.5	176.7	25.7	2.99	3.05	-2.0	0.896	0.960	-6.7
	Run No. R38, T = 322.2°C, P = 280 cm Hg, Feed 5.3 Volume Percent NH_3, Balance O_2									
1	0.0549	9.8	261.0	7.3	13.0	13.0	0.0	5.92	5.83	0.9
2	0.104	7.8	255.8	10.2	9.86	9.95	-0.9	3.97	4.13	-3.9
3	0.193	5.8	256.3	13.5	7.05	7.15	-1.4	2.68	2.67	0.4
4	0.275	4.9	255.8	14.9	5.62	5.90	-3.7	1.89	2.07	-8.7
5	0.468	3.3	253.7	17.2	3.86	3.96	-2.5	1.20	1.22	-1.6
6	0.690	2.5	253.2	18.4	2.92	2.90	0.7	0.787	0.808	-2.6
7	0.883	2.1	253.2	19.1	2.40	2.40	0.0	0.581	0.626	-7.1
8	1.19	1.7	252.1	19.6	1.91	1.90	0.5	0.416	0.432	-3.7
	Run No. R39, T = 322.2°C, P = 280 cm Hg, Feed 16.5 Volume Percent NH_3, Balance O_2									
1	0.0528	31.6	219.6	21.3	33.1	32.9	0.6	22.5	22.3	0.9
2	0.100	25.8	214.0	29.9	25.1	24.3	3.3	16.3	15.3	6.5
3	0.191	20.2	208.3	38.0	17.8	17.3	2.9	10.1	10.0	1.0
4	0.844	9.0	197.4	54.3	6.37	6.47	-1.5	2.65	2.83	-6.4
5	1.170	7.2	196.4	56.8	4.87	5.00	-2.6	1.94	2.02	-4.
	Run No. R40, T = 322.2°C, P = 216 cm Hg, Feed 9.7 Volume Percent NH_3, Balance O_2									
1	.0705	15.5	197.4	0.0	19.3	18.9	2.1	10.5	9.98	5.8
2	0.133	12.5	199.0	0.0	16.1	15.3	5.2	7.91	7.46	6.0
3	0.248	8.17	200.5	0.0	9.49	10.1	-6.0	3.97	4.24	-6.4
4	0.352	5.12	202.6	0.0	6.64	6.35	4.5	2.50	2.27	10.1
5	0.600	3.23	202.6	0.0	4.24	4.00	6.	1.34	1.22	9.8
6	0.855	2.64	203.1	0.0	3.25	3.27	-0.6	0.952	0.929	2.5
	Run No. R41, T = 322.2°C, P = 176 cm Hg, Feed 16.5 Volume Percent NH_3, Balance O_2									
1	0.474	13.6	152.5	0.0	14.6	14.2	2.8	6.86	7.17	-4.6
	Run No. R42, T = 322.2°C, P = 280 cm Hg, Feed 5.3 Volume Percent NH_3, Balance O_2									
1	0.275	4.2	269.8	0.0	5.96	6.19	-3.7	2.17	2.08	4.3
	Run No. R43, T = 322.2°C, P = 280 cm Hg, Feed 16.5 Volume Percent NH_3, Balance O_2									
1	0.190	17.4	244.4	0.0	23.2	24.0	-3.3	12.2	13.1	-6.8
	Run No. R44, T = 322.2°C, P = 176 cm Hg, Feed 5.3 Volume Percent NH_3, Balance O_2									
1	0.691	3.3	70.8	0.0	2.14	2.07	3.4	0.675	0.635	6.3
	Run No. R45, T = 322.2°C, P = 251 cm Hg, Feed 16.5 Volume Percent NH_3, Balance O_2									
1	0.844	8.7	180.9	47.5	6.30	6.20	1.6	2.78	2.67	4.1
2	1.17	6.8	180.0	50.0	4.84	4.75	1.9	1.93	1.88	2.7
3	2.40	5.2	177.8	52.7	3.46	3.48	-0.6	1.33	1.25	6.4
4	3.76	3.3	174.2	54.8	2.06	2.13	-3.3	0.694	0.650	6.8
5	6.87	2.1	173.6	56.8	1.41	1.37	2.9	0.373	0.363	2.8

TABLE B-1 (CONT'D)

Measurement No.	Contact Time, min · 10^3	P_{NH_3}, cm Hg	P_{O_2}, cm Hg	P_{H_2O}, cm Hg	$Rate_{N_2}$ (Data), $cm^3\ min^{-1}\ gm^{-1}$	$Rate_{N_2}$ (Calc), $cm^3\ min^{-1}\ gm^{-1}$	% Dev	$Rate_{N_2O}$ (Data), $cm^3\ min^{-1}\ gm^{-1}$	$Rate_{N_2O}$ (Calc), $cm^3\ min^{-1}\ gm^{-1}$	% Dev
	Run No. R46, T = 345.5°C, P = 176 cm Hg, Feed 16.5 Volume Percent NH_3, Balance O_2									
1	0.0908	21.4	139.0	11.3	25.6	26.2	-2.3	21.4	22.2	-3.6
2	0.171	17.8	135.9	18.6	20.6	20.2	0.2	16.2	16.0	1.2
3	0.328	13.7	132.3	20.5	14.8	15.0	-1.3	11.1	10.9	1.8
4	1.16	7.0	126.1	32.2	6.71	6.77	-0.9	3.94	3.88	1.5
5	1.45	6.2	124.5	33.4	5.77	5.87	1.7	3.09	3.22	-4.0
6	2.02	4.8	123.5	35.4	4.57	4.45	2.7	2.22	2.23	-0.5
	Run No. R47, T = 345.5°C, P = 216 cm Hg, Feed 9.7 Volume Percent NH_3, Balance O_2									
1	0.0677	13.7	188.1	10.7	20.5	20.7	-1.0	14.5	14.9	-2.7
2	0.128	10.7	185.0	15.1	15.5	15.5	0.0	11.0	10.3	6.8
3	0.237	8.1	182.4	18.7	11.2	11.2	0.0	6.60	6.72	-1.8
4	0.588	4.8	178.9	24.7	6.22	6.23	-1.6	3.14	3.11	1.0
5	0.837	3.8	178.3	25.4	4.61	4.90	-5.9	2.05	2.26	-0.9
6	1.05	2.9	177.8	26.8	3.90	3.71	5.1	1.63	1.56	4.5
7	1.46	2.3	177.2	27.4	3.05	2.98	2.3	1.14	1.16	-1.7
	Run No. R48, T = 345.5°C, P = 280 cm Hg, Feed 5.3 Volume Percent NH_3, Balance O_2									
1	0.0525	8.3	258.9	9.8	15.3	15.5		9.22	9.44	
2	0.0992	6.0	256.3	12.6	11.0	10.9		6.45	5.90	
3	0.185	4.2	255.3	15.8	7.35	7.14		3.97	3.54	
4	0.263	3.4	254.2	17.2	5.96	5.86		2.66	2.59	
5	0.448	2.2	253.2	18.8	4.01	3.83		1.55	1.47	
6	0.658	1.7	251.2	19.6	2.92	2.97		0.994	1.05	
7	0.843	1.5	251.1	19.9	2.38	2.47		0.742	0.813	
8	1.14	1.1	250.8	20.5	1.87	1.86		0.514	0.553	
	Run No. R49, T = 345.5°C, P = 216 cm Hg, Feed 9.7 Volume Percent NH_3, Balance O_2									
1	0.0677	13.4	199.0	0.0	23.5	22.8		17.4	16.4	
2	0.128	10.4	199.5	0.0	17.5	17.8		11.6	11.7	
3	0.237	7.7	201.5	0.0	12.4	13.2		7.27	7.81	
4	0.338	5.7	201.6	0.0	10.0	9.87		5.43	5.27	
5	0.588	3.8	202.6	0.0	6.79	6.48		3.30	2.98	
6	0.837	2.8	203.1	0.0	5.06	4.78		2.10	1.98	
	Run No. R50, T = 345.5°C, P = 176 cm Hg, Feed 16.5 Volume Percent NH_3, Balance O_2									
1	0.328	12.6	153.4	0.0	18.6	18.2		12.5	12.8	
	Run No. R51, T = 345.5°C, P = 280 cm Hg, Feed 5.3 Volume Percent NH_3, Balance O_2									
1	0.185	4.0	269.8	0.0	8.17	8.32		3.67	3.93	
	Run No. R52, T = 345.5°C, P = 176 cm Hg, Feed 5.3 Volume Percent NH_3, Balance O_2									
1	0.691	3.1	70.8	0.0	2.51	2.61		1.06	1.13	

APPENDIX C

SAMPLE CALCULATIONS

1. Calculation of Reaction Rates and Partial Pressures from Raw Data

Measurements from the gas chromatographic analysis of the reactor effluent are in the form

$$\frac{\text{Area}_{N_2}}{\text{Area}_{N_2O} + \text{Area}_{O_2}} \equiv D_1 \qquad (C.1)$$

$$\frac{\text{Area}_{N_2O}}{\text{Area}_{N_2O} + \text{Area}_{N_2} + O_2} \equiv D_2$$

From these area ratios and the relationship between percentage area and mole fractions as determined by calibration, mole fractions of nitrogen and nitrous oxide in the effluent are calculated

$$(\text{Mole Fraction})_{N_2} = 1.01\ D_1 \equiv F_{N_2}$$
$$(\text{Mole Fraction})_{N_2O} = 0.716\ D_2 \equiv F_{N_2O} \qquad (C.2)$$

Using these mole fractions and taking a basis of 100 standard cm^3 of oxygen in the product stream, the ratios

$$\frac{100\ N_2}{O_2} = \frac{100\ F_{N_2}}{1 - F_{N_2}} = (N_2)_{out} \qquad (C.3)$$

$$\frac{100\ N_2O}{O_2} = \frac{F_{N_2O}}{(1-F_{N_2O})(1-F_{N_2})} = (N_2O)_{out}$$

are computed. The percent nitrous oxide yield is now defined as that percentage of reacted ammonia which has been converted to nitrous oxide, i.e.,

$$\% \, N_2O \text{ Yield} = \frac{(N_2O)_{out}}{(N_2)_{out} + (N_2O)_{out}} \tag{C.4}$$

Throughout the remaining calculation, a basis of 100 standard cm^3 of oxygen in the product stream is used. The overall stoichiometric equations are

$$\begin{aligned} 4 \, NH_3 + 3 \, O_2 &= 2 \, N_2 + 6 \, H_2O \\ 2 \, NH_3 + 2 \, O_2 &= N_2O + 3 \, H_2O \end{aligned} \tag{C.5}$$

Hence the standard cm^3 of ammonia reacted to form the nitrogen and nitrous oxide is

$$(NH_3)_{reacted} = 2(N_2)_{out} + 2(N_2O)_{out}, \; cm^3 \tag{C.6}$$

The oxygen which reacted with this ammonia is

$$(O_2)_{reacted} = 1.5(N_2)_{out} + 2(N_2O)_{out}, cm^3 \tag{C.7}$$

Total oxygen entering the system is

$$(O_2)_{in} = 100 + (O_2)_{reacted}, \; cm^3 \tag{C.8}$$

Since the feed consists of a mole fraction of ammonia F_{NH_3}, balance oxygen, the ammonia accompanying the $(O_2)_{in}$ is

$$(NH_3)_{in} = \frac{(F_{NH_3})(O_2)_{in}}{1 - F_{NH_3}}, \; cm^3 \tag{C.9}$$

The fraction of ammonia conversion is then

$$C_{NH_3} = \frac{(NH_3)_{reacted}}{(NH_3)_{in}} \qquad (C.10)$$

The total rate of nitrogen and nitrous oxide formation, equal to twice the rate of ammonia reaction, is then calculated.

$$(r)_{N_2+N_2O \text{ formation}} = \frac{(\text{Feed Rate})(F_{NH_3})(NH_3)}{(2)(\text{Catalyst Weight})}, \ cm^3 \ min^{-1} \ gm^{-1} \qquad (C.11)$$

Use of Equations (C.4) and (C.11) now gives the individual rates of nitrogen and nitrous oxide formation.

The partial pressures of the individual gases in the recycle loop remain to be calculated. Realizing that

$$(NH_3)_{out} = (NH_3)_{in} - (NH_3)_{reacted}, \ cm^3 \qquad (C.12)$$

and, from stoichiometry,

$$(H_2O)_{out} = 3(N_2)_{out} + 3(N_2O)_{out} \qquad (C.13)$$

a total volumetric product rate $(T)_{out}$ is easily calculated.

$$(T)_{out} = 100 + (NH_3)_{out} + (N_2)_{out} + (N_2O)_{out} + (H_2O)_{out} \qquad (C.14)$$

Letting P represent the pressure setting of the back pressure regulator, taken as equal to the reaction pressure, the partial pressure of ammonia is then

$$p_{NH_3} = \frac{(P)(NH_3)_{out}}{(T)_{out}} \qquad (C.15)$$

The remaining partial pressures are calculated in a similar manner.

2. Evaluation of Constants in Rate Equations

The method used to evaluate the rate equation constants K_{N_2}, $b_{O_2}^{1/2}$ and b_{H_2O} in

$$r_{N_2} = \frac{K_{N_2} p_{NH_3}^{1.0} p_{O_2}^{1.0}}{(1 + b_{O_2}^{1/2} p_{O_2}^{1/2} + b_{H_2O} p_{H_2O})^2} \qquad (C.16)$$

at 273.5°C is here detailed. Rearrangement of Equation (C.16) yields

$$\left(\frac{p_{NH_3}}{r_{N_2}}\right)^{1/2} = \left(\frac{1}{K_{N_2}^{1/2}}\right) p_{O_2}^{-1/2} + \left(\frac{b_{H_2O} p_{O_2}^{-1/2}}{K_{N_2}^{1/2}}\right) p_{H_2O} + \frac{b_{O_2}^{1/2}}{K_{N_2}^{1/2}} \qquad (C.17)$$

Using data for which $p_{H_2O} \cong 0$, a plot of (p_{NH_3}/r_{N_2}) vs. $p_{O_2}^{-1/2}$ yields a straight line with slope equal to $K_{N_2}^{-1/2}$ and intercept equal to $b_{O_2}^{1/2} K_{N_2}^{-1/2}$. Such a plot for nitrogen rate data is presented in Figure C.1. Using data from the nitrogen plot,

$$K_{N_2}^{-1/2} = \frac{1.705 - 1.475}{.08 - .06} = 11.5, \text{ or } K_{N_2} = .0075 \text{ cm}^3 \text{ min}^{-1} \text{ gm}^{-1} \text{ cm Hg}^{-2} \qquad (C.18)$$

The intercept of the nitrogen plot is easily calculated to be 0.785. Using this value and the value of $K_{N_2}^{-1/2}$ from Equation (C.18),

$$b_{O_2}^{1/2} = \frac{0.785}{11.5} = 0.068 \text{ cm Hg}^{-1/2} \qquad (C.19)$$

The term b_{H_2O} remains to be evaluated. This term is established from Equation (C.17) by plotting $(p_{NH_3}/r_{N_2})^{1/2}$ vs. p_{H_2O} for data in which p_{O_2} is essentially constant. Such a plot is shown in Figure C.2. The slope of the straight line is equal to $b_{H_2O} p_{O_2}^{-1/2} K_{N_2}^{-1/2}$. In Figure C.2 the slope of the curve for the nitrogen rate measurements is easily computed

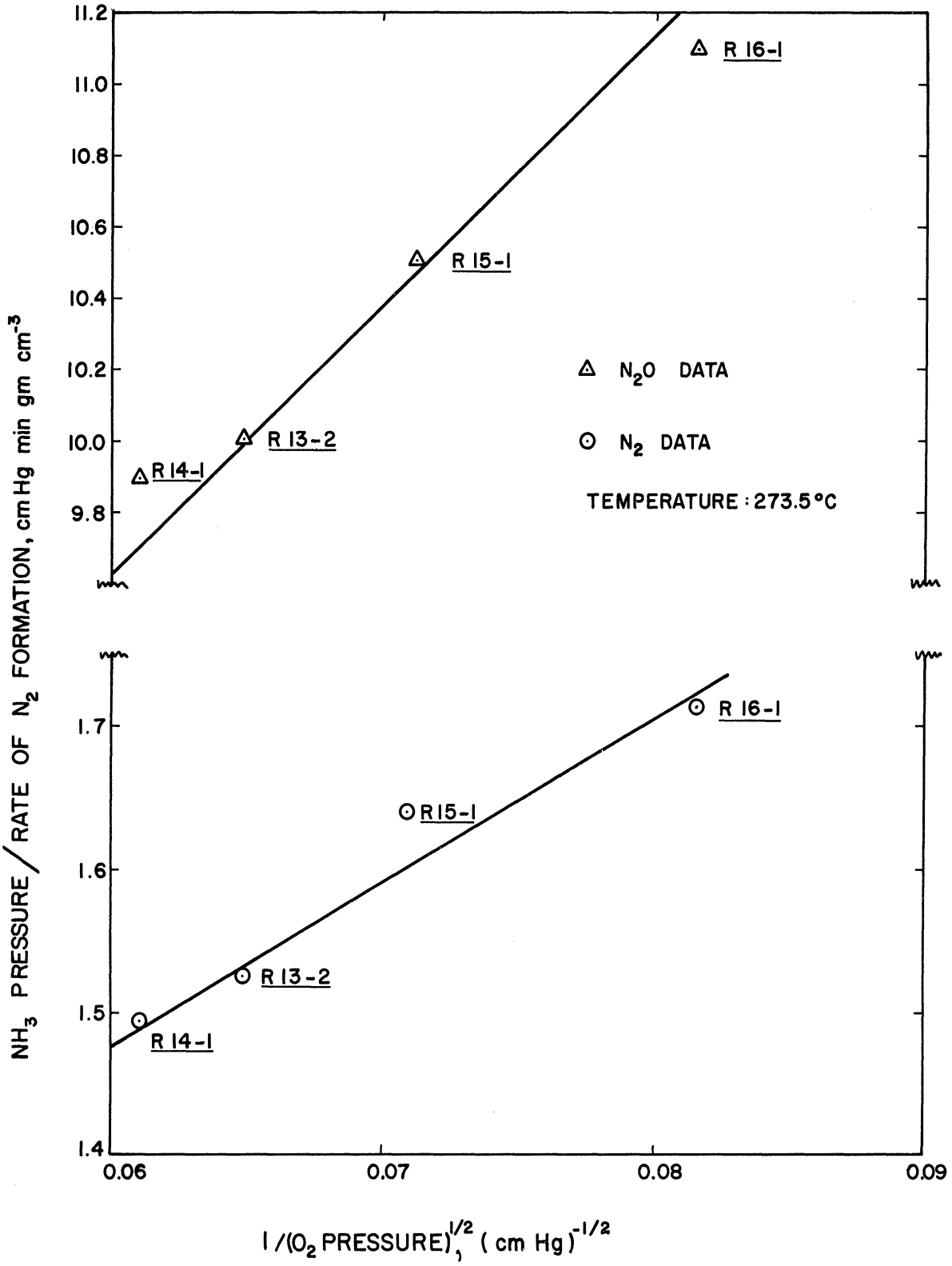

Figure C.1. Plot for Evaluation of Rate Constants.

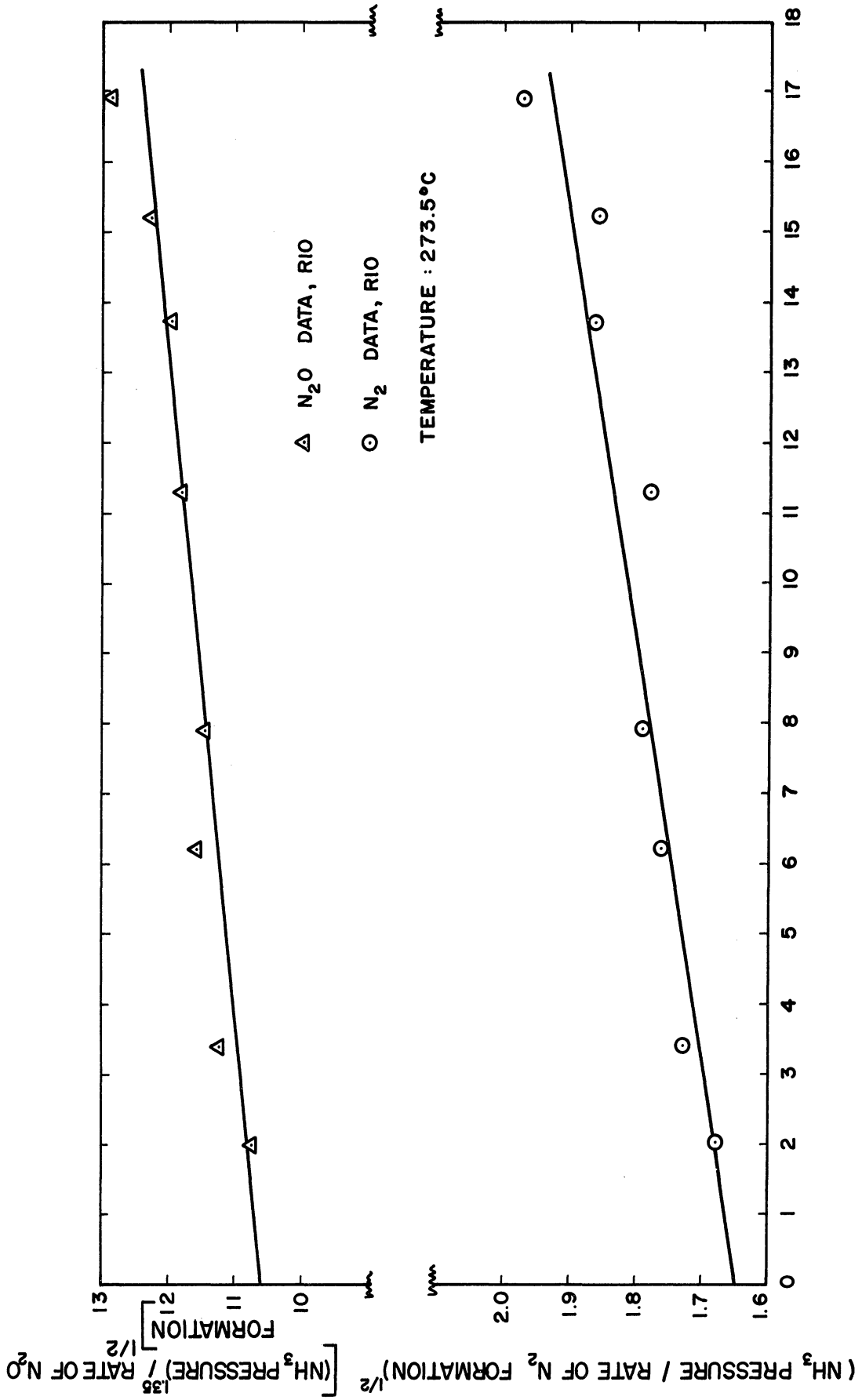

Figure C.2. Plot for Evaluation of Rate Constants.

to be 0.0169. The oxygen partial pressure for the data plotted is 188 cm Hg as seen for R10 data in Appendix B. Using these values and the value for $K_{N_2}^{-1/2}$ determined in Equation (C.18),

$$b_{H_2O} = (0.0169)(188)^{1/2}(.0075) = 0.020 \text{ cm Hg}^{-1} \qquad (C.20)$$

3. Calculation of Experimental Heat of Adsorption

The experimental heat of adsorption λ is related to the equilibrium adsorption constant b by the equation

$$b = b_o \exp(\lambda/RT) \qquad (C.21)$$

The adsorption heat can consequently be evaluated by use of

$$\lambda = \frac{R d\ln b}{d(1/T)} \qquad (C.22)$$

Values of $\ln(b_{O_2}^{1/2})$ have been plotted vs. $1/T$ in Figure (6.2). Using data from the figure,

$$\lambda_{O_2} = \frac{1.98 \ln (9.4/3.7)^2}{(1.93 - 1.61)\ 10^{-3}} = 11.3 \text{ kcal gm mole}^{-1} \qquad (C.23)$$

4. Calculation of Theoretical Heat of Adsorption

The theoretical heat of adsorption of oxygen is calculated from the equation(51)

$$(\lambda)_{o,\ theo,\ O_2} = E[R_u = R_u] + 46.12\ \mu^2 \qquad (C.24)$$

The value of the ruthenium-oxygen polar moment μ is estimated as a first approximation to be equal to the difference in electronegativities of ruthenium

and oxygen, from which[40]

$$\mu = 3.5 - 2.2 = 1.3 \qquad (C.25)$$

The energy of a single bond between ruthenium atoms supported on the alumina, E[Ru-Ru] , is estimated to be one sixth the heat of sublimation of ruthenium metal, and the energy of a double bond, E[Ru=Ru] , is taken as twice the single bond energy. The heat of sublimation of ruthenium is 160 kcal gm mole^{-1}.[12] Hence

$$(\lambda)_{o,\ theo,\ O_2} = \frac{1}{3}(160) + 46.12(1.3)^2 = 131.3 \text{ kcal gm mole}^{-1} \qquad (C.26)$$

5. Calculation of the Experimental b_o

The relationship between b_o , b and temperature is

$$b = b_o \exp(\lambda/RT) \qquad (C.27)$$

Solving Equation (C.27) for b_o gives

$$b_o = b \exp(-\lambda/RT) \qquad (C.28)$$

Experimental values of b_{O_2} have been presented in Table VI-2 and a plot of ln (b_{O_2}) vs. 1/T appears in Figure 6.2. From the slope of this plot, λ_{O_2} = 11.3 kcal gm mole^{-1}. Using this value and taking $b^{1/2}$ = .057 cm Hg$^{-1/2}$ at 296.1°C from Table VI-2, Equation (C.28) becomes

$$(b_o)_{exptl,O_2} = \frac{b_{O_2}}{\exp(\lambda/RT)} = \frac{(.057)^2}{\exp(11{,}300/(1.98)(569))} = 1.48 \cdot 10^{-7} \text{ cm Hg}^{-1} \qquad (C.29)$$

6. Calculation of the Theoretical b_o

The theoretical b_o value is computed from the equation

$$(b_o)_{theo} = \frac{V_m}{vd(2\pi MRT)^{1/2}} \qquad (C.30)$$

These values hold for oxygen at 300°C: $V_m = 28.1$ cm^3 gm mole^{-1}; $v = 10^{13}$ sec^{-1}; $T = 573$°K; $M = 32$; $d = 6$ Angstroms;[26] $R = 6{,}340$ cm^3 cm Hg. Substituting into Equation (C.30),

$$(b_o)_{theo,O_2} = \frac{28.1}{(10^{13})(6\cdot10^{-8})(2\pi(32)(6240)(573))^{1/2}} = 1.73\cdot10^{-7} \text{ cm Hg}^{-1} \qquad (C.31)$$

7. Calculation of the Experimental Entropy of Adsorption

Experimental adsorption entropy is calculated from the equation

$$(\Delta S)_{exptl} = \frac{-\lambda}{T} + R\ln b \qquad (C.32)$$

The value of adsorption heat λ was found to be 11.3 kcal gm mole^{-1} for oxygen. Taking the $b_{O_2}^{1/2}$ value of 0.097 cm Hg$^{-1/2}$ at 246.2°C from Table VI-2 and substituting into Equation (C.32),

$$(\Delta S)_{exptl,O_2} = \frac{-11{,}300}{519} + (1.98)\ln(.097)^2(76) = -23.1 \text{ e.u.} \qquad (C.33)$$

8. Calculation of E for Power Rate Law

The activation energy E appearing in the power rate law equation

$$r = k_o\, p_A^m\, p_B^n \exp(-E/RT) \qquad (C.34)$$

can be evaluated from the expression

$$E = -R(d\ln r/d(1/T))_{p_{NH_3},\ p_{O_2},\ p_{H_2O}\ \text{constant}} \qquad (C.35)$$

The data plotted in Figure 5.3 may be conveniently used for this calculation. At p_{NH_3} = 20 cm Hg , the rates appearing in Table C-1 are read from the figure cited.

TABLE C-1

MEASUREMENTS USED TO EVALUATE ACTIVATION ENERGY IN POWER RATE LAW

Temp °C	$(1/T°K)\cdot 10^3$	$r^1_{NH_3}$ rxn	$r^2_{N_2O}/r_{N_2}$	$2r^1_{N_2}$	$2r^1_{N_2O}$
273.5	1.83	10.2	.068	9.55	0.65
296.1	1.76	19.7	.165	15.9	2.78
310.8	1.715	31.5	.35	23.3	8.18
322.2	1.68	52.	.58	33.	19.
345.5	1.61	82.	.85	44.3	37.7

1. rates in $cm^3 min^{-1} gm^{-1}$
2. data from Figure 5.17

The data appearing in Table C-1 are plotted in Figure C.3. Taking data from the figure,

$$E_{N_2} = \frac{(1.98)\ln(44.5/11.0)}{(1.83 - 1.61)\ 10^{-3}} = 12.6 \text{ kcal gm mole}^{-1} \qquad (C.36)$$

$$E_{N_2O} = \frac{(1.98)\ln(42.0/0.85)}{(1.83 - 1.61)\ 10^{-3}} = 35.0 \text{ kcal gm mole}^{-1} \qquad (C.37)$$

9. Calculation of Power Rate Law Experimental Pre-Exponential Factor

From Table VI-2 at 322.2°C,

$$(k_o)_{exptl,N_2} \exp(-E_{N_2}/RT) = 0.30 \qquad (C.38)$$

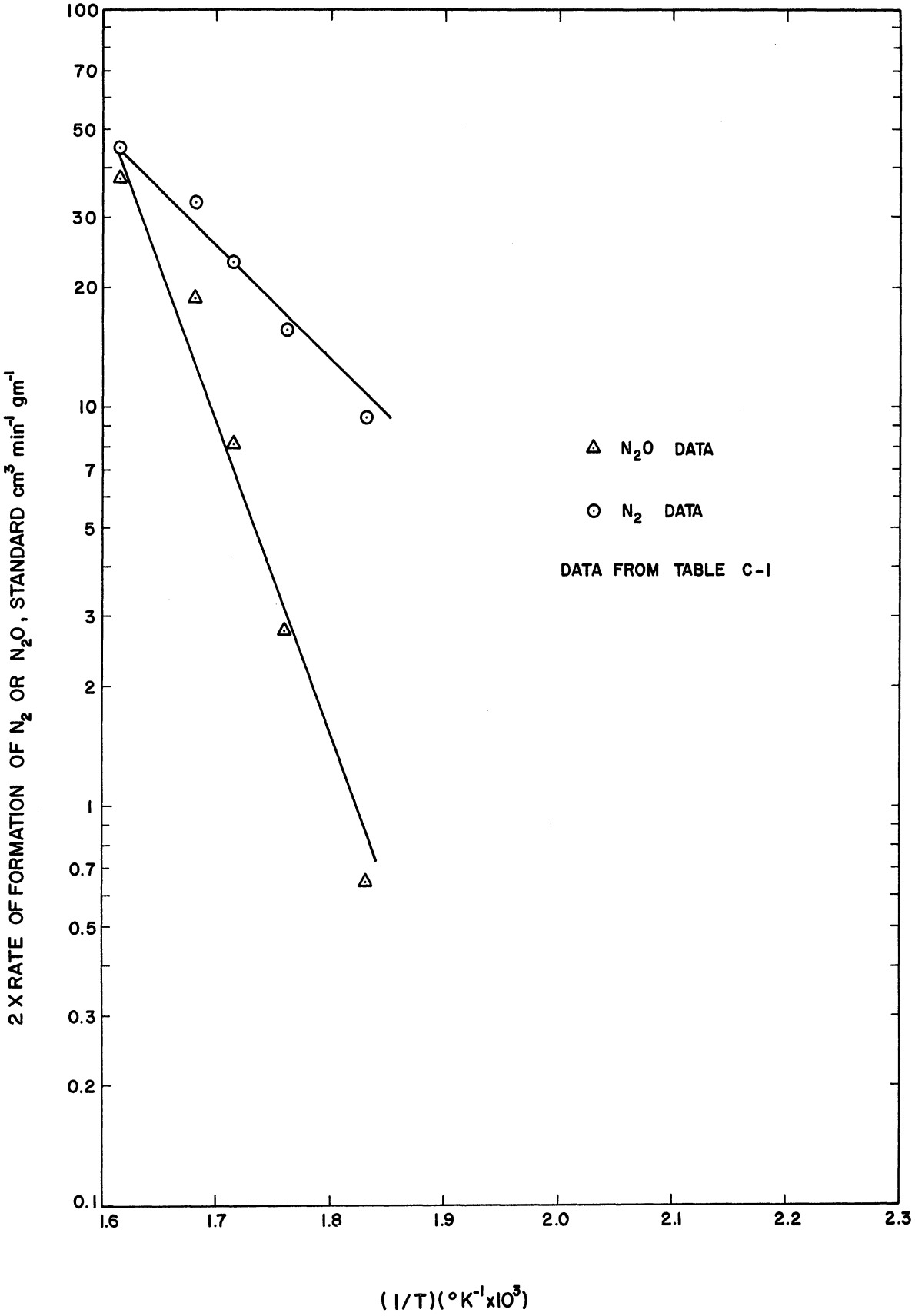

Figure C.3. Plot for Evaluation of Power Rate Law Activation Energy.

Using E_{N_2} = 12.6 kcal gm mole^{-1} as computed in Appendix C under 9. and substituting into Equation (C.38),

$$(k_o)_{exptl,N_2} = 0.03 \exp(12{,}600/(1.98)(595)) = 1.33 \cdot 10^4 \text{ cm}^3 \text{ min}^{-1} \text{ gm}^{-1} \quad (C.39)$$

This value must now be converted to units of molecules site^{-1} sec^{-1}. The factor by which the value in Equation (C.39) must be multiplied to effect this conversion is easily calculated to be 0.0151 under the assumption that each ruthenium atom represents one site. The reasonableness of this assumption is established quantitatively as Item 12 in this Appendix. Using this factor, Equation (C.39) becomes

$$(k_o)_{exptl,N_2} = 2.01 \cdot 10^2 \text{ molecules site}^{-1} \text{ sec}^{-1} \quad (C.40)$$

10. Calculation of Power Rate Law Theoretical Pre-Exponential Factor

The theoretical value of the power rate law pre-exponential factor is given by

$$(k_o)_{theo} = (kT/h) \exp[(a\phi_{NH_3} + b\phi_{O_2} + C\phi_{H_2O})/R] \quad (C.41)$$

Terms are defined in Nomenclature. At a temperature of 600°K, using the free energy function values listed in Table VI-3 and the values of a , b , and c given in Equation (6.63), we have

$$(k_o)_{theo,N_2} = \frac{(1.38 \cdot 10^{-16})(600)}{(6.62 \cdot 10^{-27})} \exp\left[\frac{-43{,}826 + (.458)(-46.968) - (.396)(-42.766)}{1.98}\right]$$

$$= 9.1 \cdot 10^2 \text{ molecules site}^{-1} \text{ sec}^{-1} \quad (C.42)$$

11. Calculation of Percentage Surface Covered by Atomic Oxygen

$$\theta_o = \frac{b_{O_2}^{1/2} p_{O_2}^{1/2}}{1 + b_{O_2}^{1/2} p_{O_2}^{1/2} + b_{H_2O} p_{H_2O}} \qquad (C.43)$$

Typical Data at 300°C: $b_{O_2}^{1/2} = .05$

$p_{O_2} = 196$ cm Hg

$b_{H_2O} = .012$

$p_{H_2O} = 30$ cm Hg

$$\theta_o = \frac{(.05)(14)}{1+(.05)(14)+(.012)(30)} = 34\% \qquad (C.44)$$

12. Validity of Assumption that Number of Reaction Sites Equals Number of Ruthenium Atoms

The relationship between the weight of a catalytic agent and the weight of carrier required for monolayer distribution of the agent on the carrier is

$$\frac{\text{weight of catalytic agent}}{\text{weight of carrier}} = \frac{10^4 S d^{2/3} M^{1/3}}{N^{1/3}} \qquad (C.45)$$

For the present calculation, all quantities in Equation (C.45) are known except S, the specific area of the catalyst, square meters per gram, required for monolayer coverage by the agent. Using the values $M_{Ru} = 101.1$, $d_{Ru} = 12.2$ grams per cubic centimeter and the usual value for the Avogardo number N, and recalling that the catalyst bears 0.5 weight percent ruthenium, the value for S is

$$S = \frac{(0.005/0.995)(6.023 \cdot 10^{23})^{1/3}}{(101.1)^{1/3}(12.2)^{2/3}(10^4)} = 1.71 \text{ m}^2/\text{gram} \qquad (C.46)$$

The area given in Equation (C.46) assumes that the catalytic agent is uniformly distributed over the carrier. In this case, the ruthenium is deposited on the surface of 1/8 inch cylindrical pellets. If the ruthenium is estimated to penetrate 5% of the way into the pellet interior, corresponding to a penetration of 0.0159 cm, then the volume of the carrier covered by the ruthenium is easily shown to be 27.1% of the total carrier volume. The 5% penetration would require a specific surface area of

$$S = 1.71/0.271 = 6.32 \text{ m}^2/\text{gram} \qquad (C.47)$$

for deposition of the ruthenium in a monolayer. The actual area of the alumina pellets used by Engelhard Industries, Inc., in production of the 0.5 weight percent ruthenium catalyst has been given as in the vicinity of 120 m^2/gram.[48] Hence the assumption of monolayer deposition is plausible.

It is of interest to calculate how deeply the ruthenium can be expected to penetrate the catalyst interior under conditions of monolayer deposition, given that the carrier area is 120 m^2/gram. Calculation with Equation (C.45) shows that under this condition only 1.45% of the pellet need be contacted by the ruthenium. This corresponds to a penetration of 0.2% of the catalyst pellet, or penetration to a depth of 0.0064 cm.

13. Calculation of Theoretical Entropy of Adsorption of Oxygen

Postulating that oxygen loses three degrees of translational freedom upon adsorption and is dissociatively adsorbed, the entropy change expected to accompany this process is given by

$$\Delta S = -_3 S_{trans} + S_{config} , \qquad (C.48)$$

where

$$ {}_3S_{trans} = R\ln M^{3/2}T^{5/2} - 2.3 \qquad (C.49) $$

and

$$ S_{config} = 2R[2(x-1/4)\ln(x-1/4)+\ln 2-x\ln x-(x-1)\ln(x-1)] \qquad (C.50) $$

Evaluating Equation (C.49) for oxygen at 600°K,

$$ {}_3S_{trans} = (1.98)(2.3)\log(32)^{3/2}(600)^{5/2} = 39.5 \text{ e.u.} \qquad (C.51) $$

Taking $\theta = 1/2$, then $x = 2$ because $x = 1/\theta$. Evaluation of Equation (C.50) for oxygen then gives

$$ S_{config} = (2)(1.98)[(3.5)(2.3)\log(3.5)+(2.3)\log 2-(2)(2.3)\log 2] $$

$$ S_{config} = 14.6 \text{ e.u.} \qquad (C.52) $$

Combining the results of Equations (C.51) and (C.52),

$$ S = -39.5 + 14.6 = -24.9 \text{ e.u.} \qquad (C.53) $$

APPENDIX D

HEAT AND MASS TRANSFER CONSIDERATIONS

1. Calculation of Pressure Drop Between Bulk Gas and Catalyst Surface

It was shown experimentally that, for the flow rates used in this work, mass transfer to the catalyst surface is not the slow step in the oxidation of ammonia over ruthenium. It is of interest, however, to compute the expected pressure drop of reactants due to diffusion from the bulk gas to the exterior catalyst surface. The mass transfer calculation has been considered in detail by Yang and Hougen[56] and their development will be used here. The pressure drop between the bulk gas and the catalyst surface is given by

$$\frac{\Delta p_A}{p_A} = \left(\frac{r}{p_A}\right)\left(\frac{p_f (a_p)^{1/2} M_m}{1.25\ \mu a_m}\right)\left(\frac{\mu}{\rho D_{Am}}\right)^{2/3}\left(\frac{(a_p)^{1/2} G}{\mu}\right)^{-.59} \qquad (D.1)$$

It is observed that $\Delta p_A/p_A$ is linearly dependent on the ratio of reaction rate to partial pressure of diffusing species A. The equation thus will be evaluated at 345.5°C, where the maximum ratio of reaction rate to ammonia partial pressure occurred. It is true that the effect of viscosity, increasing with temperature, is to decrease Δp_A. The viscosity temperature coefficient is, however, more than offset by the rate temperature coefficient.

Table D-1 lists the Equation (D.1) values which obtain at 345°C:

TABLE D-1

NUMERICAL VALUES USED IN MASS TRANSFER EQUATION

Value	Comment
$\mu = .082$ lb ft^{-1} hr^{-1}	The viscosity of O_2 is used to approximate the gas viscosity.
$M_m = 29$	Average molecular weight of the gas is somewhat less than that of O_2.
$\rho = .039P$ lb ft^{-3} atm^{-1}	Density has been left as a function of reaction pressure P, in atm.
$D_{Am} = 3.71P$ ft^2 atm hr^{-1}	The diffisivity of NH_3 in O_2 has been approximated as equal to NH_3 diffusivity in air, and has been left as a function of reaction pressure P, in atmospheres.
$p_f = P$ atm	Gas film pressure is taken equal to reaction pressure.
$a_p^{1/2} = .0225$ ft	Pellet area a_p has been taken equal to the surface area of a 1/8" X 1/8" cylinder.
$a_m = 5.35$ ft^2 lb^{-1}	This figure represents the external surface area per pound of pellets.
$G = 35{,}500$ lb hr^{-1} ft^{-2}	Mass rate at reaction pressure 2.32 atm
$G = 40{,}800$ lb hr^{-1} ft^{-2}	Mass rate at reaction pressure 2.84 atm
$G = 47{,}600$ lb hr^{-1} ft^{-2}	Mass rate at reaction pressure 3.68 atm

When the values listed in Table D-1 are substituted into Equation (D.1) and an appropriate correction factor is introduced so that reaction rate may be expressed in cm^3 min^{-1} gm^{-1} and p_A may be expressed in cm Hg, these equations result:

$$\frac{\Delta p_A}{p_A} = .00174 \frac{r}{p_A} \quad \text{(at 2.32 atm rxn pressure)} \qquad (D.2)$$

$$\frac{\Delta p_A}{p_A} = .00193 \frac{r}{p_A} \quad \text{(at 2.84 atm rxn pressure)} \qquad (D.3)$$

$$\frac{\Delta p_A}{p_A} = .00227 \frac{r}{p_A} \quad \text{(at 3.68 atm rxn pressure)} \qquad (D.4)$$

The largest value of r/p_A occurs for measurement R48-1 and has a value of 5.88 $cm^2\ min^{-1}\ gm^{-1}\ cm^{-1}$. Using the applicable Equation, (D.4):

$$\left(\frac{\Delta p_A}{p_A}\right)_{max} = .0133 \qquad (D.5)$$

Equation (D.5) shows that the ammonia pressure drop due to diffusion from the bulk gas to the catalyst surface is less than 1.5% of the bulk ammonia pressure for the most rapid rate of ammonia oxidation encountered in this work. This fact justifies the direct use of recycle stream partial pressures in the rate equations.

No mention was made of catalyst pores in the above considerations. It is demonstrated quantitatively under Item 12 in Appendix C that monolayer deposition of 0.5 weight percent ruthenium on 1/8 inch alumina pellets corresponds to a ruthenium penetration of 0.2% into the pellet interior. Pore diffusion is therefore not considered to be a factor in this case.

2. Calculation of Temperature Drop Between Bulk Gas and Catalyst Surface

The strongly exothermic ammonia oxidation can easily lead to severe temperature gradients in a catalyst bed unless experimental conditions are carefully controlled by limiting the rate of reaction, diluting

the reactants, providing a large heat transfer area, or all three. One of the advantages in using a recirculation-type differential bed reactor is that relatively accurate temperature control can be realized. For a given overall conversion, adiabatic temperature rise is but a fractional part of the adiabatic temperature rise existing in a once-through reactor.

Temperature rise in the reactant stream is plotted in Figure D.1 as a function of the rate of ammonia reaction, standard cm^3 min^{-1}. Three curves are shown, one at each of the three major pressure levels of operation. Since most of the heat released went to increase the sensible heat of the recycle stream, temperature rise was dependent on recycle rate, which in turn was dependent on reaction pressure. Temperature of the reactant stream leaving the first catalyst section was measured by a thermocouple positioned just below the catalyst charge. Sufficient heat transfer area was provided between the three catalyst sections so that the reactants cooled to bath temperature before contacting the next catalyst charge in sequence. This fact was established experimentally with a thermocouple positioned ahead of each catalyst section.

Not all temperature increase measurements have been included in Figure D.1. The data shown, however, are completely representative. Temperature rise depends only on the reaction rate, cm^3 min^{-1}, and the recycle rate. Note that if the total catalyst charge had been used in one catalyst section rather than three, a temperature rise almost three times as large would have been experienced. The maximum gas stream temperature rise occuring in this work was 2.4°C.

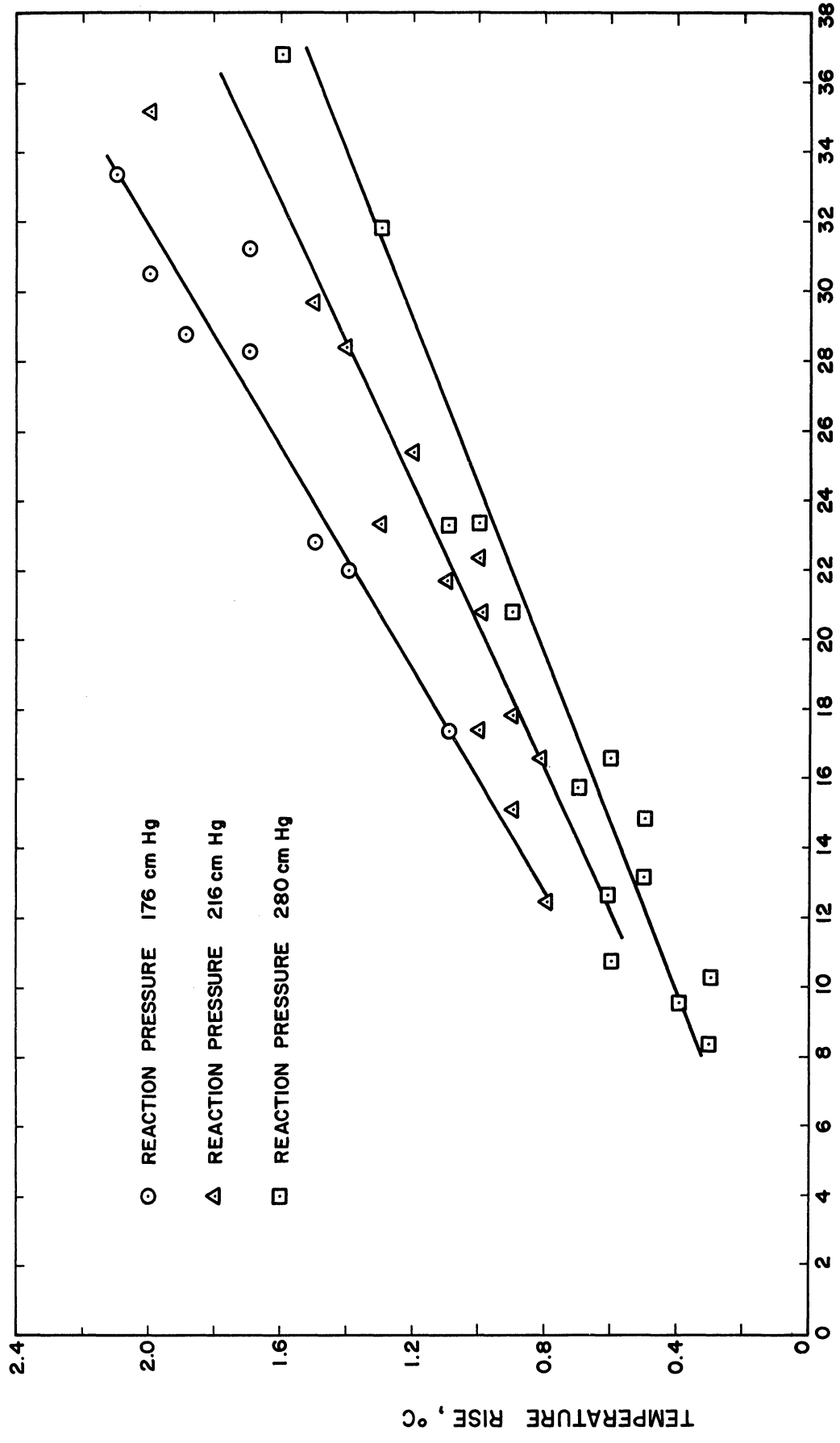

Figure D.1. Experimental Temperature Rise in Reactant Stream.

At an overall ammonia conversion level of 56% and at a reaction pressure of 280 cm Hg, temperature rise using the 16.5 volume percent NH_3, balance O_2, feed was 1.1°C. Using a one pass reactor, an adiabatic temperature rise of 963°C would result at the same level of conversion. This effectively illustrates the temperature control advantage gained by using a recirculation-type reactor.

Temperature rises shown in Figure D.1 are about 90% of the calculated adiabatic temperature rise. Small heat transfer area contained in the reactor tubes resulted in this near-adiabatic condition.

In addition to the temperature rise of the reactant stream, the temperature difference between the reactant stream and the catalyst surface must be considered. Yang and Hougen[56] have treated this problem. Their development will be used here.

The temperature difference Δt between the main gas stream and the catalyst surface is:

$$\frac{\Delta t}{T} = \left(\frac{r}{T}\right) \left(\frac{\Delta H\ (a_p)^{1/2}}{1.35\ \mu\ c_p a_m}\right) \left(\frac{c_p \mu}{k}\right)^{2/3} \left(\frac{(a_p)^{1/2} G}{\mu}\right)^{-.59} \qquad (D.6)$$

Terms used in Equation (D.6) are defined under Nomenclature. Equation (D.6) will be evaluated at 345°C, where the maximum rate and consequently the maximum Δt is encountered. Table D-2 lists the values in effect at 345°C:

TABLE D-2

NUMERICAL VALUES USED IN HEAT TRANSFER EQUATION

Value	Comment
$\frac{C_p}{k} = 0.77$	The Prandtl Number is taken as that for air.
$\mu = .082$ lb ft^{-1} hr^{-1}	The viscosity is taken as that of O_2.
$C_p = 0.45$ Btu lb^{-1} $^oF^{-1}$	Heat capacity used is that of O_2.
$k = .048$ Btu ft^{-1} $^oF^{-1}$	Thermal conductivity used is that of O_2.
$\Delta H = 136{,}000$ Btu $(lb\ mol)^{-1}$	ΔH is the heat of reaction when one pound mole of NH_3 is converted to N_2: $4NH_3 + 3O_2 = 2N_2 + 6H_2O$
$a_p^{1/2} = .0225$ ft	Pellet area has been taken equal to the surface area of a 1/8" X 1/8" cylinder.
$a_m = 5.35$ ft^2 lb^{-1}	a_m equals the external pellet surface area per pound of pellets.
$G = 35{,}500$ lb hr^{-1} ft^{-2}	Mass rate at reaction pressure 2.32 atm
$G = 40{,}800$ lb hr^{-1} ft^{-2}	Mass rate at reaction pressure 2.84 atm
$G = 47{,}600$ lb hr^{-1} ft^{-2}	Mass rate at reaction pressure 3.68 atm

When the values listed in Table D-2 are substituted into Equation (D.6) and an appropriate correction factor is introduced so that reaction rate may be expressed in standard cm^3 min^{-1} gm^{-1}, these equations result:

$$\frac{\Delta t}{T} = .115\ \frac{r}{F} \quad \text{(rxn pressure = 2.32 atm)} \tag{D.7}$$

$$\frac{\Delta t}{T} = .105\ \frac{r}{F} \quad \text{(rxn pressure = 2.84 atm)} \tag{D.8}$$

$$\frac{\Delta t}{T} = .0955\ \frac{r}{F} \quad \text{(rxn Pressure = 3.68 atm)} \tag{D.9}$$

The maximum rate of ammonia oxidation is 94 cm^3 min^{-1} gm^{-1} at measurement R46-1. Using appropriate Equation (D.7):

$$\left(\frac{\Delta t}{T}\right)_{max} = .0175 \qquad (D.10)$$

Equation (D.10) predicts that at a temperature of 345.5°C, a temperature differential of some 11°C will exist between the catalyst surface and the bulk gas stream. Such a temperature increment would be incompatible with accurate kinetic measurements. Reference to Equation (D.6) shows that Δt is inversely proportional to a_m, the catalyst surface area per pound. Table D-2 indicates that the a_m value used in calculating Equations (D.7) through (D.9) was 5.35 ft^2 lb^{-1}, based on the assumption that pellet surface area equals the surface area of 1/8" X 1/8" cylinders. It is clear that this is a conservative assumption. The actual area of the alumina pellets used by Engelhard Industries, Inc., in production of the 0.5 weight percent ruthenium catalyst has been given as in the vicinity of 120 m^2 gm^{-1},[48] or 5,050 ft^2 lb^{-1}. Taking exterior surface irregularities into account, it is not unreasonable to suppose that a_m is at least an order of magnitude greater than 5.35 ft^2 lb^{-1}. In this event, the maximum Δt between the catalyst surface and the bulk gas stream would be a more tolerable 1.1°C.

The above consideration was confirmed experimentally by measuring the catalyst pellet temperature at 345.5°C. A small hole was cored in the bottom of the last pellet contacted by the reactant stream when a 10 pellet charge was used. A bare chromel-alumel thermocouple was then positioned in this hole. The ceramically-shielded thermocouple wires were led through

a Swagelok fitting at the bottom of the reactor and then out of the molten salt inside 1/4" O.D. stainless steel tubing. Then the wires were led from their reaction pressure environment to atmospheric pressure through a rubber sealing septum. Pellet temperature measurements were made in this manner for the first three measurements of each of runs R46, R47 and R48. These measurements correspond to the fastest reaction rates encountered in this work. Measured pellet temperature for all 9 points was never more than 0.6°C greater than the exit stream temperature.

3. Relationship Between Mass Transfer Coefficient and Reactor Diameter

The relationship between the j-factor for mass transfer and the mass transfer coefficient is given by

$$j_D = \frac{k}{v}\left(\frac{\mu}{\rho D}\right)^{1/2} \qquad (D.11)$$

and has been related to the superficial mass velocity by Gordon[21] as

$$j_D = \left(\frac{\epsilon DG}{\mu}\right)^{-1/2} \qquad (D.12)$$

Substitution of (D.12) into (D.11) and subsequent solution for k yields

$$k = \frac{\rho}{\epsilon}\frac{v}{G}1/2 \qquad (D.13)$$

It is seen in (D.13) that the mass transfer coefficient is directly proportional to v, the superficial velocity through the reactor, and inversely proportional to the square root of G, the superficial velocity through the reactor. G and v are both inversely proportional to the square of the reactor diameter. Hence we see that

$$k\alpha \frac{(1/D^2)}{(1/D^2)^{1/2}} = \frac{1}{D} \qquad (D.14)$$

APPENDIX E

VALUES OF CONSTANTS IN RATE EQUATIONS

TABLE E-1

VALUES OF CONSTANTS IN RATE EQUATIONS AND PERCENTAGE DEVIATIONS OF DATA FIT

Temp °C	K_{N_2}	K_{N_2O}	$b_{O_2}^{1/2}$	b_{H_2O}	N_2+% Dev	N_2O+% Dev
246.2	.0053[1]		.097[3]	.031[4]	3.7	
273.5	.0075	.000177[2]	.068	.020	3.4	3.4
296.1	.01038	.00597	.057	.013	2.5	2.8
310.8	.01239	.00147	.049	.011	2.7	3.1
322.2	.0206	.00598	.039	.0065	2.4	4.8

[1]Units: $cm^3\ min^{-1}\ gm^{-1}\ (cm\ Hg)^{-2}$
[2]Units: $cm^3\ min^{-1}\ gm^{-1}\ (cm\ Hg)^{-2.35}$
[3]Units: $(cm\ Hg)^{-1/2}$
[4]Units: $(ch\ Hg)^{-1}$

APPENDIX F

FREE ENERGY FUNCTIONS OF AMMONIA, OXYGEN AND WATER

TABLE F-1

FREE ENERGY FUNCTIONS OF AMMONIA, OXYGEN AND WATER (cal $^{\circ}C^{-1}mole^{-1}$)

Temp °K	$-\phi_{NH_3}$	$-\phi_{O_2}$	$-\phi_{H_2O}$
500	42.249	45.675	41.293
600	43.826	46.968	42.766
700	45.209	48.071	44.024

APPENDIX G

DETERMINATION OF REACTION RATES IN A STIRRED FLOW SYSTEM

Rates of reaction may in general be measured in two major types of systems, batch or continuous flow. If the reaction

$$aA + bB = cC + dD$$

is carried out batchwise, the rate of disappearance of A is expressed by a differential equation as

$$dA/dt = kA^aB^b \qquad (G.1)$$

so that integration of the equation

$$t = \int \frac{dA}{kA^aB^b} \qquad (G.2)$$

is necessary to obtain the amount of A remaining at any time t . For many reaction systems, the integration may not be straightforward and simplifying assumptions may be required. A continuous flow system, on the other hand, involves mathematics which are quite simple relative to the differential equation in (G.1). Continuous flow systems may be either of the stirred flow type or of the tubular variety. In either case, concentration is independent of time under steady state conditions. Assuming efficient stirring occurs in the stirred flow reactor, sometimes referred to as a capacity flow reactor, the concentration of reactants is uniform throughout the reaction vessel and equals the concentration in the product stream. The concentration in a tubular reactor, however, depends on position along the length of the reactor tube.

The mathematics describing the operation of a stirred flow reactor follow from the mass balance for reactant A,

$$F_iA_i - F_oA_o = V(dA/dt) + VkA^aB^b, \qquad (G.3)$$

written generally in Equation (G.3) as input minus output equals the rate of change of reactant in the reactor vessel plus the rate of disappearance due to reaction. After enough time has elapsed under conditions of steady flow, dA/dt approaches zero and the equation

$$F_iA_i - F_oA_o = VkA^aB^b \qquad (G.4)$$

results. The reaction rate constant k can therefore be evaluated by measurement of steady state concentrations.

For a heterogeneously-catalyzed reaction system operating under stirred-flow conditions, the variable influencing the reaction rate is not the reaction vessel volume V but the catalyst weight W. In this case, Equation (G.4) becomes

$$F_iA_i - F_oA_o = Wr, \qquad (G.5)$$

where the rate of reaction r per unit weight of catalyst has been used to replace the term kA^aB^b. The last-mentioned term usually requires more complex representation when a solid-catalyzed gas reaction occurs. The important advantage of Equation (G.5) is that a differential rate of reaction can be determined under time-independent conditions. This fact greatly simplifies the interpretation of rate data, since it eliminates the need to either integrate proposed rate equations for use with integral

rate measurements or to difference integral rate data for use with differential rate equations.

An obvious requirement of the capacity flow experimental method is that rapid stirring of the fresh feed be effected as it enters the system. When the reactants constitute a non-solid, one phase system, stirring can be satisfactorily accomplished in a simple tank by introduction of a mechanical agitator. For a system in which gas phase reactants are catalyzed by a solid, stirring is more satisfactorily accomplished by recirculating the gas phase at high velocities over the catalyst.

A second requirement for use of the stirred flow method is that the proper combination of stirrer and inlet and outlet positions be used so that no bypassing of the fresh feed through the system can occur. An additional condition for use of this technique is that it must be possible to carry out analysis of the steady state composition successfully. Finally, for solid-catalyzed gas reactions, there must be no homogeneous reactions which can take place between reactants and products during holdup of the reactant stream in the recycle loop or in the reaction vessel.

BIBLIOGRAPHY

1. Amano, A. and Paravano, G., Adv. in Catalysis, 9, 716 (1957).

2. Amano, A. and Taylor, H. S., J. Am. Chem. Soc., 76, 4201 (1954).

3. Andrussow, L., Angew. Chemie, 39, 321 (1926).

4. Andrussow, L., Angew. Chemie, 40, 174 (1927).

5. Andrussow, L., Angew. Chemie, 41, 207 (1928).

6. Andrussow, L., Chem. Ing. Tech., 27, 469 (1955).

7. Balandin, A., Vasyunina, N., Barysheva, G. and Chepigo, S., Izvest. Akad. Nauk SSSR, Otdel. Khim. Nauk, 392 (1957).

8. Baron, T., Manning, W. and Johnstone, H., C.E.P., 48, 125 (1952).

9. Benton, A. F. and Drake, L. C., J.A.C.S., 56, 255 (1934).

10. Berkowitz, L. M. and Rylander, P. N., J. Org. Chem., 24, 708 (1959).

11. Bond, G. C. and Webb, G., Plat. Metals Review, 6, 12 (1962).

12. Bond, G. C., Catalysis by Metals, Academic Press (1960).

13. Bodenstein, M., Angew. Chemie, 40, 174 (1927).

14. Bodenstein, M. and Buettner, G., Angew. Chemie, 47, 364 (1934).

15. Bodenstein, M., Z. Elektrochemie, 41, 466 (1935).

16. Bretiner, E., Roginski, E. and Rylander, P. N., J. Org. Chem., 24, 1855 (1959).

17. Butt, J. B., Dissertation, Yale University, New Haven, Conn. (1959).

18. Eyring, H., J. Chem. Phys., 3, 107 (1935).

19. Fischer, F., Tropsch, H. and Dilthey, P., Brennstoff-Chemie, 6, 16, 466 (1935).

20. Giordano, N., Cavaterra, E. and Zema, D., La Chimica a E L'industria, 45, 14 (1963).

21. Gordon, K. F., "A Cell Model for Mass and Heat Transfer in a Fixed Bed," Presented AIChE Washington Meeting, 1960.

22. Gresham, W. F., U. S. Pattent 2, 535,060, Dec. 26, 1950.

23. Guyer, P., Thomas, D. and Guyer, A., Helv. Chim. Acta, 42, 481 (1959).

24. Hulbert, H. M. and Srini Vasan, C. D., A.I.Ch.E.J., 1, 143 (1961).

25. Keith, P. C., U. S. Patent 2,558,760, July 3, 1951.

26. Kemball, C., Adv. in Catalysis, 2, 233 (1950).

27. Kemp, L. C., Jr., U. S. Patent 2,461,064, Feb. 8, 1949.

28. Kokes, R. J., Tobin, H. and Emmett, P. H., J.A.C.S., 77, 5860 (1955).

29. Krauss, W., Z. physik. Chemie, B39, 83 (1938).

30. Krauss, W. and Schuleit, H., Z. physik. Chemie, B45, 1 (1939).

31. Krauss, W. and Neuhaus, A., Z. physik. Chemie, B50, 323 (1941).

32. Krauss, W., Z. Elektrochemie, 54, 264 (1950).

33. Kuhlmann, K., Ann., 29, 281 (1839).

34. Laidler, K. J., Catalysis, 1, 75 (1954).

35. Mueller, E. and Mueller, F., Z. Elektrochemie, 31, 41 (1925).

36. Mueller, E. and Mueller, F., Z. Elektrochemie, 31, 45 (1925).

37. Parravano, G. and Moreno, V., Gazz. Chim. Ital., 91, 479 (1961).

38. Parravano, G., Chimica e Industria, 36, 85 (1954).

39. Parravano, G., Ind. Eng. Chem., 49, 266 (1957).

40. Pauling, L., Nature of the Chemical Bond, Cornell University Press (1960).

41. Perkins, T. K. and Rase, H. F., A.I.Ch.E.J., 4, 351 (1958).

42. Petrov, A., Minachev, Kh., Ponomarenko, V., Sokolov, B. and Odabashyan, G., Doklady Akad. Nauk SSSR, 112, 273 (1947).

43. Raschig, F., Angew. Chemie, 40, 1183 (1927).

44. Raschig, F., Angew. Chemie, 41, 207 (1928).

45. Rea, A. E. and Bebbington, M., Annotated Bibliography on Ruthenium, Rhodium and Iridium as Catalysts, The International Nickel Company, New York (1959).

46. Schwab, G. M. and Theopholides, N., J. Phys. Chem., 50, 427 (1946).

47. Schwab, G. M., Adv. in Catalysis, 2, 257 (1950).

48. Seligman, Bernard, Personal Communication.

49. Smith, W. V., J. Chem. Phys., 11, 110 (1943).

50. Sommerfield, J., Dissertation, University of Michigan, Ann Arbor, Michigan (1963).

51. Trapnell, B., Chemisorption, Academic Press Inc. (1955).

52. Trotter, I. P., Dissertation, Princeton University, Princeton, New Jersey (1959).

53. van Reijen, L. L. and Schuit, G., Bull. Soc. Chim, Belg., 67, 489 (1958).

54. von Nagel, A., Z. Elektrochemie, 36, 754 (1930).

55. von Nagel, A., Z. physik. Chemie, B41, 75 (1938).

56. Yang, K. H. and Hougen, O. A., C.E.P., 46, 146 (1950).

57. Wicke, E. and Hedden, K., Z. Elektrochemie, 57, 636 (1953).

58. Weisz, P. B. and Prater, C. D., Adv. in Catalysis, 6, 156 (1954).

59. Wynkoop, R. and Whilhelm, R. H., C.E.P., 46, 300 (1950).

60. Zawadzki, J., Trans. Faraday Soc., Disc., No. 8, 140 (1950).